The Andes and Hotspots: Mutual Evidence

Rex H Pilger, Jr
10630 W 66th Avenue
Arvada, Colorado USA
rexpilger@yahoo.com
https://orcid.org/my-orcid?orcid=0000-0003-3715-5084

Key Points

Subduction beneath western South America of two hotspot traces on the Nazca Plate since 70 Ma is reflected in gaps and eastward displacement of the Andean volcanic arc as a result of trace-induced low-angle subduction.
The locations of the inferred effects of subducted traces in the Andean magmatic record are consistent with a single hotspot reference frame beneath the Pacific extending from Hawaii to the Juan Fernandez island-seamount chain offshore Chile and covering at least 150 Ma
The role of variations in convergence rate on Andean magmatism from 80 Ma to the Present is not obvious in the distribution of isotopic dates, perhaps correlations with geochemical trends would provide more insight in the future.

Abstract

Improved plate-to-plate reconstructions in the southwest Pacific, South Atlantic, and southwest Indian Ocean, and plate-to-hotspot models for the Pacific plate, combined with published igneous dates of the South American Andes produce apparent correspondence of predicted with observed magmatic patterns in the mountain range. The inferred Easter-Nazca (EN) and Juan Fernandez (JF) hotspot traces, long inferred to control low-angle subduction and contemporary volcanic gaps along the Andean crest, when reconstructed match the traces' present bathymetric expression and seismic clusters within the South American plate. Global reconstructions of the Nazca to the South American plate predict the subducted portions of the traces through time. Gaps in magmatism over the past 10-15 Ma correspond with the reconstructed position of the traces beneath Peru (EN) and Chile and Argentina (JF). The predicted JF trace also matches trends in magmatism, especially mafic rocks, including eastward shifts and gaps as early as 60 Ma in Bolivia, southern Peru, Chile, and Argentina from the 80-90 Ma segments of the trace. The magmatic pattern provide a kind of "image" of the hotspot traces projected onto the Cenozoic of the Andes. The correspondences also increase confidence in the existence of a stable hotspot reference frame beneath the plates of the Pacific over the past ~90 m.y.

Key Words

3040 Plate tectonics
8157 Plate motions: past
8178 Tectonics and magmatism
3037 Oceanic hotspots and intraplate volcanism

Plain Text Summary

Application of advances in plate tectonic theory to the Andes of South America strengthens models of anomalous oceanic plate from mantle hotspots which produce low-angle subduction and volcanic gaps and shifts as oceanic and continental plates converge. Combined plate reconstructions and hotspot models of the Pacific predict when and where anomalous parts of the oceanic plate encountered South America; the calculated positions correspond with observed gaps and shifts in volcanism in the Andes over the past 60 million years.

1. Introduction

The South American Andes, which has developed above a continuously active subduction zone for the plates beneath the Pacific throughout the Cenozoic and extending into the Late Cretaceous, provides the ongoing opportunity for understanding the mutual relationships of mountain-building, magmatism, and subduction to plate kinematics, oceanic plate age, subducting plate fracture zones, and hotspot traces. Ongoing enhancements to the characterization of the ocean basins from magnetic and bathymetric surveys and satellite geoid and gravity measurements, resulting in higher resolution plate reconstructions, provide comparable evolving resolution of global reconstructions of the Nazca/Farallon and Antarctic plates relative to South America. Similarly, studies of the contemporary configuration of the subduction zone from seismicity, tomography, and potential field modeling, and the structure and magmatic evolution of the mountain range, provide a basis of comparison with the plate reconstructions and kinematics. From such analysis, insight into other mountain ranges formed above oceanic subduction zones may be provided, as well as improved characterization of geohazards and effective development of existing and newly discovered mineral resources.

The hotspot/plume hypothesis of Wilson (1963) and Morgan (1971, 1972) continues to influence research on plate kinematics, as well as dynamics, both whether hotspots provide one or more distinct reference frames, and the nature of their origin and relation to the driving mechanism. An auxiliary proposal, that island-seamount chains, inferred traces of hotspots, decrease the angle of subduction, thereby extinguishing or shifting loci of arc magmatism and resulting in Rocky Mountain-type deformation and backarc subsidence (e.g. Cross and Pilger, 1978b, 1982, Pilger, 1981, 1984), has simmered, lacking an abundance of data to establish a correspondence of observed island-seamount chains and their inferred, reconstructed traces with magmatic patterns in the one mountain range in which it is possible, the South American Andes. Since the original 1981 proposal for the Andes a number of workers have applied the idea of gaps in magmatism as indicative of low-angle subduction (although periods of reduced convergence rate, arc-parallel displacement between plates, and/or spreading ridge subduction may also play a role), without application of particular kinematic models for the production of near-flat subduction. Additional implications for magmatic, deformational, and dynamic elevation effects from variations in subduction kinematics have also been a matter of speculation, even as global reconstructions have increased in resolution.

Progressive advances in a wide variety of fields over the intervening forty-plus years provides the opportunity for addressing the magmatic history, plate kinematics, hotspot-frame, and trace subduction effects together for the past 80 Ma. The advances include the generation and publication of thousands of isotopic dates of igneous rocks in the Andes by multiple laboratories in the Americas, Europe, Asia, and Australia, and improved, higher resolution plate-pair reconstructions (especially recent results from the South Atlantic and Southwest Indian Oceans to supplement earlier Pacific Ocean studies) and plate-hotspot reconstructions (especially in the Pacific Ocean, based on more accurate argon-argon dating and improved modeling techniques).

2. Rationale and Methodology

At present, the Andean subduction zone is readily subdivided into five zones, as recognized and defined from the seismicity by Barazangi and Isacks (1976, 1979), three with a maximum dip of 40-45 degrees of the descending plate between 100 to 300 km in depth, and two with nearly horizontal dips just below 100 km in depth (Figure 1). Deeper seismicity appears to be separated from the shallow zone, within 500 and 800 km. The shallow, low-angle segments, beneath central Chile and adjacent Argentina and beneath central and northern Peru, are also distinctive in the absence of active volcanism along the Andean crest, in contrast with the other three, more steeply dipping shallow segments.

Three inferred hotspot traces on the Nazca plate appear to be undergoing subduction beneath the Andes of South America, the Juan Fernandez chain, the Nazca Ridge, and the Carnegie Ridge. The first two are offshore of the contemporary low-angle subduction segments prompting the suggestion of a genetic relationship of the traces to the anomalous subduction (e.g., Pilger, 1981). The traces' inferred sources are, respectively, the proposed Juan Fernandez, Easter, and Galapagos hotspots (Figure 2).

Numerous kinematic models for the production of the hotspot traces on the Pacific plate, assuming relatively fixed hotspots, have been produced since Morgan's (1971) original proposal. Pilger and Handschumacher (1981) showed how the models of Clague and Jarrard (1973) and Jarrard and Clague (1977) could be extended to the three inferred traces on the Nazca plate via relative reconstructions of the Pacific and Nazca/Farallon plates (the Nazca plate is the largest of several to have formed from the fragmentation of the larger Farallon plate at about 25 Ma as recognized by Handschumacher, 1976). Reconstructions of the Nazca plate relative to the South American plate, first calculated by Pilger (1981, extended in 1983) were derived via the plate pair circuit South American > African > Indian > Antarctic > Pacific > Nazca. Subsequently, in Pilger (1984), the circuit was shortened when newly published African > Antarctic reconstructions could replace the longer and less precisely defined African > Indian > Antarctic sub-circuit. A number of other workers have provided updates to the reconstructions within the circuit, including Cande (1985), Cande and Leslie (1986), Pardo-Casas and Molnar (1987), Somoza (1998), and Somoza and Ghidella (2012), and Muller et al. (2019). (Reconstructions by Yáñez et al., 2001, are based on the absolute motions of the Nazca and South American plates according to Gordon and Jurdy, 1986, assuming that the hotspot frameworks of the Pacific and Atlantic are fixed relative to one another. All of the other reconstructions cited do not make this assumption, relying only on relative plate-pair reconstructions.) Recognition that East and West Antarctica have acted at times as separate plates (Cande and Stock, 2000) introduced their replacement of a single Antarctic plate within the circuit, included in the latter two circuit calculations. In each ocean basin, periodically updated plate-pair reconstructions have been published by a number of workers. Thus it is possible to derive documented Nazca/Farallon - South American reconstructions as early as 84 Ma (for earlier times, the connection through Antarctica to the Pacific is speculative). A few alternate circuits have been proposed, as further considered below.

As noted, the correspondence of the two hotspot traces with segments of low-angle subduction could be genetic. Thickened plate beneath aseismic ridges, formed at spreading centers could decrease the density contrast with the shallow asthenosphere at the subduction zone, resulting in shallower inclination of the oceanic plate. Intraplate hotspot traces might produce a decreased contrast due to heating of the plate along with marginal increase in thickness of the crust by the magmatic activity. Both proposed mechanisms have been modeled by several workers with divergent results. As shown by Pilger and Handschumacher (1981), the Nazca ridge was likely formed at the Pacific-Nazca spreading center between 50 to 25 Ma, perhaps beginning even earlier (with older portions undergoing subduction beneath Peru). The Juan Fernandez chain is clearly younger than the surrounding Nazca plate and smaller in dimensions than the Nazca Ridge, so its effect on the subduction zone might be expected to be less significant than that of the Easter/Nazca trace.

The contemporary correspondence of hotspot traces and low-angle subduction can be further tested by reconstructions of the hotspot traces relative to the Nazca/Farallon plate (extending the Pacific-hotspot models via Nazca-Pacific plate-pair reconstructions), and the latter relative to the South American plate via the global circuit, for comparison with the magmatic history of the Andes. Pilger (1981, 1984) applied this approach with lower-resolution plate-pair reconstructions and a very small number of published isotopic dates of Andean igneous rocks. Then available dates showed the expected correspondence over the last 13 to 15 m.y., for the Easter-Nazca and Juan Fernandez traces; that is within the two studied segments, dated magmatism along the Andean crest and younger than the calculated timing of trace subduction was observed to be absent. However, the paucity of dating over much of the Andes limited confidence in the anticipated correspondence, especially for earlier times.

Higher resolution plate pair reconstructions are now available within some plate pairs within the circuit South American > African > East Antarctic > West Antarctic > Pacific > Nazca/Farallon (*SA-AF-EA-WA-PC-NF*), although a few limitations persist. One of the most significant shortcomings is the inability to propagate reconstruction uncertainties throughout since common magnetic isochrons for plate pair reconstructions within the circuit do not exist.

Over the past forty years thousands of isotopic dates of Andean igneous rocks have been produced by laboratories in South and North America, Europe, Asia, and Australia. A compilation of greater than 20,000 dates on igneous rocks from the Andes and adjacent areas from published sources (including more than 10,000 younger than 100 Ma) provides a basis for comparison with the reconstructions.)

If the hotspot trace subduction effect exists, gaps or landward shifts in the magmatic foci should be observed for dates on the order of or younger than the reconstructed hotspot traces. (In addition, the reconstructions are also an implicit test of models of relatively fixed hotspots beneath the Pacific Ocean and the separate Atlantic-Indian Ocean hotspots.)

Other postulated controls on subduction zone configuration, such as convergence rate, motion of the upper plate relative to the deeper mantle (i.e., “absolute motion”), and age of the subducting oceanic plate may also be relevant (e.g., Cross and Pilger, 1982), but, with the exception of the first, are not so easily distinguished. Convergence rate variations are readily calculated from the reconstructions, so semi-quantitative comparisons are possible, recognizing the limitation of unknown uncertainties. Convergence rate inferences made in the first few decades of reconstructions (e.g., Pilger, 1983; Pardo-Casas and Molnar, 1987) suffered from inaccuracies and imprecision in the geomagnetic time scale, which appear to have decreased in recent years as more isotopic dating of sedimentary and volcanic sequences and correlation with solar cycle measurements have been incorporated (e.g. Gradstein et al., 2020).

Unfortunately, motion of the South American plate in a hotspot frame is poorly constrained and of relatively low resolution in most extended models (e.g., Pilger, 2007); some analysis may be tentatively undertaken, nevertheless.

3. Relative Plate Reconstructions

Table 1 lists the primary sources of the relative plate-pair reconstructions within the South American-African-Antarctic-West Antarctic-Pacific-Nazca/Farallon (SA-AF-AN-WA-PC-NF) and SA-AF-AN-WA-NF circuits and hotspot-Pacific and hotspot-Africa (HS-PC, HS-AF; these pairs are addressed further below). Supplementary Table 1 lists the actual parameters and assigned ages. DeMets et al. (2015) and DeMets and Merkoviev (2019) have provided high resolution reconstructions for AF-EA (since ~20 Ma) and SA-AF (since ~34 Ma), while Croon et al. (2008) have calculated high resolution reconstructions for WA-PC for virtually the full time interval of interest. Pérez-Díaz & Eagles’ (2014) parameters complete SA-AF, while Royer and Chang (1991), Cande et al. (2010), Bernard et al. (2005), Nankivell (1997) complete AF-EA, with both sets at variable resolution. Wilder’s (2003) PC-NF reconstructions are confined to the interval 12 to 28

Ma, supplemented by partial reconstructions of Wright et al. (2015) and Seton et al. (2012) from the North Pacific for older times and two PC-NF reconstructions younger than 12 Ma, calculated from Tebbens and Cande's (1987) WA-NF and Croon et al.'s WA-PC parameters (PA-NF is equivalent, of course, to PA-WA-NF, but with added uncertainty). A shorter circuit, involving SA to AN directly but of lower resolution, is also presented in Table 1 from Livemore et al. (2005), Eagles and Vaughn (2009), and Eagles and Jokat (2014). It is compared with the primary circuit below.

The circuit reconstructions require interpolation since only a few isochrons are identified within all of the plate pairs. Conventional interpolation (e.g., Atwater and Molnar, 1973) utilizes constant stage poles and rates of rotation (introduced by Pitman and Talwani, 1972, and Weissel and Hayes, 1972) between reconstructed isochrons at discrete times. Piecewise polynomial interpolation (e.g., cubic splines) is an alternative approach (Pilger, 1981b, 2003, 2007), which allows for continuous change in kinematics; constant stage poles and rates force changes to correspond with the discrete isochron reconstructions (the most confidently identified isochrons are those formed during apparent periods of constant rotation pole, if not constant rate; forcing changes to correspond with just such times is very likely incorrect). Rather than select discrete isochrons, reconstruction parameters are calculated at unit m.y. Intervals via the splines. Logically, meaningful reconstruction uncertainties cannot be determined by interpolation; by definition, interpolation provides synthetic parameters for times in which such parameters are unavailable. Uncertainties for discrete reconstructions derived by conventional means (e.g., Kirkwood et al., 1997) are linearized approximations of nonlinear forms which do not have a temporal dependency since they are derived for individual isochrons whose assigned ages are irrelevant. (Livermore et al. 2014, did apply a method of simultaneous reconstructions of sequences of isochrons via flowlines, including uncertainties, after Shaw and Cande, 1990, but the approach has not been expanded upon, probably because the number of reconstruction and flowline parameters sought can become unwieldy.)

The geomagnetic timescale of Ogg (2020) is utilized for the reconstructions and cubic spline interpolation. The spline interpolation is applied to each plate pair, converting the spherical coordinates to Cartesian with magnitude equal to the average rotation rate. The algorithms of Press et al. (1992) produce the spline coefficients and interpolated pseudovector parameters, converted to quaternion parameters. The latter parameters are combined utilizing the derivation of Francheteau (1973; LePichon et al. 1973) and ultimately converted back to spherical coordinates. (Supplementary Table 2 provides the interpolated parameter sets for each pair at 1 m.y. intervals.)

Table 2 provides the calculated parameters for the reconstructions of the Nazca/Farallon plate to the South American plate at 1 m.y. Intervals. Resolution is best achieved between 12 and 20 Ma, and, to a lesser extent, between 20 and 33 Ma. Pacific to Nazca/Farallon reconstructions are probably the least certain in the primary circuit because of the sparsity of magnetic survey coverage of the east-central Pacific Ocean; this is particularly unfortunate since this boundary has the highest average spreading rates of the entire circuit (e.g. Pilger, 1983), thereby providing the greatest contribution to the net kinematics.

4. Hotspot - Plate Reconstructions

Since Morgan's (1972) original parameterization of the Hawaiian-Emperor (H-E) hotspot trace (together with the Tuamotus and Line Islands) a number of workers have revised the parameters based on progressive isotopic dating of volcanism along not only the H-E trace, but also others on the Pacific plate . Critical to modeled parameters was in the introduction of argon-argon dating which demonstrated many measured island/seamount potassium-argon dates are apparently too young, most familiarly, the bend in the H-E chain, which is now accepted to be closer to 48 Ma based on argon-argon dating (Sharp and Clague, 2006; O'Connor et al. 2013) rather than the K/Ar date of 43 Ma and an even earlier, projected 27 Ma (Clague and Jarrard, 1973), while the Line Islands are much more complex than Morgan had interpreted. Harada and

Hamano's (2000) model for the Pacific hotspot traces derived an implicit age of 48 Ma for the bend, even before Sharp and Clague's (2006) revised date was published and independent of relative plate motion evidence

The most recent models of Pacific - hotspot motion which incorporate the 48 Ma age for the bend and other, newly recognized traces are Wessel and Kroenke (2008) and Gaastra et al. (2022). Some workers argue that the dating and paleomagnetic measurements require significant relative motion of the Hawaiian and Louisville hotspots; Gaastra et al. (see sources cited in their paper) show that one issue is the presumption of where the point in the latter chain corresponding to the HE bend is located; their revised model fits the two primary traces plus parts of additional traces recognized on the Pacific plate resulting in minimal motion between hotspots.

It should be noted that most Pacific hotspot models do not take the apparent traces on the Nazca and Cocos plates into account; one exception is that of Pilger and Handschumacher (1981; also Pilger, 1983) who noted that the Easter-Nazca trace is better fit by an age for the HE bend close to isochron 21 or 22, now dated between 45.724 and 49.344 Ma (Ogg, 2020), than the then widely accepted 43 Ma; the older age also corresponds with a significant change in motion of the Farallon and Pacific plates, another point of contention with the 43 Ma date (e.g., Norton, 1995)...

Because both models, Wessel and Kroenke (2008) and Gaastra et al. (2022), for Pacific-hotspot motion are based entirely on isotopic ages, they do not need to be adjusted for changes in the geomagnetic time scale. However, in order to test the models against the traces on the Nazca plate, which involve magnetic reversal isochrons for the Pacific-Nazca/Farallon plate reconstructions, it is necessary to document the timescale used, in this case, that of Ogg (2020). Supplementary Table 1 includes the two Pacific-hotspot model parameter sets; Supplementary Table 2 includes the cubic spline-interpolated parameters by the same procedure used for the relative plate reconstructions plus the calculated Nazca-hotspot parameters for the two hotspot models.

5. Nazca and Cocos Plate Hotspot Loci at Present

Note: It is suggested that the reader obtain the Keyhole Markup Language files in the Supplementary Data and display them in Google Earth (or another GIS software program which also displays regional geographic features, such as coastlines, trenches, islands and seamounts, and country boundaries). The descriptions in the next sections are more easily visualized in this manner.

Figure 2 illustrates back-tracked loci of individual dated volcanic samples from inferred hotspot traces on the Pacific, Nazca, and Cocos plates, using the model of Gaastra et al. (2022; "*GGW22*") for Pacific-hotspot motion, extended to the two other plates; at the scale of the two figures, the model of Wessel and Kroenke (2008, "*WK08*") would not produce obvious differences. At a larger scale (Figure 3), loci for the two models of hotspot motion relative to the Nazca/Farallon plate (from application of the parameters in Table 3; see also Supplementary Keyhole Markup Language, "**.kml*," files), based on *WK08*, and *GGW22*, are calculated for the three inferred contemporary hotspots with respect to the Nazca plate, propagated from the Pacific plate as described above. As WK08 extends to 140 Ma and GGW22 only to 80 Ma, the stage parameters from 80 to 140 Ma calculated from the former are used to extend the latter to 140 Ma. The hotspot locations are adjusted to best fit the bathymetric expression of each trace to the GGW22 loci. (There are a number of published dates for the Juan Fernandez, Easter/Nazca, and Galapagos/Carnegie hotspot traces, included in a Supplementary Data *kml* file; they are not inconsistent with the calculated loci described in this paper.)

The extensions of the modeled loci into the South American plate (Figure 3 and subsequent illustrations below) are *not* adjusted for the configuration of the subducted slab, since it is not clear what the kinematic path along the slab should be, nor, for past reconstructions, is the slab configuration in the independently

known; the individual loci could be relocated several tens of kilometers or more to the southwest or west of the modeled surface locations.
Figure 3 shows that both WK08 and GGW22 fit the 25 Ma bend in the Easter-Nazca trace fairly well, but with different inferred locations for the Easter hotspot (its contemporary location is poorly constrained). However, there is a significant deviation of the younger part of the Juan Fernandez (*JF*) and Galapagos-Carnegie (*GC*) loci from the observed bathymetry for those based on the WK08 model compared with the GGW22 model; the WK08 model would fit better if the contemporary JF hotspot location were further southwest of the westernmost extent of the JF chain; even so its orientations are still significantly different than those of the JF and GC traces.
For the purposes of this study, the GGW22 Pacific-hotspot model is utilized because of its better fit to the observed portions of the JF and GC traces and the other data presented below. Before further consideration of the relationship of the GGW22 loci to other geological observations, it is convenient to summarize the shape of the loci through time. The Juan Fernandez locus, from present into the past extended east-west from 0 to ~25 Ma, to the northeast between ~25 and ~85 Ma, more easterly from ~85 to ~110 Ma, and northerly between ~110 to ~120 Ma; it then curves back to the west to north-north easterly from ~120 to ~140 Ma. (The part of the locus between 105 and 125 Ma, termed herein the “hammerhead,” appears in another guise below.) The abrupt “kink” in the locus about 50 Ma is inherited from the parameters of the GGW22 Pacific-hotspot model close to the HE bend and is independent of the Pacific-Nazca/Farallon parameters. (Recall that the 80 to 140 Ma part of GGW22 is based on the equivalent part of WK08A combined with the 80 Ma GGW22 parameters.)
It is possible that the older parts of the locus, assumed attached to the Farallon plate, may never have formed in the first place as another plate may well have existed above the JF hotspot at that time, if the hotspot, also, then existed. Other evidence for the trace and plate is essential to provide support for the hotspot’s existence and expression at progressively earlier times.
Returning to the younger part of the loci, the GGW22 modeled JF trace corresponds well with the shallow-to-intermediate-depth seismicity pattern in central Chile extending into Argentina (Figure 4), and lesser shallow seismic clusters appear along the GGW22 extensions of the Nazca and Carnegie Ridge loci (Figure 1). If the ridges indeed extend where the model suggests, instead of hotter, partially molten asthenosphere in the wedge between the subducting slab and the upper plate, drag against the upper plate by the shallowly dipping lower plate could induce resistance, propagating enhanced shallow deformation and seismicity into the upper (South American) plate above the subducting trace.
As recognized by Barazangi and Isacks (1976), contemporary volcanism along the crest of the Andes is present within the more steeply dipping segment of the subduction zone from southern Peru into northern Chile, and absent within the low-angle subduction segments. The respective presence and absence of the asthenospheric wedge is invoked to explain the difference (see also Cross and Pilger, 1982).
The reconstructed loci in their contemporary locations require only the Pacific-hotspot kinematic models and Pacific-Nazca/Farallon reconstructions (without attempting to address their deformation in the subduction zone). To compare the loci through time relative to the magmatic history of the Andes requires the global circuit plate reconstructions.

6. Nazca Plate Hotspot Loci Relative to South America since 80 Ma

The three Model GGW22 hotspot trace loci (Figure 3) are further reconstructed relative to South America for discrete times, via the global circuits to 80 Ma. Figure 5 shows the loci in relation to the continental plate at 5 m.y. intervals. From Figure 5 one may infer that essentially east-west subduction at the latitude of the JF Ridge occurred over the last twenty million years, with most rapid convergence of the Nazca and South American plates between 25 and 15 Ma (higher resolution analysis of convergence rate and direction

variations is addressed further, below). Additionally, the reconstructions imply that subduction of the JF trace was largely confined to the contemporary zone of low-angle subduction for the past ~13 m.y. (which is consistent with Pilger's 1984 reconstructions over the same period). Between 25 and 13 m.y., the locus intersection with the trench progressed southward from northernmost to central Chile. (Since the trench may have been in a more oceanward position, the intersection points would be farther to the southwest relative to the stable interior of the South American plate.) From ~45 to ~25 Ma, the reconstructed JF trace implies roughly east-west convergence within a narrow zone beneath southern Peru, northern Chile, Bolivia, and northern Argentina; the reconstructed trace first encountered the subduction zone about between 70 and 65 Ma.

The reconstructed Easter-Nazca (EN) trace first encountered the Trench offshore present-day northern Colombia between 45 and 40 Ma, maintaining a southwesterly migrating intersection with the trench onshore Colombia and Ecuador until about 18 Ma, when the intersection migrated to the south-southeast more rapidly, to its contemporary position off southern Peru. As with the JF trace, the position of the trench may have been farther west relative to the interior of the continent at progressively earlier times, contributing some additional uncertainty to the intersection locales.

The reconstructed Galapagos-Carnegie Ridge Trace (GC) first intersected the Nazca-Pacific boundary between 25 and 20 Ma, near the Caribbean-South American-Nazca triple junction, extending beneath the complex Caribbean-South American boundary of northern Colombia and Venezuela. It is not clear whether it has any effect on the configuration of the contemporary subducting slab (Figure 1).

As observed above, the older parts of the loci may never have developed on the older part of the Farallon plate if the corresponding portions of the latter did exist; the projected part of the Farallon plate is based on isochrons in the northwest Pacific. Corresponding parts of the Pacific plate with those projected under South America are also unknown because they are presumably beneath the northeastern Australian plate, having been subducted, if they, also, ever did exist. The reconstructions of Clennett et al. (2020), focused on the northeast Pacific, do include an existent, subducting Farallon plate offshore South America as early as 80 Ma; prior to that time, they infer accreting terranes, island arc fragments, as far south as Colombia, with another intervening plate which completed subduction before the end of the Cretaceous. (Clennett et al.'s reconstruction circuit includes most of the components of the circuit utilized in this study, except their primary concern is North, not South, America relative to the plates of the Pacific and Mesozoic accreted terranes.)

7. Volcanic history of the Andes and reconstructed hotspot loci

As anticipated, the patterns of magmatism in the Andes apparently reflected interaction with subducting hotspot loci in spatial/temporal gaps or landward displacement of igneous foci from then sparsely available potassium-argon isotopic dates (Pilger, 1981, 1984). The more recently acquired abundant dating, much of it argon-argon and uranium-lead, by multiple workers from the Andes and adjacent areas (compiled as part of the current study and accessible via GEOROC, http://georoc.mpch-mainz.gwdg.de/georoc/) provides additional testing of the hypothesis. Display of four-dimensional data in comparison with reconstructed loci is a challenge, however, and would require a large number of two dimensional maps and graphs and/or projection into three dimensions via digital goggles and sophisticated visualization software. In order to produce a small set of two-dimensional and pseudo-three dimensional portrayals, the intersections of loci with the trench and sub-parallel landward segmented lines have been calculated for display in age versus distance from the trench graphs in addition to the maps provided in the Supplementary Data (the data sets are also available in spreadsheet and kml formats within Supplementary Data files).

(In the Supplementary Data, Google Earth views of the JF and EN hotspot trace loci and isotopic dates of igneous rocks in the Andes in 10 m.y. Increments from 80 Ma to the Present are displayed together with the

preferred model loci.. It is apparent in such views that it is difficult to recognize the correlation of the JF trace with magmatic patterns except for the most recent period, 0-10 Ma. To a greater extent the apparent absence of significant magmatism for the same period from central to northern Peru, corresponds with the reconstructed EN loci.)

Plots of magmatic isotopic age versus distance along the Andes is more enlightening. Figure 6a illustrates the Peru-Ecuador-Colombia part of the Nazca-South American boundary in a set of charts with the trench, dates, and loci rotated 24.5° around a pole at 15.8° S latitude and -74.8° W longitude (the rotation parameters are chosen to approximately orient the Andean crest and the average trench north-south). Each chart incorporates rotated dates and loci points (calculated at 1 m.y.) in intervals of 1° east-west distance (~111 km) from the trench along parallels (rotated coordinates). The distribution of the isotopic dates from Peru and Ecuador younger than 15 Ma closely corresponds, as expected, with the projected locus points of the Easter-Nazca trace, producing a time-transgressive cessation from north to south, parallel with the locus intersections, lagging the loci (Figure 6a A-D, and strengthening the tentative correlation previously observed with the much sparser data set (Pilger, 1984). Resumption of magmatism is apparent along the northern part of the segment. Loci from the Juan Fernandez hotspot also reach into this segment and largely correspond with gaps in dates between 40 and 30 Ma. (There are obvious limitations with the rotated dates in the southern part of the segment in that the trend of the Andes undergoes a change from NNW to nearly NS.) Even with the increase in number of isotopic dates from the mid-1980s, there is still a paucity from northern Peru, although it is possible that a significant igneous history is hidden by late Cenozoic sedimentation in the upper Amazon basin, which appears to have formed in response to the onset of low-angle subduction (Cross and Pilger, 1978b).

Figure 6b shows a similar (unrotated) plot for the isotopic dates between 0 to 80 Ma, south of 15.8° S latitude, in 1° intervals, similarly bounded by the project loci points as in Figure 6a; a more subtle correlation appears to be present. The cessation of volcanism above the contemporary central Chilean-northern Argentinian low-angle subduction segment is inferred to have begun at approximately 13 Ma along the Andean crest, based on the isotopic dates; the locus of the projected Juan Fernandez trace stabilized in the segment at approximately the same time, as Pilger (1981, 1984) showed.

What was not obvious in previous work, due to sparsity of data, was an apparent correspondence of date distributions with the JF loci prior to 13 Ma,. The significantly larger number of isotopic dates from Chile, Argentina, Bolivia and southernmost Peru allow for closer examination. For dates within 300 km of the trench, the absence of such dates for the last 10 m.y. In the region where the JF locus intersects the trench and the parallel line segments 150 and 300 km east of the trench is quite apparent, as noted above – the contemporary zone of low-angle subduction (Barazangi and Isacks, 1979). Earlier, between 25 and 13 Ma there is an onset of increasing density of dates paralleling the JF locus extending from north to south from the contemporary low-angle segment in each chart. For dates greater than 300 km from the trench, there is an even greater correspondence with the loci; that is, a greater density of dates far from the trench is observed paralleling and the locus intersections from 3 to 7° (approximately 333 to 777 km). There are a number of earlier dates apparent prior to the predicted location of the JF ridge. What is the significance of the correlation? It is inferred that the JF trace produced a tentative increase in magmatism after it had progressively moved from north to south; in other words, a short-lived period of low-angle subduction interrupted normal subduction and was quickly followed by resumption of magmatism after passage of the trace; the low-angle subduction expanded the zone of magmatism to the east which then persisted after passage of the ridge beneath. Note that the oldest parts of the loci in each diagram records the “hammerhead” in map view above (Figure 5); note also that the distribution of oldest igneous dates in Figure 6b A, C-E, and F, also produce a similar shape, but older than the trace points

That the loci intersections overlap with somewhat older dates in the same area with other factors may be involved; the other possible mechanisms include: (1) the age progression along the Hawaiian trace may be

older than the combined GGW22 and W08 model, which would increase the age of the intersection of the consequently longer and more easterly trending JF locus; (2) the JF hotspot may be located farther east; (3) reconstructions between the Pacific and Nazca/Farallon plate since about 25 Ma are in error, due to sparsity of isochron identifications (the high resolution identifications across the other plate-pair boundaries are unlikely to be significantly erroneous); (4) the north-south zone of influence of the subducting trace may have been significantly wider, affecting magmatism to the south of the southward-migrating intersection.
Pilger and Handschumacher (1981) provided several rationales for an older age of ~50 Ma for the Hawaiian-Emperor bend, especially the observed change in Pacific-Farallon motion around that time. That dates from seamounts may be as much as 3 m.y. younger than the onset of their formation has been suggested by O'Connor et al. (1995) and Ray et al. (2012) as applied to the Easter-Nazca chain (Maia et al. 2005, based on magnetic surveys and modeling of the near-ridge part of the Foundation seamount chain on the Pacific Plate, argue that seamount formation occurs within a period as short as 1 m.y.)..
To test the possible variation in age of the Pacific-hotspot model, the parameters of Gaastra et al. (2022) are retained but linearly assigned progressively older dates from 10 to 25 Ma to 10 to 28 Ma; original dates from 25 to 48 Ma in their model are linearly adjusted to between 28 and 50 Ma and from 48 to 80 to 50 to 80 Ma, with adjustment to the reconstructions and age/latitude plots as shown in Figures 7 and 8. The adjusted loci encounter the subduction at earlier times and seemingly better fit the isotopic age data, at least from ~23 Ma and younger. Older ages could be applied to all of the parameters in the combined model to better fit the isotopic dates.
That Juan Fernandez ridge subduction has been responsible for rotation of the region south of 15, i.e., oroclinal bending (Isacks, 1988), has been proposed by a number of workers (e.g., Arriagada et al., 2013). The magnitude and timing of this deformation, ~20-25 Ma, is supported in part by paleomagnetic evidence (e.g., Dupont-Nivet et al., 1996, Arriagada et al. 2013, Puigdomenech et al., 2021) and corresponds with the calculated intersection of the JF trace with the trench (Pilger, 1981, 1984, this paper).

8. Alternatives

A number of workers have proposed alternative mechanisms for the production of low-angle subduction, especially the two segments of the Andes in which flat slabs are observed, including DeCelles et al. (2009), et al. (1976), Skinner and Clayton (2013), Schepers et al. (2017), and Schellart WP (2020). In each case, some aspects of convergence rate, age of subducted plate, crustal thickening within the upper plate, duration of subduction episode, and/or surface erosion are invoked to explain the "anomalous" subduction without or minimizing the hotspot trace convergence effect. In most cases the workers have only considered the contemporary structures and phenomena without considering the geohistorical evolution of the region. Testing of plate reconstructions of the plates and hotspot traces over time is not incorporated into their models, nor evidence for the evolution of the volcanic gaps through time.

The inferred inadequacy of a buoyancy effect in such models may point to the need to consider auxiliary phenomena if the modeling cannot reproduce low-angle subduction. The observation of low-velocity mantle beneath the subducting slab beneath southern Peru, below the recognized continuation of the Nazca ridge (Bishop et al., 2017) is particularly striking. That is, the buoyancy effect of the thickened crust may be augmented by low-density mantle beneath the subducting plate. Paleomagnetic evidence from southern Peru indicates late Cenozoic deformation of the Andes (Rousse et al., 2017). This corresponds with the progressive southern migration of the Nazca ridge along the Andes, and, by inference, the subducting ridge and its underlying anomaly. Other aspects of apparent Nazca ridge migration, on the trench side, and the foreland side of the Peruvian arc are also worthy of further investigation. (That physical modeling has come up short in some cases does not invalidate the other evidence for ridge subduction effects.)

One remaining issue is the persistence of low-angle subduction beneath northern Peru after inferred passage of the Easter-Nazca trace beneath, as the contemporary position of the trace is predicted to continue well to the east. Note that all trace reconstructions do not incorporate conformance of the traces onto the inferred subduction zone. Were such calculations added, the position of the trace would be farther to the west, but it is not clear if the apparent anomaly would be fully resolved by such a “correction.” Figure 12 illustrates one more possible factor: younger plate is undergoing subduction beneath northern Peru than plate beneath central and southern Peru. As is apparent beneath southern Chile, younger plate subducts at lower angles than older plate (Cande and Leslie, 1986).

9. Convergence Rates and Directions

The reconstructions derived in this study also provide estimates of variations in convergence rate and direction across the Nazca/Farallon - South American plate boundary. Significant revisions to the geomagnetic timescale result in differing convergence rate calculations from those in the 1980s (e.g., Pilger, 1981, 1983; Cande, 1985; Pardo-Casas and Molnar, 1987) on top of the higher resolution of newer plate-pair reconstructions. Cande and Kent’s (1995) timescale has been the standard for most subsequent plate kinematic analyses, e.g. Muller et al. (2019) and previous University of Sydney syntheses; the latest timescale of Ogg (2020), utilized in this study, produces results not that much different from Cande and Kent, even as it is aligned with the orbital-tuning refinements incorporated into the latest geological time scale (Harland et al. 2020).

Figure 13a illustrates the calculated instantaneous convergence rate variations over the last 80 m.y., as derived from the global plate reconstructions via spline interpolation of pseudo-vectors and their gradients (Pilger, 1983, 2003) at several locations along the South American-Nazca plate boundary. At a resolution of 1 m.y., variations in apparent rates are significant, but perhaps misleading. The variations could represent uncertainties in isochron picks, the spline interpolation, and/or the geomagnetic timescale which are magnified by calculation of the gradient.

By undertaking a moving average (Figure 13b) four distinct relative peaks in convergence rates are recognizable. The first, just before the end of the Cretaceous, between 78 and 68 Ma, is followed by a deep minimum between 65 and 55 Ma. Three more peaks, each greater than the previous, follow, between 54 and 49, 45 and 40, and 22 and 15 Ma. The drop-off since 18 Ma includes some apparent stationarity between 14 and 9 Ma, with a smaller “shoulder” around 7 to 5 Ma. It is important to keep in mind that the highest rates of motion in the circuit are between the Nazca/Farallon and South American plates which has the lowest resolution, especially in the past 15 m.y., and prior to 30 Ma.

A simple histogram of all of the compiled dates 80 Ma or younger, at 5 m.y. bins (FIgure 14a), when compared with the convergence rates, does not demonstrate any obvious visual correspondence. Perhaps a finer comparison, focused on date frequency relative to distance from the trench and age would reveal a better correlation (Figure 14b); however, there still is no obvious correspondence.

If there is a correlation between convergence rate and magmatism, it might be manifested in a certain amount of lag time between the time of subduction and its manifestation in a change in magmatic volume (for which the dates are a proxy). Simple correlation of the number of dates in one-million year bins versus convergence rate normal to the margin produces a value of 0.26. For simple convergence rate, the value is 0.07. Cross-correlation over 0-80 m.y., at a 1 m.y. Is displayed in Figure 15.

The absence of a sharp peak implies the absence of a simple lag from subduction to magmatism. The broad peak, cresting between 13 and 22 m.y. could be interpreted as an integrated effect of waves of magmatism complexly correlated with convergence rate over a broad lag in time. Of course, it is important to recognize that sampling of the igneous activity in the Andes has not been focused on measuring changes in volumes of magmatism over time; that is the histograms maybe only vaguely indicative of magmatic intensity.

10. Southern Andes and Spreading Center - Trench Interaction

The southern Andes differ from the central and northern parts of the range insofar as the latter have apparently interacted with the Nazca/Farallon plate most of the Cenozoic, while the former has been affected by proximity to the Nazca-West Antarctic spreading center for at least the Late Cenozoic (Cande and Leslie, 1986) and, consequently, slow subduction of the young, hot WA plate. The updated global reconstructions as part of this study have been applied to identified WA-NF isochrons and restored to both their apparent positions relative to SA at the time they formed but also projected forward in time at 1 m.y. Increments to provide apparent positions of younger, now subducted isochrons reconstructed to the SA plate as well (Fig. 16). The synthetic assumption for the younger reconstructed isochrons is that spreading continued after subduction at the same rate and geometry as the rest of the still active part of the NF-WA spreading center. So the reconstructed isochrons approximate the hypothetical spreading center beneath SA at the age of the rotated isochron. This is not to imply that spreading actually did persist for millions of years after the first encounter of the ridge with the trench. However, the pattern of the the reconstructed isochrons relative to the pattern of isotopic ages from the same nearest the trench are intriguing: Reconstructed isochrons along the trench and along segmented lines approximately parallel to the trench at 150 km spacings are plotted along with isotopic ages in age versus latitude charts (Figure 17). Note the similarity in patterns of reconstructed isochrons along the trench,150 km east of the trench and isotopic ages between the two segmented lines (Figure 17a). The pattern is not apparent in the next segment to the east, between 150 and 300 km from the trench (Figure 17b). The near-trench patterns have two obvious implications: hotter subducting plate resulted in closer proximity of volcanism, very similar to the pattern observed in the North Pacific as parts of the Farallon-Pacific spreading center approached the California subduction zone beginning about 25 Ma (Pilger and Henyey, 1979). The corresponding patterns in the southern Andes, with this interpretation, provide additional support for the resilience of the global plate reconstructions for the past 45 m.y., while the hotspot trace patterns described above support the reconstructions since at least 60 Ma.

11. Other Hotspot Reference Frames

It is not enough to demonstrate an apparent correspondence of hotspots in one reference frame, in the Pacific, with subduction-related magmatic patterns. Other hotspot reference frames outside of the Pacific have also been proposed. Müller et al.'s classic (1993; “M93”) hotspot-plate model for the plates of the Indian and Atlantic Oceans is one example and a globally-averaged hotspot reference frame is another (Muller et al., 2019, “M19”)..

There are two rationales for using Müller et al. (1993) in addition to their own documentation. First, as first recognized Oxburgh and Turcotte (1974) mid-to-late Cenozoic isotopic dates from East Africa imply a southward progression of volcanic inception; Pilger (2003), based on a larger data set, Inferred two southward progressions of inception, from 60 Ma (southern progression – the one Oxburgh and Turcotte recognized) and from 40 Ma (northern progression). What is intriguing is that the progressions are both

consistent with M93. That is, the asthenospheric magmatic sources responsible for the two groups of East African volcanism appear to be fixed relative to the other hotspots that comprise the foundation of M93.
The second rationale is provided by Müller et al. (1999) who showed that reconstructions of the paleo-positions of the Caribbean island arc are also consistent with the M93 reference frame. Using Pindell and Kennen's (1991) reconstructions of the Caribbean plate relative to North America, restoration via the circuit Caribbean-North American-African-Hotspot, the restored arc positions overlie one another. That is, the Caribbean subduction zone apparently maintained a stable position in the same reference frame as the hotspots beneath the Indian and Atlantic Oceans, as defined by M93. In contrast, the moving hotspot reference frame, M19, and its earlier progenitors (e.g., O'Neill et al., 2005, and Torsvik et al., 2010, Doubrovine, 2012) do not both fit the East African volcanic date pattern and restore the Caribbean arc as well as M93.
Assuming the three hotspots of the Nazca plate are fixed to each of those reference frames, connected through the global relative reconstruction circuit used above, reconstructed JF loci along with the GGW22 locus are shown in Figure 18 and with examples of their relationship with the magmatic dates in Figure 19. One recognizes overall similarities in the calculated loci to those constructed from GGW22, with the 25 Ma bend present in all three, along with the "hammerhead." The extension of M93 to the Nazca plate shows the 25 Ma bend farther east and extended M19 farther west from the extended GGW22 model. The similarity in bends is not surprising, as the Pacific-Nazca spreading center, with its prominent 25 Ma motion change, at the time of fragmentation of the southern Farallon plate into the Cocos and Nazca plates, dominates contributions to the global reconstruction circuit (Pilger, 1983). The alternative models are also displaced from the observed JF and Galapagos-Carnegie traces; depending on the location of the Easter hotspot, each of the three loci could fit the Easter trace, with the extended M19 and M93 models having comparable orientations to the Nazca Ridge. Comparison of the alternative models with the Andean isotopic dates shows a significant offset of the predicted loci intersections from the igneous patterns, however, again realizing that the placement of the Easter hotspot is critical to the position of the loci intersections relative to the Peruvian trench. In sum, the extended GGW22 model, with older ages for pre-25 Ma parameters, appears to fit all of the data sets (physiography, shallow seismicity clusters, igneous isotopic dates) better than those of WK08, M93, and M19, in the context of the same global reconstruction circuit (for the latter two models).

12. Mafic Magmatic Evidence

With the exception of data 13 Ma and younger, the evidence for JF interaction in the magmatic evidence shown above might be questioned by some:in a progressive north-to-south increased intensity in magmatic activity represented by the increased density of isotopic dates, in parallel with the trace intersections? In an effort to examine evidence for possible back-arc extension, independent of testing for the proposed JF "effect," isotopically dated samples of identified mafic rocks were filtered from the larger Andean igneous data set. These included basalt, basaltic andesite, diabase, and gabbros as well as more generally defined mafic and basic rock types. Identifications appear to extend from field examination to thin section analysis in the original publications. (Modal analyses based on geochemistry of dated samples are not as common, and, therefore, are not incorporated.)
Figure 18a illustrates the mafic samples, binned into segments of 1° of arc from the trench (measured along parallels). Adjacent segments are shown in Figure 18b-f along with modeled JF and EN hotspot traces, using the older reconstruction model (and rotation of northern samples) as described above.
Note that the modeled traces serve as incomplete envelopes bracketing magmatic episodes older and younger than the traces at each latitudinal point. On the older side, the JF trace bounds mafic samples which progress from west to east and north (~12° S) to south (35° S), terminating from ~80 Ma to the

present. In some cases, the mafic magmatic episodes appear to expire several million years prior to the calculated intersection of the trace. On the younger side, the JF trace bounds the onset of mafic magmatism, particularly farther east from the trench, from 50 Ma at 15 S° to the Present at 28° S. This pattern appears to be more obvious than within the total data set from 0-80 Ma, although the interpreted larger data distribution relative to the modeled traces is consistent with the more obvious pattern in the mafic dates. The mafic data from the northern Andes is consistent with the location of the EN trace intersections recognized in the larger data set, without obvious trends in inception and cessation of mafic magmatism.

The mafic dates are more clearly consistent with JF interaction as modeled by the reconstructions, strengthening the inference as applied to the larger data set. The larger as well as the smaller mafic data sets are also consistent with interaction of the EN trace with the Andean subduction zone. Further, simple comparison of loci calculated in the other hotspot reference frames indicates a “best fit” of the extended, older GGW22 model.

13. Conceptual Implications: Gap and Delamination?

If one tentatively accepts the possible correlation of the intersection of the Juan Fernandez hotspot trace with the Andean subduction zone and onset of increased magmatism shortly after, the question naturally arises: what is the mechanism for apparent increased melting of source material in relation to the trace? This scenario is envisioned: (1) Normal subduction of the Farallon plate is accompanied by modest magmatism along the Andean crest, as a result of the encounter of the top of the oceanic plate with the asthenosphere beneath the South American plate. (2) At a particular latitude along the trench the hotspot trace begins to be subducted; when the top of the thickened oceanic plate reaches ~100 km in depth, the lower net density of the subducting plate begins moving horizontally, cutting off melting and therefore the supply of magma, resulting in gradual cessation of volcanism. (3) Eventually the oceanic crust of the hotspot trace experiences the phase change from basalt/gabbro to denser eclogite and begins to sink at a steeper angle, coming into contact with the asthenosphere at a larger distance from the trench, with minor magmatism resulting. (4) While subduction is nearly east-west, the orientation of the subducting trace results in migration of the intersection with the trench from north to south. Each intersection point experiences a short period of low-angle subduction of the trace, followed by resumption of subduction of normal oceanic plate. (4) As the last part of the trace reaches a depth of ~100 km and moves horizontally, the normal oceanic plate detaches from the thicker part and begins to sink at a steeper angle. (5) The remaining part of the trace continues to move to the east, resulting in a gap emerging between the trace and the detached, now normally subducting plate. As a consequence, asthenospheric mantle begins to fill in the gap. As a consequence, a rapidly widening flare of magmatism begins behind the horizontally moving plate.

The contemplated gap may be associated with inferred delamination of the South American plate (e.g., Kay et al., 1994, Risse et al., 2013) beginning beneath the Central Andes of Bolivia and northern Chile and Argentina (Kay et al., 2019) and extending to just north of the contemporary low-angle subduction segment beneath Chile and Argentina (Mulcahy et al., 2014).

The proposed gap between the subducting hotspot trace fragment and reinstituted normally subducting oceanic plate is geometrically comparable to, if signficantly smaller than, the conjectured window in the Southern Andes between the subducted of the Nazca- (West) Antarctic spreading center and the remnant of the subducting Nazca plate (Cande and Leslie, 1986; and, e.g., Navarette et al., 2020) Only minor subduction of the West Antarctic plate, if any, follows the cessation of spreading.

Thus, the subducting JF trace, while producing only a short hiatus in magmatism as it obliquely subducts, is followed by a flare of magmatism. The hiatus is almost unobservable in the total data set, but more

apparent in the smaller mafic data set, because of the remnant of magmatic activity from the prior episode of normal subduction and the following flare.. The apparent intensification of magmatism following the oblique trace subduction may represent decompression melting of hotter and/or more fertile asthenosphere previously beneath the thickened subducting plate and under the accompanying delaminatiing upper plate, The zone of concentrated mafic dates at 27-28ºS from ~13 Ma to the Present is approximately located above the inferred gap between moderate and low-angle subduction. Perhaps the gap is responsible for the enhanced mafic magmatism in this locale as well as the inferred delamination at an earlier time, farther north.

14. Hotspots and Reference Frames

While the primary focus of this investigation has been on the magmatic evolution of the Andes in relation to subduction of inferred hotspot traces, the implications of the recognition of additional evidence for the subduction effect for the nature of hotspots themselves is worthy of further consideration. The evidence for the trace effect on subduction in the context of the Pacific hotspot reference frame and distinct from an Atlantic-Indian Ocean reference frame prompts questions about the reference frames themselves. That the motions of the plates relative to hotspots of the two domains apparently incompatible with one another was recognized already in the 1980s by the work of Molnar and colleagues (e.g., Molnar and Atwater, 1973; Molnar and Francheteau, ….). Resolution of the inconsistency b,etween the Pacific and Atlantic/indian Ocean domains would require detection of a yet unrecognized plate boundary between the central South Pacific and the Indian Ocean, most likely within the Antarctic plate. Cenozoic movement between East and West Antarctic within the Cenozoic has indeed been documented, but the detected displacement (Cande and Stock, 2000; Granot et al., 2013; Granot and Dyment, 2018).is inadequate relative to the discrepancy between the two hotspot frames The idea of a “moving hotspot” reference frame (O’Neill et al., 2005) presents other difficulties, however. Each hotspot within the Atlantic and Indian Ocean domain is assumed to move semi-independently from one another, in effect displaced by a kind of mantle wind. Modeling of whole earth convection with embedded hotspots is the mechanism assigned to such movement; however, the scheme suffers from several defects. Most importantly, it is profoundly underdetermined; perturbations of convection are performed so as to fit each of a small number of hotspot traces, constrained by gross mantle structure (seismic velocity with inferred density and viscosity), plate boundaries and kinematics. Parameters describing hotspot motion, conventional pole latitude and longitude and rotation angle relative to either the global frame or one of the continental plates (usually Africa) are difficult to rationalize; they may describe an individual hotspot’s motion relative to a particular frame, but how are such parameters interpolated? That is, the approach does not provide a means of estimating the motion of other hotspots which are not part of the framework; the application of M19, above, to the JF trace, illustrates the problem. Does a global convection model fit the hotspots of the Pacific? Oddly, as Gaastra et al. (2022) show, a single hotspot reference frame appears to provide a satisfactory reference frame for the hotspots of the Pacific plate; extrapolated to the Nazca plate, it also appears to fit the Andean “images” of subducted hotspot traces, with slight adjustments to the age progression.

What are the implications of the observation that (1) a single reference frame beneath the Pacific Ocean appears to have existed for at least 80 m.y. and (2) an inferred hotspot reference frame beneath the Indian and Atlantic Oceans fits volcanic patterns in northeast Africa for 60 m.y. and a Caribbean island arc for 70 Ma? Further, (3) the motion of the Pacific plate in the Hawaiian hotspot frame also fits the orientation of lineations in the observed gravity field (Haxby and Weissel, 1986), structures that have a shallow origin? This implies that the hotspot reference frames are shallow – not manifestations of the location of deep mantle plumes.

15. Conclusion

This short contribution is built upon an enormous amount of data produced by many workers: field observation, petrographic, geochemical and isotopic laboratory analysis, shipboard magnetic and bathymetric profiling, aeromagnetic surveying, satellite navigation and geoid observation with gravity extraction and bathymetric estimation, magnetic isochron modeling and identification, fracture zone characterization, marine dredging and drilling, plate pair reconstruction, data compilation... Much finer analysis of the isotopic date distribution and the plate reconstructions could be undertaken, especially incorporating more detailed petrology and geochemistry. The relationship to the deformation and uplift history of the Andes since 80 Ma is not explored in this study, other than the observation that late Cenozoic faulting in the Pampean Ranges of northern Argentina occurs within the low-angle subduction segment in which the reconstructions imply subduction of the Juan Fernandez trace for over 10 m.y., implying a genetic relationship (originally recognized by Pilger, 1981). Further, the reconstructions that indicate apparent subduction of the older parts of the JF trace between 60 and 45 Ma beneath northernmost Chile and Argentina, southernmost Peru, and Bolivia may indicate contribution of the trace to the intense deformation that produced the so-called Andean Orocline (Isacks, 1987) and its associated structures.

It is apparent that the two reconstructed hotspot traces compared with seismicity, bathymetry, and igneous isotopic ages, imply controlling influences on the angle of dip of the Andean subduction zone and consequent location of volcanic loci by the traces. The Easter-Nazca trace-igneous date correspondence is clearer than the Juan Fernandez trace, perhaps indicative of the significantly larger dimensions of the Nazca Ridge than the Juan Fernandez trace, with a larger, more persistent low-angle subduction effect. Pilger (1981) had suggested that the “mirror-image” of the Nazca Ridge on the Pacific plate might have contributed further to the extent of the low-angle subduction segment, a suggestion other workers have subsequently made (It is difficult to point to any other independent evidence in support of this auxiliary proposal).

The reconstructions and corresponding patterns of magmatism in the Andes provide indirect support of the hypothesis that the hotspots of the Pacific Ocean form a stable self-consistent reference frame extending beyond the limits of the Pacific plate. That is, the combined and modified model of Gaafstra et al. (2022) and Wessel and Kroenke (2008) extended to the Nazca and South American plates not only fits the observed parts of the Easter-Nazca and Juan Fernandez island-seamount-ridges, but also the distribution of magmatic activity in the central and northern Andes for the past 65-70 m.y.

It is difficult to recognize obvious relations of convergence rate and magmatism in the Andes from the reconstructions and age distribution of igneous isotopic dates. Similarly, the relation of motion of South America to the hotspots beneath the Atlantic and Indian Oceans and any possible control on Andean magmatism has been proposed by numerous authors. The most recent models for these hotspots imply motion relative to one another as well as those of the Pacific set (e.g., Müller et al., 2019, and references therein). Consequently, it is uncertain how to extend the model to the South American plate for testing beyond the simple examples presented above.

Subduction of very young plate and the actual spreading center appears to be manifest in the igneous history of the southern Andes as Cande and Leslie (1986) first recognized. Patterns of igneous activity appear to correspond closely with reconstructed isochrons. This correspondence provides additional confidence in the robustness of the global plate reconstructions for at least the last 40-50 m.y.

That the Juan Fernandez and Hawaiian hotspot traces, along with the other traces of the Pacific and Nazca plates can be characterized by an internally consistent reference frame is an additional striking result of this study. While the propagation of uncertainties in the reconstructions is not possible using contemporary formulations and existing isochron identifications and their derivative reconstruction parameters, the visual correspondences with Andean igneous dates should motivate higher resolution magnetic and bathymetric surveys of the older parts of the SA-AF and AF-EA systems and especially the PA-NF and WA-NF systems for the full time period since Chron 34. The PA-NF pair, with the highest average spreading rates in the full circuit, is an especially desirable target for near-future surveys; one might expect to find evidence of multiple small plates, like the present-day Easter plate (e.g., Handschumacher et al., 1981; Naar and Hey, 1991) which only high resolution surveys could resolve. Could semi-autonomous, solar-powered drones, with satellite GPS, three-component magnetometers and laser ranging, and intermittent satellite connection for data uploads provide a relatively economical fleet for aeromagnetic surveys of the remote regions of the South Pacific and southwest Indian Oceans most lacking in data? The correspondences demonstrated in this work may motivate the additional proposed study, especially in relation to continued mineral exploration and development, geothermal prospecting for electrical energy generation, geological hazards related to contemporary volcanism, uplift, and hydrothermal activity, and enhanced geoclimatic history in and of Andes. Such improved understanding may provide useful analogs for studies of other subduction-related mountain melts. .

Figure 19 illustrates the reconstructed Juan Fernandez trace, based on GGW22, assuming 50 Ma Hawaiian-Emperor bend and 85 Ma for older end, and extended to the Nazca plate, in turn reconstructed relative to a fixed South American plate at 1 m.y. increments. This figure provides a basis for further consideration of possible controls by subduction of the trace on the uplift, magmatic and tectonic evolution of the central Andes in the Late Cenozoic.

Supplementary Data

The compilation of isotopic dates from igneous rocks has been archived by GEOROC. Spreadsheets and keyhole markup language (kml, kmz) files include the charts, reconstruction parameters, and map data sets.

Acknowledgements

The research made use of the following software: Microsoft Office, Visual Studio, Google Earth, Google Sheets, Google Docs.

References

Arriagada, César, Ferrando, Rodolfo, Córdova, Loreto, Morata, Diego, Roperch, Pierrick, 2013, The Maipo Orocline: A first scale structural feature in the Miocene to Recent geodynamic evolution in the central Chilean Andes, Andean Geology 40, 419-437, doi: 10.5027/andgeoV40n3-a02.

Atwater, T. and Molnar, P., 1973, Relative motion of the Pacific and North American plates deduced from sea-floor spreading in the Atlantic, Indian, and South Pacific Oceans, Proc. Conf. on Tectonic Problems of the San Andreas Fault System, Geological Sciences XIII, School of Earth Sciences, Stanford Univ. Publications, 136-148.

Barazangi, M., and Isacks, B., 1976. Spatial distribution of earthquakes and subduction of the Nazca plate beneath South America, *Geology*, 4, 686–692.

Barazangi, Muawia, and Isacks, Bryan L., 1979, Subduction of the Nazca plate beneath Peru: evidence from spatial distribution of earthquakes, Geophysical Journal International, 57, 537–555, https://doi.org/10.1111/j.1365-246X.1979.tb06778.x.

Bello-González, Juan Pablo, Contreras-Reyes, Eduardo, Arriagada, César, 2018, Predicted path for hotspot tracks off South America since Paleocene times: Tectonic implications of ridge-trench collision along the Andean margin, Gondwana Research, 64, 216-234, DOI: 10.1016/j.gr.2018.07.008

Bernard, A., Munschy, M., Rotstein, Y. and Sauter, D. (2005), Refined spreading history at the Southwest Indian Ridge for the last 96 Ma, with the aid of satellite gravity data. Geophysical Journal International, 162: 765-778. https://doi.org/10.1111/j.1365-246X.2005.02672.x

Cande, Steven C.,1985, Nazca-South America plate interactions since 50 M.Y.B.P., Ocean Margin Drilling Program, Regional Atlas Series, Peru-Chile Trench Off Peru, Atlas 9, Hussong, D. M., Dang, S. P., Kulm, L, D., Couch, R. W., and Hilde, T. W. C., Editors.

Cande, Steven C., Leslie, Rob B., 1986, Late Cenozoic tectonics of the Southern Chile Trench, Journal of Geophysical Research: Solid Earth, 91, 471-496, https://doi.org/10.1029/JB091iB01p00471 .

Cande, S. C., Kent, D. V., 1995, Revised calibration of the geomagnetic polarity timescale for the Late Cretaceous and Cenozoic, Journal of Geophysical Research: Solid Earth, 100, 6093-6095, DOI:10.1029/94JB03098

Cande, S. C., C. A. Raymond, J. Stock, and W. F. Haxby, 1995, Geophysics of the Pitman fracture zone and Pacific-Antarctic plate motions during the Cenozoic, Science, 270, 947-953

Cande, S. C., J. M. Stock, R. D. Müller, and T. Ishihara, 2000, Cenozoic motion between East and West Antarctica, Nature, 404, 145-150.

Cande, Steven C., and Stock, Joann M., 2004, Pacific–Antarctic–Australia motion and the formation of the Macquarie Plate, Geophysical Journal International, 157, 399–414 doi: 10.1111/j.1365-246X.2004.02224.x

Cande, S. C., P. Patriat, and J. Dyment, 2010, Motion between the Indian, Antarctic and African plates in the early Cenozoic, Geophysical Journal International, 183, 127-149.

Cande, Steven C., and Patriat, Philippe, 2015, The anticorrelated velocities of Africa and India in the Late Cretaceous and early Cenozoic, Geophysical Journal International, 200, 227–243.

Clague, David A., and Jarrard, Richard D. 1973, Tertiary Pacific Plate Motion Deduced from the Hawaiian-Emperor Chain, Geological Society of America Bulletin, 84, 1135–1154 https://doi.org/10.1130/0016-7606(1973)84<1135:TPPMDF>2.0.CO;2

Clennett, E. J., Sigloch, K., Mihalynuk, M. G., Seton, M., Henderson, M. A., Hosseini, K., et al. (2020). A quantitative tomotectonic plate reconstruction of western North America and the eastern Pacific basin. Geochemistry, Geophysics, Geosystems 20, e2020GC009117 https://doi.org/10.1029/2020GC009117

Coira, B., Kay, S.M., and Viramonte, J., 1993, Upper Cenozoic magmatic evolution of the Argentine Puna—A model for changing subduction geometry: International Geology Review, v. 35, p. 677–720.

Croon, M. B., S. C. Cande, and J. M. Stock (2008), Revised Pacific-Antarctic plate motions and geophysics of the Menard Fracture Zone, Geochemistry, Geophysics, Geosystems, 9, 7.

Cross, T. A., and Pilger, R. H., Jr., 1978a, Constraints on absolute motion and plate interactions inferred from Cenozoic igneous activity in the western United States, American Journal of Science, 278, 865-902.

Cross, T. A., and Pilger, R. H., Jr., 1978b, Tectonic controls of Late Cretaceous sedimentation, western interior, U.S.A., Nature, 274, 653-657.

Cross, Timothy, Pilger, Rex, 1982, Controls of subduction geometry, location of magmatic arcs, and tectonics of arc and back-arc regions, Geological Society of America Bulletin 93, 545–562, DOI: 10.1130/0016-7606(1982)93<545:COSGLO>2.0.CO;2

Dalrymple, G.B., and Clague, D.A., 1976, Age of the Hawaiian Emperor bend: Earth and Planetary Science Letters, v. 31, p. 313-329, doi: 10.1016/0012- 821X(76)90113-8.

DeMets, C., Gordon, R.G., Argus, D.F., and Stein, S., 1990. Current plate motions. Geophysical Journal International 101(2), 425–78.

DeMets, C., Gordon, R.G., Argus, D.F., and Stein, S., 1994, Effect of recent revisions to the geomagnetic reversal time scale on estimates of current plate motions: Geophysical Research Letters, v. 21, no. 20, p. 2191-2194, doi: 10.1029/94GL02118.

DeMets, C., Gordon, R.G., Argus, D.F., 2010, Geologically current plate motions, .Geophysical Journal International, 181, 1–80, doi: 10.1111/j.1365-246X.2009.04491.x

DeMets, C., Merkouriev, S., and Sauter, D., 2015, High-resolution estimates of Southwest Indian Ridge plate motions, 20 Ma to present, Geophysical Journal International, 203, 1495–1527 doi: 10.1093/gji/ggv366

DeMets, C., & Merkouriev, S., 2019,. High-resolution reconstructions of Nubia, North America, and Antarctic plate motions relative to South America: 34 Ma to present. Geophysical Journal International, 217(3), 1821–1853. https://doi.org/10.1093/gji/ggz087

Doubrovine, P. V., Steinberger, B., and Torsvik, T. H., 2012, Absolute plate motions in a reference frame defined by moving hot spots in the Pacific, Atlantic, and Indian oceans, Journal of Geophysical Research, 117, B09101, doi:10.1029/2011JB009072.

Dupont-Nivet, G., Roperch, P., Gautier, P., Chauvin, A., Gerard, M., and Carlier, G., 1996, Clockwise rotations in northern Chile: oroclinal bending and in situ tectonic rotations, Third ISA, St. Malo, France, 355-358.

Eagles, Graeme, Gohl, Karsten, Larter, Robert D., 2008, Animated tectonic reconstruction of the Southern Pacific and alkaline volcanism at its convergent margins since Eocene times Tectonophysics, 464, 21-29, https://doi.org/10.1016/j.tecto.2007.10.005

Eagles, Graeme, and Jokat, Wilfried, 2014, Tectonic reconstructions for paleobathymetry in Drake Passage, Tectonophysics 611, 28–50

Eagles, Graeme, and Vaughan, Alan P. M., 2009, Gondwana breakup and plate kinematics: Business as usual, Geophysical Research Letters, 36, L10302, doi:10.1029/2009GL037552.

Engebretson, D.C., Cox, A., and Gordon, R.G., 1985, Relative motions between oceanic and continental plates in the Pacific basin: Geological Society of America, Special Papers, v. 206, p. 1–60, http://dx.doi.org/10.1130/SPE206-p1.

Francheteau, Jean, 1970, Paleomagnetism and Plate Tectonics, PhD dissertation, University of California, San Diego.

Gaastra, Kevin Mitchell, Gordon, Richard G., Woodworth, Daniel, 2022?, Quantification of Pacific Plate Hotspot Tracks Since 80 Ma and the Relative Timing of Eocene Plate Tectonic Events, submitted to Tectonics, https://doi.org/10.1002/essoar.10506394.2

Gaina, C., Müller, D. R., Royer, J.-Y., Stock, J., Hardebeck, J., and Symonds, P. (1998), The tectonic history of the Tasman Sea: A puzzle with 13 pieces, J. Geophys. Res., 103(B6), 12413– 12433, doi:10.1029/98JB00386.

Gradstein, F. M., and Ogg, J. G., 2020, The chronostratigraphic scale, Geologic Time Scale, 2020, Gradstein, F. M., Ogg, J. G., Schmitz, M. D., Ogg, G. M., editors, Elsevier, Amsterdam, 1, 21-32.

Granot, R., Cande, S. C., Stock, J. M., and Damaske, D., 2013, Revised Eocene-Oligocene kinematics for the West Antarctic rift system, Geophysical Research Letters, 40, 279–284, doi:10.1029/2012GL054181,

Granot, R., Dyment, J. Late Cenozoic unification of East and West Antarctica. *Nat Commun* 9, 3189 (2018). https://doi.org/10.1038/s41467-018-05270-w

Hamilton, W., 1969, The volcanic Central Andes: A modern model for the Cretaceous batholiths and tectonics of western North America, Oregon Department of Mineral Industries Bulletin, 655, 175-1984.

Handschumacher, D.W., 1976, Post-Eocene plate tectonics of the Eastern Pacific, in The Geophysics of the Pacific Ocean Basin and its Margins, in The Geophysics of the Pacific Ocean Basin and its Margins, AGU Monograph 19, ed.G.H.Sutton, et al., Washington: AGU, pp. 177-202.

Harada, Y., and Hamano, Y., 2000, Recent progress on plate motions relative to hot spots, in The History and Dynamics of Global Plate Motions, Geophysical Monograph Series, 121, edited by Richards, M. A., Gordon, R. G., and van der Hilst, R. D., 327–338, AGU, Washington, D. C.

Haxby, W.F. and Weissel, J.K. (1986). Evidence for small-scale mantle convection from Seasat altimeter data. Journal of Geophysical Research 91: doi: 10.1029/JB091iB03p03507. issn: 0148-0227.

Hayes, G. P., Moore, G. L., Portner, D. E., Hearne, M., Flamme, H., Furtney, M., and Smocsyk, G. M., 2018, Slab2, a comprehensive subduction zone geometry model, Science, 362, 48-61. https://doi.org/10.1126/science.aat4723

Herron, E. M. (1972), Sea-floor spreading and the Cenozoic history of the east-central Pacific, Geological Society of America Bulletin, 83, 1671-1692.

Isacks, Bryan L., 1988, Uplift of the Central Andean Plateau and Bending of the Bolivian Orocline, Journal of Geophysical Research: Solid Earth, 93, 3211-3231

Jarrard, R.D., and Clague, D.A., 1977, Implications of Pacific Island and seamount ages for the origin of volcanic chains, Reviews of Geophysics and Space Physics, 15, 57-76.

Kay, S. M., Coira, B., and Viramonte, J., 1994, Young mafic back arc volcanic rocks as indicators of continental lithospheric delamination beneath the Argentine Puna Plateau, central Andes, J. Geophys. Res., 99(B12), 24323– 24339, doi:10.1029/94JB00896.

Kay, S. M. & Abbruzzi, J. M., 1996, Magmatic evidence for Neogene lithospheric evolution of the Central Andean flat-slab between 30 and 32°S, Tectonophysics 259, 15–28.

Kay, Suzanne M., Kato, Joseph J., Coira, Beatriz L., Jimenez, N., 2018, Isotopic and Geochemical Signals of the Neogene Los Frailes Volcanic Complex as Recorders of Delamination and Lower Crustal Flow under the Southern Altiplano of the Central Andes, South American symposium on isotope geology, 11th SSAGI, Cochabamba, Bolivia, 22-25 July.

Kirkwood, B. H., J. Y. Royer, T. C. Chang, and R. G. Gordon (1999), Statistical tools for estimating and combining finite rotations and their uncertainties, *Geophysical Journal International,* 137(2), 408– 428.

König, Matthias, Jokat, Wilfried, 2010, Advanced insights into magmatism and volcanism of the Mozambique Ridge and Mozambique Basin in the view of new potential field data, Geophysical Journal International 180(1):158 - 180 DOI: 10.1111/j.1365-246X.2009.04433.x

Larter, Robert D., Cunningham, A. P., Barker, P. F., Gohl, K., Nitsche, F. O., 2002, Tectonic evolution of the Pacific margin of Antarctica 1. Late Cretaceous tectonic reconstructions, Journal of Geophysical Research-Solid Earth 107, 2345.

Le Pichon, X., Francheteau, J., & Bonnin, J. (1973). Plate Tectonics. *Elsevier*, 1973.

Livermore, Roy, Nankivell, Adrian, Eagles, Graeme, Morris, Peter, 2005 Paleogene opening of Drake Passage, Earth and Planetary Science Letters 236 (2005) 459 – 470

Lonsdale, P., 2005, Creation of the Cocos and Nazca plates by fission of the Farallon plate, Tectonophysics, 404, 237-264

Maia, Marcia, Dyment, Jérôme, Jouannetaud, David, 2005, Constraints on age and construction process of the Foundation chain submarine volcanoes from magnetic modeling, Earth and Planetary Science Letters, Volume 235, 183-199, https://doi.org/10.1016/j.epsl.2005.02.044.

Marks, K., Stock, J. Evolution of the Malvinas Plate South of Africa. Marine Geophysical Researches 22, 289–302 (2001). https://doi.org/10.1023/A:1014638325616

Matthews, K. J., Williams, S. E., Whittaker, J. M., Müller, R. D., Seton, M., & Clarke, G. L. (2015). Geologic and kinematic constraints on Late Cretaceous to mid Eocene plate boundaries in the southwest Pacific. Earth-Science Reviews, 140, 72–107. https://doi.org/10.1016/j. Earscirev.2014.10.008

Morgan, W.J., 1971, Convection plumes in the lower mantle: Nature, v. 230, p. 42-43.

Morgan, W.J., 1972, Plate motions and deep mantle convection: Boulder, Colorado, Geological Society of America Memoir 132, p. 7-22.

Mulcahy,P., C.Chen, S.M.Kay, L. D. Brown, B. L. Isacks, E. Sandvol, B.Heit, X.Yuan,and B.L.Coira (2014),Central Andean mantle and crustal seismicity beneath the Southern Punaplateau and the northern margin of the Chilean-Pampean flat slab, Tectonics, 33, 1636–1658, doi:10.1002/2013TC003393.

Müller, R.D., Royer, J.-Y. & Lawver, L. A., 1993, Revised plate motions relative to the hotspots from combined Atlantic and Indian Ocean hotspot tracks. Geology 21, 275–278.

Müller, R.D., Cande, S.C., Royer, J.-Y., Roest, W.R., Maschenkov, S., 1999. New constraints on the Late Cretaceous/Tertiary plate tectonic evolution of the Caribbean. In: Mann,

Müller, R. Dietmar, Roest, Walter R., Royer, Jean-Yves, Gahagan, Lisa M., Sclater, John G., 1997, Digital isochrons of the world's ocean floor, Journal of Geophysical Research, 102, 3211-3214

Müller, R. D., Sdrolias, M., Gaina, C., and Roest, W. R. (2008), Age, spreading rates, and spreading asymmetry of the world's ocean crust, Geochemistry, Geophysics, Geosystems, 9, Q04006, doi:10.1029/2007GC001743.

Müller, R. D., Zahirovic, S., Williams, S. E., Cannon, J., Seton, M., Bower, D. J., Tetley, Michael G., Heine, Christian, Le Breton, Eline, Liu, Shaofeng, Russell, Samuel H. J., Yang, Ting, Leonard, Jonathon, and Gurnis, Michael, 2019, A global plate model including lithospheric deformation along major rifts andorogens since the Triassic, Tectonics, 38,1884–1907. https://doi.org/10.1029/2018TC005462

Naar, D. F., and Hey, R. N., 1991, Tectonic evolution of the Easter Microplate, J. Geophys. Res., 96, 7961 – 7993.

Nankivell A.P., 1997. Tectonic evolution of the southern ocean between Antarctica, South America and Africa over the last 84 Ma, *PhD thesis* , Univ. of Oxford, Oxford, p. 303.

Navarrete, César, Gianni, Guido, Massaferro, Gabriela, Butler, Kristina, 2020, The fate of the Farallon slab beneath Patagonia and its links to Cenozoic intraplate magmatism, marine transgressions and topographic uplift, Earth-Science Reviews, 210, 103379, https://doi.org/10.1016/j.earscirev.2020.103379

Norton, I.O., 1995: Plate motions in the North Pacific: the 43 Ma non-event. Tectonics, 14, 1080-1094.

Norton, I. O., 2000, Global hotspot reference frames and plate motion, in Richards, M.A., Gordon, R. G., and van der Hilst, R. D., eds., The History and Dynamics of Global Plate Motions: American Geophysical Geophysical Monograph, 121, 339–357.

Nürnberg, D., Müller, R. D., The tectonic evolution of the South Atlantic from Late Jurassic to present, Tectonophysics 191, 27 (1991).

O'Connor, J. M., Stoffers, P. & McWilliams, M. O., 1995, Time-space mapping of Easter Chain volcanism. Earth and Planetary Science Letters, 136, 197-212

O'Connor, John M., Steinberger, Bernhard, Koppers, Anthony A. P., Wijbrans, Jan R., Haase, Karsten M., Stoffers, Peter, Jokat, Wilfried, and Garbe-Schönberg, Dieter, 2013, Constraints on past plate and mantle motion from new ages for the Hawaiian-Emperor Seamount Chain, Geochemistry, Geophysics, Geosystems, 14, doi:10.1002/ggge.20267

Ogg, J. G., 2020, Geomagnetic Polarity Time Scale, in Geologic Time Scale, 2020, Gradstein, F. M., Ogg, J. G., Schmitz, M. D., Ogg, G. M., editors, Elsevier, Amsterdam, 1, 159-192.

O'Neill, Craig, Müller, R. Dietmar, Steinberger, Bernhard, 2005, On the uncertainties in hot spot reconstructions and the significance of moving hot spot reference frames, Geochemistry-Geophysics-Geosystems, Volume 6, Number 4, Q04003, doi:10.1029/2004GC000784

Pardo Casas, Frederico, and Molnar, Peter, 1987, Relative motion of the Nazca (Farallon) and South American Plates since Late Cretaceous time, Tectonics 6, 233-248.

Pérez-Díaz, L., and G. Eagles, 2014, Constraining South Atlantic growth with seafloor spreading data, Tectonics,33, 1848–1873, doi:10.1002/2014TC003644

Pilger, Rex H., Jr., 1978, A method for finite plate reconstructions, with applications to Pacific-Nazca Plate evolution, Geophysical Research Letters, 5, 469-472, https://doi.org/10.1029/GL005i006p00469.

Pilger, Rex H., Jr., and Henyey, T., 1979, Pacific-North American plate interaction and Neogene volcanism in coastal California, Tectonophysics, 57, 189-209, DOI: 10.1016/0040-1951(79)90148-3

Pilger, Rex H., Jr., 1981a, Plate reconstructions, aseismic ridges, and low-angle subduction beneath the Andes, Geological Society of America Bulletin, 92, 448–456, https://doi.org/10.1130/0016-7606(1981)92<448:PRARAL>2.0.CO;2

Pilger, Rex H., Jr., and Handschumacher, David, 1981, The fixed-hotspot hypothesis and origin of the Easter—Sala y Gomez—Nazca trace, Geological Society of America Bulletin, 92, 437–446. https://doi.org/10.1130/0016-7606(1981)92<437:TFHAOO>2.0.CO;2

Pilger, Rex H., Jr., 1981b, Interpolation of plate reconstructions using cubic splines: a means of estimating instantaneous kinematics, AGU Annual Meeting, San Francisco, CA, USA, EOS Transactions, American Geophysical Union, 62, 45, November 10, TE-1-A-1.

Pilger, Rex H., Jr., 1983, Kinematics of the South American subduction zone from global plate reconstructions, In Geodynamics of the Eastern Pacific Region, Caribbean and Scotia Arcs Geodynamics of the Eastern Pacific Region, Caribbean and Scotia Arcs, 9, Editor: Cabré , Ramón, S.J., https://doi.org/10.1029/GD009p0113

Pilger, Rex H., Jr.,1984 Cenozoic plate kinematics, subduction and magmatism: South American Andes, Journal of the Geological Society, 141(5):793-802, DOI: 10.1144/gsjgs.141.5.0793

Pilger, Rex H., Jr., 2003, Geokinematics, Prelude to Geodynamics, Springer, New York, DOI:10.1007/978-3-662-07439-8, ISBN: 978-3-642-05608-6

Pilger, Rex H., Jr., 2007, The Bend: Origin and significance, Geological Society of America Bulletin, 119, DOI 10.1130/B25713.1

Pilger, Rex H., Jr., 2012, Fractal plate reconstructions with spreading asymmetry, Marine Geophysical Research, 33, DOI: 10.1007/s11001-012-9152-6

Pindell, J., and Kennan, L., 2001, Kinematic evolution of the Gulf of Mexico and Caribbean, Transactions, Gulf Coast Association of Geological Societies.

Pitman, Walter C., and Talwani, Manik, 1972, Sea-Floor Spreading in the North Atlantic, Geological Society of America Bulletin, 83, 619–646, https://doi.org/10.1130/0016-7606(1972)83[619:SSITNA]2.0.CO;2

Press, William H., Teukolsky, Saul A., Vetterling, William T., Flannery, Brian P., 1992, Numerical Recipes in C - The Art of Scientific Computing, Second Edition, Cambridge University Press, Cambridge, UK, 994 p.

Puigdomenech, C., Alarcón, S., Ruiz González, V., Rossel, P., Orts, D., Zaffarana, C., 2021, Tectonic rotations in central Chile: New insights on the southern limit of the Maipo Orocline, Journal of South American Earth Sciences, 106, doi.org/10.1016/j.jsames.2020.103012

Ramos, 1999, Victor A., Plate tectonic setting of the Andean Cordillera, Episodes, 22, 183-190.

Ramos, V. A., Cristallini, E. O. & Pérez, D.J 2002. The Pampean flat-slab of the Central Andes. Journal of South American Earth Sciences 15(1), 59–78.

Ray, Jyotiranjan S., Mahoney, John J., Duncan, Robert A., Ray, Jyotisankar, Wessel, Paul, Naar, David F., 2012, Chronology and Geochemistry of Lavas from the Nazca Ridge and Easter Seamount Chain: an ~30 Myr Hotspot Record , Journal of Petrology, 53, 1417–1448, https://doi.org/10.1093/petrology/egs021

Raymond, C.A., Stock, J.M., and Cande, S.C., 2000, Fast Paleogene motion of the Pacific hotspots from revised global plate circuit constraints, in Richards, M.A., Gordon, R.G., and van der Hilst, R.D., editors, History and Dynamics of Plate Motions, AGU Geophysical Monograph, 121, 359-375.

Risse, A., Trumbull, R. B., Kay, S. M., Coira, B., Romer, R. L., 2013, Multi-stage Evolution of Late Neogene Mantle-derived Magmas from the Central Andes Back-arc in the Southern Puna Plateau of Argentina, Journal of Petrology, 54, 1963–1995, https://doi.org/10.1093/petrology/egt038

Rousse, Sonia, Gilder, Stuart, Farber, Daniel, McNulty, Brendan, Patriat, Philippe, Torres, Victorr, and Sempere, Thierry, 2003, Paleomagnetic tracking of mountain building in the peruvian andes since 10 Ma, Tectonics, 22, 1048.

Royer, J. and Chang, T., 1991, Evidence for relative motions between the Indian and Australian Plates during the last 20 m.y. From plate tectonic reconstructions: Implication for the deformation of the Indo-Australian plate. Journal of Geophysical Research 96: doi: 10.1029/91JB00897. issn: 0148-0227.

Schellart, W. P., 2020, Control of subduction zone age and size on flat slab subduction, Frontiers in Earth Science, 8:26. doi: 10.3389/feart.2020.00026

Seton, M., Müller, R.D., Zahirovic, S., Gaina, C., Torsvik, T., Shephard, G., Talsma, A., Gurnis, M., Turner, Maus, S., Chandler, M., 2012, Global continental and ocean basin reconstructions since 200Ma, Earth-Science Reviews, 113, 212 - 270, https://doi.org/10.1016/j.earscirev.2012.03.002

Seton, M., J. Whittaker, P. Wessel, R. D. Müller, C. DeMets, S. Merkouriev, S. Cande, C. Gaina, G. Eagles, R. Granot, J. Stock, N. Wright, and S. Williams, 2014, Community infrastructure and repository for marine magnetic identifications, Geochemistry, Geophysics, Geosystems, 5, 1629-1641, doi:10.1002/2013GC005176

Royer J.Y. Chang T., 1991. Evidence for relative plate motions between the Indian and Australian plates during the last 20 m.y. from plate tectonic reconstructions: implications for the deformation of the Indo-Australian plate, *J. geophys. Res.*, 96, 11779–11802.

Royer, J.-Y., P. Patriat, H. Bergh, and C. R. Scotese, 1988, Evolution of the Southwest Indian Ridge from the Late Cretaceous (anomaly 34) to the middle Eocene (anomaly 20), Tectonophysics, 155, 235-260.

Sharp, W.D. and D.A. Clague, 2006, 50-Ma Initiation of Hawaiian-Emperor Bend Records Major Change in Pacific Plate Motion, Science, 313: 1281-1284

Shaw, P. and Cande, S., 1990, High-Resolution Inversion for South Atlantic Plate Kinematics Using Joint Altimeter and Magnetic Anomaly Data,J. Geophys. Res. 80, 4815–4822.

Somoza, Rubén, 2005, Cenozoic convergence in western South America: Subduction of the Nazca, Farallon, and Aluk plates, 6th International Symposium on Andean Geodynamics (ISAG 2005, Barcelona), Extended Abstracts: 681-684.

Somoza, Rubén, and Ghidella, M.E., 2005, Convergence in the western margin of South America during the Cenozoic: Subduction of Nazca, Farallon and Aluk plates, Revista de la Asociacion Geologica Argentina, 60(4):797-809, http://hdl.handle.net/20.500.12110/paper_00044822_v60_n4_p797_Somoza

Somoza, Rubén, and Ghidella, M.E., 2012, Late Cretaceous to recent plate motions in western South America revisited, Earth and Planetary Science Letters, 331-332 , pp. 152-163.

Tebbens, S. F., Cande, S. C., 1997, Southeast Pacific tectonic evolution from Early Oligocene to Present, Journal of Geophysical Research: Solid Earth, 102, 12061-12084.

Tetley, Michael G., Williams, S. E., Gurnis, Michael, Flament, Nicolas, Müller, R. D., 2019, Constraining Absolute Plate Motions Since the Triassic, Journal of Geophysical Research: Solid Earth, 124, https://doi.org/10.1029/2019JB017442

Torsvik, Trond H., Steinberger, Bernhard, Gurnis, Michael, Gaina, Carmen, 2010, Plate tectonics and net lithosphere rotation over the past 150My, Earth and Planetary Science Letters, 291, 106-112, https://doi.org/10.1016/j.epsl.2009.12.055.

.

Weissel, J. K. and D. E. Hayes, 1972, Magnetic anomalies in the Southeast Indian Ocean, in Antarctic Oceanology II: The Australian-New Zealand Sector, Antarctic Research Series, 19, edited by D.E. Hayes, pp. 165-196, AGU, Washington, D.C.

Wessel, P., and L. W. Kroenke, 2008, Pacific absolute plate motions since 145 Ma, Journal of Geophysical Research, 113, B06101, doi:10.1029/2007JB005499.

Whittaker, J. M., R. D. Müller, G., Leitchenkov, H. Stagg, M. Sdrolias, C. Gaina, and A. Goncharov, 2007, Major Australian-Antarctic plate reorganization at Hawaiian-Emperor bend time, Science, 318, 83–86, doi:10.1126/science.1143769.

Wilder, D. T. (2003), Relative motion history of the Pacific-Nazca (Farallon) plates since 30 million years ago, M.S. Thesis, U. S. Florida.

Williams, S. E., Whittaker, J. M., & Müller, R. D., 2011. Full-fit, palinspastic reconstruction of the conjugate Australian-Antarctic margins. Tectonics, 30, TC6012. https://doi.org/10.1029/2011TC002912

Wilson, J.T., 1963, A possible origin of the Hawaiian islands: Canadian Journal of Physics, v. 41, p. 863-870.

Wright, Nicky, Müller, Dietmar, Seton, Maria, and Williams, Simon, 2015, Revision of Paleogene plate motions in the Pacific and implications for the Hawaiian-Emperor bend, Geology, 43, 455-458, DOI: 10.1130/G36303.1.

Yáñez, G. A., Ranero, C. R., von Huene, R., and Díaz, J., 2001, Magnetic anomaly interpretation across the southern central Andes (32°–34°S): The role of the Juan Fernández Ridge in the late Tertiary evolution of the margin, J. Geophys. Res., 106(B4), 6325– 6345, doi:10.1029/2000JB900337.

Supplementary Table References

Andrews, D. L., R. G. Gordon, and B. C. Horner-Johnson, 2006, Uncertainties in plate reconstructions relative to the hot spots: Pacific-hot spot rotations and uncertainties for the past 68 million years, Geophys. J. Int., 166, 939–951, doi:10.1111/j.1365-246X.2006.03029.x.

Bernard, A., Munschy, M., Rotstein, Y. and Sauter, D., 2005, Refined spreading history at the Southwest Indian Ridge for the last 96 Ma, with the aid of satellite gravity data. Geophysical Journal International, 162: 765-778. https://doi.org/10.1111/j.1365-246X.2005.0267t2.x

Cande, S. C., and Kent, D. V., 1995, Revised calibration of the geomagnetic time scale for the Late Cretaceous and Cenozoic, Journal of Geophysical Research, v. 100, p. 6093-6095.

Cande, S. C., Kent, D. V., 1995, Revised calibration of the geomagnetic polarity timescale for the Late Cretaceous and Cenozoic, Journal of Geophysical Research: Solid Earth, 100, 6093-6095, DOI:10.1029/94JB03098

Cande, S. C., P. Patriat, and J. Dyment, 2010, Motion between the Indian, Antarctic and African plates in the early Cenozoic, Geophysical Journal International, 183, 127-149.

Cande, Steven C., and Patriat, Philippe, 2015, The anticorrelated velocities of Africa and India in the Late Cretaceous and early Cenozoic, Geophysical Journal International, 200, 227–243.

Cande, Steven C., and Stock, Joann M., 2004, Pacific–Antarctic–Australia motion and the formation of the Macquarie Plate, Geophysical Journal International, 157, 399–414 doi: 10.1111/j.1365-246X.2004.02224.x

Croon, M. B., S. C. Cande, and J. M. Stock, 2008, Revised Pacific-Antarctic plate motions and geophysics of the Menard Fracture Zone, Geochemistry, Geophysics, Geosystems, 9, 7.

DeMets, C., & Merkouriev, S., 2019. High-resolution reconstructions of Nubia, North America, and Antarctic plate motions relative to South America: 34 Ma to present. Geophysical Journal International, 217(3, 1821–1853. https://doi.org/10.1093/gji/ggz087

DeMets, C., & Merkouriev, S., 2019, High-resolution reconstructions of Nubia, North America, and Antarctic plate motions relative to South America: 34 Ma to present. Geophysical Journal International, 217(3, 1821–1853. https://doi.org/10.1093/gji/ggz087

DeMets, C., Gordon, R.G., Argus, D.F., 2010, Geologically current plate motions, Geophysical Journal International, 181, 1–80, doi: 10.1111/j.1365-246X.2009.04491.x

DeMets, C., Merkouriev, S., and Sauter, D., 2015, High-resolution estimates of Southwest Indian Ridge plate motions, 20 Ma to present, Geophysical Journal International, 203, 1495–1527 doi: 10.1093/gji/ggv366

Doubrovine, P. V., Steinberger, B., & Torsvik, T. H., 2012, Absolute plate motions in a reference frame defined by moving hot spots in the Pacific, Atlantic and Indian oceans. Journal of Geophysical Research, 117, B09101. https://doi.org/10.1029/2011JB009072

Eagles, Graeme, and Jokat, Wilfried, 2014, Tectonic reconstructions for paleobathymetry in Drake Passage, Tectonophysics 611, 28–50

Eagles, Graeme, and Vaughan, Alan P. M., 2009, Gondwana breakup and plate kinematics: Business as usual, Geophysical Research Letters, VOL. 36, L10302, doi:10.1029/2009GL037552, 2009

Eagles, Graeme, Gohl, Karsten, Larter, Robert D., 2008, Animated tectonic reconstruction of the Southern Pacific and alkaline volcanism at its convergent margins since Eocene times Tectonophysics, 464, 21-29, https://doi.org/10.1016/j.tecto.2007.10.005

Gaastra, Kevin Mitchell, Gordon, Richard G., Woodworth, Daniel, 2022?, Quantification of Pacific Plate Hotspot Tracks Since 80 Ma and the Relative Timing of Eocene Plate Tectonic Events, submitted to Tectonics, https://doi.org/10.1002/essoar.10506394.2

Gaina, C., Müller, D. R., Royer, J.-Y., Stock, J., Hardebeck, J., and Symonds, P., 1998, The tectonic history of the Tasman Sea: A puzzle with 13 pieces, Journal of Geophysical Research, 103(B6, 12413– 12433, doi:10.1029/98JB00386.

Granot, R., Dyment, J. Late Cenozoic unification of East and West Antarctica. Nature Communications, 9, 3189 (2018). https://doi.org/10.1038/s41467-018-05270-w

Granot, R., Cande, S. C., Stock, J. M., and Damaske, D., 2013, Revised Eocene-Oligocene kinematics for the West Antarctic rift system, Geophysical Research Letters, 40, 279–284, doi:10.1029/2012GL054181,

Harada, Y., and Y. Hamano (2000), Recent progress on plate motions relative to hot spots, in The History and Dynamics of Global Plate Motions, Geophys. Monogr. Ser., vol. 121, edited by M. A. Richards, R. G. Gordon, and R. D. van der Hilst, pp. 327–338, AGU, Washington, D. C.

Koivisto, E. A., Andrews, D. L. & Gordon, R. G., 2015, Tests of fixity of the Indo-Atlantic hot spots relative to Pacific hot spots. J. Geophys. Res. 119, 661–675.

Livermore, Roy, Nankivell, Adrian, Eagles, Graeme, Morris, Peter, 2005 Paleogene opening of Drake Passage, Earth and Planetary Science Letters 236, 2005, 459 – 470

Lonsdale, P., 2005, Creation of the Cocos and Nazca plates by fission of the Farallon plate, Tectonophysics, 404, 237-264

Marks, K., Stock, J., 2001, Evolution of the Malvinas Plate South of Africa, Marine Geophysical Researches, 22, 289–302. https://doi.org/10.1023/A:1014638325616

Matthews, K. J., Williams, S. E., Whittaker, J. M., Müller, R. D., Seton, M., & Clarke, G. L., 2015, Geologic and kinematic constraints on Late Cretaceous to mid Eocene plate boundaries in the southwest Pacific, Earth-Science Reviews, 140, 72–107. https://doi.org/10.1016/j. Earscirev.2014.10.008

Müller, R. D., Zahirovic, S., Williams, S. E., Cannon, J., Seton, M., Bower, D. J., Tetley, Michael G., Heine, Christian, Le Breton, Eline, Liu, Shaofeng, Russell, Samuel H. J., Yang, Ting, Leonard, Jonathon, and Gurnis, Michael, 2019, A global plate model including lithospheric deformation along major rifts andorogens since the Triassic, Tectonics, 38,1884–1907. https://doi.org/10.1029/2018TC005462

Müller, R.D., Royer, J.-Y. & Lawver, L. A., 1993, Revised plate motions relative to the hotspots from combined Atlantic and Indian Ocean hotspot tracks. Geology 21, 275–278.

Ogg, J. G., 2020, Geomagnetic Polarity Time Scale, in Geologic Time Scale, 2020, Gradstein, F. M., Ogg, J. G., Schmitz, M. D., Ogg, G. M., editors, Elsevier, Amsterdam, 1, 159-192.

Pérez-Díaz, L., and G. Eagles, 2014, Constraining South Atlantic growth with seafloor spreading data, Tectonics, 33, 1848–1873, doi:10.1002/2014TC003644

Raymond, C. A., J. M. Stock, and S. C. Cande (2000), Fast Paleogene motion of the Pacific hot spots from revised global plate circuit constraints, in The History and Dynamics of Global Plate Motion, Geophys. Monogr. Ser., vol. 121, edited by M. A. Richards et al., pp. 359–375, AGU, Washington, D. C.

Royer, J.Y., and Chang, T., 1991, Evidence for relative plate motions between the Indian and Australian plates during the last 20 m.y. from plate tectonic reconstructions: implications for the deformation of the Indo-Australian plate, Journal of Geophysical Research, 96, 11779–11802.

Royer, J.-Y., P. Patriat, H. Bergh, and C. R. Scotese, 1988, Evolution of the Southwest Indian Ridge from the Late Cretaceous, anomaly 34, to the middle Eocene, anomaly 20, Tectonophysics, 155, 235-260.

Seton, M., Whittaker, J., Wessel, P., Müller, R. D., DeMets, C., Merkouriev, S., Cande, S., Gaina, C., Eagles, G., Granot, R., Stock, J., Wright, N., and Williams, S., 2014, Community infrastructure and repository for marine magnetic identifications, Geochemistry, Geophysics, Geosystems, 5, 1629-1641, doi:10.1002/2013GC005176

Seton, M., Müller, R.D., Zahirovic, S., Gaina, C., Torsvik, T., Shephard, G., Talsma, A., Gurnis, M., Turner, Maus, S., Chandler, M., 2012, Global continental and ocean basin reconstructions since 200Ma, Earth-Science Reviews, 113, 212 - 270, https://doi.org/10.1016/j.earscirev.2012.03.002

Steinberger, B., and Torsvik, T. H., 2008, Absolute plate motions and true polar wander in the absence of hotspot tracks. Nature, 452(7187), 620–623. https://doi.org/10.1038/nature06824

Tebbens, S. F., Cande, S. C., 1997, Southeast Pacific tectonic evolution from Early Oligocene to Present, Journal of Geophysical Research, Solid Earth, 102, 12061-12084.

Torsvik, T. H., Müller, R. D., Van der Voo, R., Steinberger, B., & Gaina, C., 2008, Global plate motion frames: Toward a unified model. Review of Geophysics, 46, RG3004. https://doi.org/10.1029/2007RG000227 T

Torsvik, Trond H., Steinberger, Bernhard, Gurnis, Michael, Gaina, Carmen, 2010, Earth and Planetary Science Letters, 291, 106–112.

Torsvik, T. H., Van der Voo, R., Preeden, U., Mac Niocaill, C., Steinberger, B., Doubrovine, P. V., van Hinsbergen, Douwe J.J., Domeier, Mathew, Gaina, Carmen, Tohver, Eric, Meert, Joseph G., McCausland, Phil J.A., Cocks, L. Robin M., 2012, Phanerozoic polar wander, paleogeography and dynamics. Earth Science Reviews, 114(3-4), 325–368. https://doi.org/10.1016/j.earscirev.2012.06.007.

Torsvik, T. H., Steinberger, B., Shephard, G. E., Doubrovine, P. V., Gaina, C., Domeier, M., et al. (2019). Pacific-Panthalassic reconstructions: Overview, errata and the way forward. Geochemistry, Geophysics, Geosystems, 20, 3659–3689. https://doi.org/10.1029/ 2019GC008402

Wessel, P., and L. Kroenke, 200, Pacific absolute plate motion since 145 Ma: An assessment of the fixed hot spot hypothesis, J. Geophys. Res., 113, B06101, doi:10.1029/2007JB005499.

Wessel, P., Y. Harada, and L. W. Kroenke, 2006, Toward a self-consistent, high-resolution absolute plate motion model for the Pacific, Geochem. Geophys. Geosyst., 7, Q03L12, doi:10.1029/2005GC001000.

Whittaker, J. M., R. D. Müller, G., Leitchenkov, H. Stagg, M. Sdrolias, C. Gaina, and A. Goncharov, 2007, Major Australian-Antarctic plate reorganization at Hawaiian-Emperor bend time, Science, 318, 83–86, doi:10.1126/science.1143769.

Wilder, D. T., 2003, Relative motion history of the Pacific-Nazca, Farallon, plates since 30 million years ago, M.S. Thesis, U. S. Florida.

Williams, S. E., Whittaker, J. M., & Müller, R. D., 2011. Full-fit, palinspastic reconstruction of the conjugate Australian-Antarctic margins. Tectonics, 30, TC6012. https://doi.org/10.1029/2011TC002912
Wright, N.M., Müller, R.D., Seton, M. and Williams, S.E., 2015. Revision of Paleogene plate motions in the Pacific and implications for the Hawaiian-Emperor bend. Geology, 43, 455-458.

	Plate Pairs								
Circuit	**SA - AF**	**SA - AN**	**AF - AN**	**AN - WA**	**WA - PC**	**PC - NF**	**AN - NF**	**HS - PC**	**HS - AF**
SA - AF - AN - WA - PC - NF	DeMets & Merkouriev, 2019; Pérez-Díaz & Eagles, 2014		Cande et al., 2010; Cande and Patriat, 2015; DeMets & Merkouriev, 2015	Granot et al., 2013	Croon et al., 2008	Wilder, 2003; Wright et al., 2015; Seton et al., 2012			
SA - AF - AN - WA - NF	DeMets & Merkouriev, 2019; Pérez-Díaz & Eagles, 2014		Cande et al., 2010; Cande and Patriat, 2015; DeMets & Merkouriev, 2015	Granot et al., 2013			Tebbens and Cande, 1997		
SA - AN - WA - PC - NF		Eagles & Jokat, 2014; Livermore et al., 2005		Granot et al., 2013	Croon et al., 2008	Wilder, 2003; Wright et al., 2015; Seton et al., 2012			
SA - AN - WA - NF		Eagles & Jokat, 2014; Livermore et al., 2005		Granot et al., 2013			Tebbens and Cande, 1997		
HS - AF - AN - WA - PC - NF			Cande et al., 2010; Cande and Patriat, 2015; DeMets & Merkouriev, 2015	Granot et al., 2013	Croon et al., 2008	Wilder, 2003; Wright et al., 2015; Seton et al., 2012			Müller et al., 1993; Müller et al., 2019
HS - PC - NF						Wilder, 2003; Wright et al., 2015; Seton et al., 2012		Wessel and Kroenke, 2008; Gaastra, 2022	

Table 1. Reconstruction sources for circuits. AF: African, AN: East Antarctic, HS: Hotspot, NF: Nazca/Farallon, PC: Pacific, SA: South American, WA: West Antarctic

Plate 1	Plate 2	Age (Ma)	Longitude (°E)	Latitude (° N)	Angle (CCW)
Nazca	South American	1	80.276	-51.577	0.658
Nazca	South American	2	80.848	-54.545	1.486
Nazca	South American	3	79.543	-55.485	2.319
Nazca	South American	4	78.382	-59.122	3.141
Nazca	South American	5	78.327	-61.340	3.959
Nazca	South American	6	78.131	-55.296	4.974
Nazca	South American	7	77.997	-49.677	6.011
Nazca	South American	8	78.566	-51.104	6.890
Nazca	South American	9	78.626	-55.923	8.155
Nazca	South American	10	78.719	-56.910	9.291
Nazca	South American	11	79.453	-57.193	10.494
Nazca	South American	12	80.470	-57.556	11.448
Nazca	South American	13	79.777	-58.836	12.322
Nazca	South American	14	76.250	-60.742	13.497
Nazca	South American	15	74.007	-61.666	15.006
Nazca	South American	16	75.654	-60.343	16.346
Nazca	South American	17	77.849	-59.123	17.976
Nazca	South American	18	80.570	-58.119	19.978
Nazca	South American	19	83.484	-57.231	22.520
Nazca	South American	20	84.899	-56.402	24.208
Nazca	South American	21	86.092	-56.118	25.345
Nazca	South American	22	87.687	-55.654	27.236
Nazca	South American	23	88.721	-55.515	28.381
Nazca	South American	24	88.715	-56.388	29.051
Nazca	South American	25	87.820	-58.145	29.519
Nazca	South American	26	86.283	-60.393	29.961
Nazca	South American	27	84.035	-62.722	30.260
Nazca	South American	28	81.299	-64.528	30.638
Nazca	South American	29	79.026	-65.663	31.244
Nazca	South American	30	76.797	-66.245	31.917
Nazca	South American	31	75.190	-66.552	32.720
Nazca	South American	32	74.060	-66.919	33.666
Nazca	South American	33	72.416	-67.330	34.519
Nazca	South American	34	70.359	-68.330	35.391
Nazca	South American	35	67.862	-69.932	36.370
Nazca	South American	36	64.267	-71.585	36.970
Nazca	South American	37	59.674	-73.548	37.878
Nazca	South American	38	53.884	-75.449	39.149

Nazca	South American	39	46.867	-76.876	40.576
Nazca	South American	40	39.726	-77.639	42.120
Nazca	South American	41	33.940	-77.690	43.610
Nazca	South American	42	29.884	-77.445	45.231
Nazca	South American	43	26.149	-77.089	46.545
Nazca	South American	44	22.081	-76.728	47.519
Nazca	South American	45	17.726	-76.409	48.337
Nazca	South American	46	13.329	-76.085	49.068
Nazca	South American	47	9.172	-75.727	49.766
Nazca	South American	48	5.562	-75.329	50.482
Nazca	South American	49	2.624	-74.909	51.231
Nazca	South American	50	0.115	-74.507	51.960
Nazca	South American	51	357.775	-74.143	52.639
Nazca	South American	52	355.408	-73.820	53.291
Nazca	South American	53	352.847	-73.530	53.946
Nazca	South American	54	350.080	-73.263	54.627
Nazca	South American	55	347.264	-73.002	55.337
Nazca	South American	56	344.589	-72.720	56.032
Nazca	South American	57	342.247	-72.395	56.654
Nazca	South American	58	340.399	-72.013	57.145
Nazca	South American	59	339.015	-71.576	57.528
Nazca	South American	60	337.931	-71.103	57.879
Nazca	South American	61	336.904	-70.604	58.257
Nazca	South American	62	335.688	-70.085	58.722
Nazca	South American	63	334.073	-69.546	59.340
Nazca	South American	64	332.397	-69.020	60.158
Nazca	South American	65	331.097	-68.541	61.155
Nazca	South American	66	330.131	-68.086	62.266
Nazca	South American	67	329.429	-67.624	63.431
Nazca	South American	68	328.917	-67.129	64.606
Nazca	South American	69	328.520	-66.574	65.751
Nazca	South American	70	328.175	-65.962	66.859
Nazca	South American	71	327.837	-65.317	67.935
Nazca	South American	72	327.470	-64.661	68.983
Nazca	South American	73	327.050	-64.012	69.995
Nazca	South American	74	326.567	-63.383	70.953
Nazca	South American	75	326.013	-62.783	71.842
Nazca	South American	76	325.396	-62.204	72.662
Nazca	South American	77	324.722	-61.631	73.421
Nazca	South American	78	323.999	-61.050	74.132
Nazca	South American	79	323.234	-60.444	74.805

Nazca	South American	80	322.437	-59.800	75.453

Table 2. South America-Nazca Reconstruction Parameters, 0-80 Ma.

Reference Frame	Plate	Age (Ma)	Longitude (°E)	Latitude (° N)	Angle (CCW)
Hawaiian Hotspot	Nazca	1	-81.507	-2.836	0.432
Hawaiian Hotspot	Nazca	2	-83.993	2.059	0.894
Hawaiian Hotspot	Nazca	3	-81.490	7.972	1.282
Hawaiian Hotspot	Nazca	4	-73.179	17.386	1.521
Hawaiian Hotspot	Nazca	5	-76.226	25.777	1.897
Hawaiian Hotspot	Nazca	6	-83.495	21.016	2.701
Hawaiian Hotspot	Nazca	7	-87.719	17.662	3.679
Hawaiian Hotspot	Nazca	8	-87.600	23.364	4.202
Hawaiian Hotspot	Nazca	9	-86.270	32.629	4.649
Hawaiian Hotspot	Nazca	10	-86.535	38.297	5.427
Hawaiian Hotspot	Nazca	11	-84.670	38.652	6.115
Hawaiian Hotspot	Nazca	12	-83.844	40.688	6.706
Hawaiian Hotspot	Nazca	13	-85.013	44.866	7.242
Hawaiian Hotspot	Nazca	14	-89.487	50.290	7.973
Hawaiian Hotspot	Nazca	15	-93.911	53.549	9.062
Hawaiian Hotspot	Nazca	16	-92.759	52.514	10.258
Hawaiian Hotspot	Nazca	17	-91.453	51.545	11.651
Hawaiian Hotspot	Nazca	18	-90.310	50.846	13.331
Hawaiian Hotspot	Nazca	19	-89.108	50.431	15.656
Hawaiian Hotspot	Nazca	20	-88.503	50.000	17.258
Hawaiian Hotspot	Nazca	21	-88.278	49.491	18.144
Hawaiian Hotspot	Nazca	22	-87.779	49.228	19.879
Hawaiian Hotspot	Nazca	23	-87.761	49.104	20.890
Hawaiian Hotspot	Nazca	24	-88.874	50.119	21.477
Hawaiian Hotspot	Nazca	25	-91.092	52.029	21.785
Hawaiian Hotspot	Nazca	26	-94.379	54.397	21.968
Hawaiian Hotspot	Nazca	27	-98.499	56.720	22.198
Hawaiian Hotspot	Nazca	28	-102.789	58.432	22.586
Hawaiian Hotspot	Nazca	29	-106.522	59.099	23.058
Hawaiian Hotspot	Nazca	30	-109.283	59.123	23.687

Hawaiian Hotspot	Nazca	31	-111.281	58.890	24.406
Hawaiian Hotspot	Nazca	32	-112.925	58.717	25.127
Hawaiian Hotspot	Nazca	33	-114.715	58.938	25.791
Hawaiian Hotspot	Nazca	34	-117.233	59.805	26.340
Hawaiian Hotspot	Nazca	35	-120.808	61.272	26.803
Hawaiian Hotspot	Nazca	36	-125.540	63.055	27.264
Hawaiian Hotspot	Nazca	37	-131.428	64.860	27.797
Hawaiian Hotspot	Nazca	38	-138.152	66.387	28.474
Hawaiian Hotspot	Nazca	39	-144.984	67.415	29.327
Hawaiian Hotspot	Nazca	40	-150.869	67.849	30.358
Hawaiian Hotspot	Nazca	41	-154.900	67.762	31.536
Hawaiian Hotspot	Nazca	42	-157.452	67.426	32.762
Hawaiian Hotspot	Nazca	43	-159.489	67.018	33.908
Hawaiian Hotspot	Nazca	44	-161.844	66.679	34.883
Hawaiian Hotspot	Nazca	45	-164.784	66.390	35.670
Hawaiian Hotspot	Nazca	46	-167.967	66.098	36.339
Hawaiian Hotspot	Nazca	47	-170.974	65.746	36.950
Hawaiian Hotspot	Nazca	48	-173.542	65.273	37.552
Hawaiian Hotspot	Nazca	49	-175.060	64.821	38.181
Hawaiian Hotspot	Nazca	50	-180.986	63.111	38.969
Hawaiian Hotspot	Nazca	51	-182.474	62.905	39.785
Hawaiian Hotspot	Nazca	52	-183.797	62.727	40.534
Hawaiian Hotspot	Nazca	53	-185.359	62.453	41.242
Hawaiian Hotspot	Nazca	54	-186.894	62.203	41.924
Hawaiian Hotspot	Nazca	55	-188.616	61.868	42.592
Hawaiian Hotspot	Nazca	56	-190.090	61.601	43.239
Hawaiian Hotspot	Nazca	57	-192.399	60.857	43.912
Hawaiian Hotspot	Nazca	58	-194.743	59.910	44.608
Hawaiian Hotspot	Nazca	59	-195.623	59.630	45.238
Hawaiian Hotspot	Nazca	60	-196.568	59.253	45.912
Hawaiian Hotspot	Nazca	61	-197.439	58.896	46.608
Hawaiian Hotspot	Nazca	62	-198.399	58.520	47.329
Hawaiian Hotspot	Nazca	63	-199.553	58.096	48.076
Hawaiian Hotspot	Nazca	64	-200.619	57.688	48.858

Hawaiian Hotspot	Nazca	65	-201.328	57.341	49.689
Hawaiian Hotspot	Nazca	66	-201.756	57.051	50.547
Hawaiian Hotspot	Nazca	67	-202.016	56.804	51.420
Hawaiian Hotspot	Nazca	68	-202.226	56.566	52.291
Hawaiian Hotspot	Nazca	69	-202.485	56.320	53.147
Hawaiian Hotspot	Nazca	70	-202.827	56.057	53.987
Hawaiian Hotspot	Nazca	71	-203.232	55.776	54.806
Hawaiian Hotspot	Nazca	72	-203.697	55.485	55.614
Hawaiian Hotspot	Nazca	73	-204.223	55.183	56.415
Hawaiian Hotspot	Nazca	74	-204.777	54.875	57.203
Hawaiian Hotspot	Nazca	75	-205.378	54.549	57.992
Hawaiian Hotspot	Nazca	76	-206.008	54.208	58.775
Hawaiian Hotspot	Nazca	77	-206.647	53.871	59.562
Hawaiian Hotspot	Nazca	78	-207.302	53.530	60.350
Hawaiian Hotspot	Nazca	79	-207.957	53.185	61.145
Hawaiian Hotspot	Nazca	80	-208.607	52.837	61.954
Hawaiian Hotspot	Nazca	81	-209.244	52.489	62.777
Hawaiian Hotspot	Nazca	82	-209.829	52.166	63.629
Hawaiian Hotspot	Nazca	83	-210.338	51.873	64.533
Hawaiian Hotspot	Nazca	84	-210.727	51.612	65.490
Hawaiian Hotspot	Nazca	85	-211.005	51.396	66.531
Hawaiian Hotspot	Nazca	86	-211.460	51.026	67.955
Hawaiian Hotspot	Nazca	87	-212.017	50.537	69.708
Hawaiian Hotspot	Nazca	88	-212.514	50.033	71.620
Hawaiian Hotspot	Nazca	89	-212.828	49.616	73.510
Hawaiian Hotspot	Nazca	90	-212.921	49.329	75.284
Hawaiian Hotspot	Nazca	91	-212.831	49.158	76.937
Hawaiian Hotspot	Nazca	92	-212.588	49.086	78.475
Hawaiian Hotspot	Nazca	93	-212.221	49.099	79.904
Hawaiian Hotspot	Nazca	94	-211.752	49.180	81.228
Hawaiian Hotspot	Nazca	95	-211.204	49.315	82.456
Hawaiian Hotspot	Nazca	96	-210.599	49.490	83.595
Hawaiian Hotspot	Nazca	97	-209.956	49.690	84.652
Hawaiian Hotspot	Nazca	98	-209.295	49.901	85.635

Hawaiian Hotspot	Nazca	99	-208.636	50.107	86.551
Hawaiian Hotspot	Nazca	100	-208.001	50.294	87.408
Hawaiian Hotspot	Nazca	101	-207.408	50.446	88.211
Hawaiian Hotspot	Nazca	102	-206.878	50.549	88.967
Hawaiian Hotspot	Nazca	103	-206.422	50.598	89.680
Hawaiian Hotspot	Nazca	104	-206.048	50.599	90.352
Hawaiian Hotspot	Nazca	105	-205.764	50.557	90.986
Hawaiian Hotspot	Nazca	106	-205.575	50.475	91.585
Hawaiian Hotspot	Nazca	107	-205.491	50.358	92.153
Hawaiian Hotspot	Nazca	108	-205.518	50.209	92.694
Hawaiian Hotspot	Nazca	109	-205.665	50.033	93.213
Hawaiian Hotspot	Nazca	110	-205.939	49.833	93.717
Hawaiian Hotspot	Nazca	111	-206.340	49.617	94.223
Hawaiian Hotspot	Nazca	112	-206.852	49.393	94.753
Hawaiian Hotspot	Nazca	113	-207.434	49.156	95.314
Hawaiian Hotspot	Nazca	114	-208.026	48.895	95.905
Hawaiian Hotspot	Nazca	115	-208.571	48.601	96.526
Hawaiian Hotspot	Nazca	116	-209.009	48.267	97.175
Hawaiian Hotspot	Nazca	117	-209.282	47.888	97.850
Hawaiian Hotspot	Nazca	118	-209.339	47.460	98.553
Hawaiian Hotspot	Nazca	119	-209.214	46.993	99.299
Hawaiian Hotspot	Nazca	120	-208.984	46.504	100.107
Hawaiian Hotspot	Nazca	121	-208.729	46.010	100.999
Hawaiian Hotspot	Nazca	122	-208.527	45.528	101.982
Hawaiian Hotspot	Nazca	123	-208.466	45.068	103.036
Hawaiian Hotspot	Nazca	124	-208.629	44.639	104.131
Hawaiian Hotspot	Nazca	125	-209.048	44.227	105.214
Hawaiian Hotspot	Nazca	126	-209.715	43.805	106.215
Hawaiian Hotspot	Nazca	127	-210.621	43.343	107.066
Hawaiian Hotspot	Nazca	128	-211.745	42.805	107.721
Hawaiian Hotspot	Nazca	129	-213.053	42.156	108.157
Hawaiian Hotspot	Nazca	130	-214.504	41.357	108.352
Hawaiian Hotspot	Nazca	131	-216.047	40.380	108.303
Hawaiian Hotspot	Nazca	132	-217.602	39.240	108.079

Hawaiian Hotspot	Nazca	133	-219.089	37.971	107.761
Hawaiian Hotspot	Nazca	134	-220.457	36.617	107.424
Hawaiian Hotspot	Nazca	135	-221.672	35.231	107.142
Hawaiian Hotspot	Nazca	136	-222.706	33.871	106.984
Hawaiian Hotspot	Nazca	137	-223.539	32.603	107.021
Hawaiian Hotspot	Nazca	138	-224.165	31.481	107.300
Hawaiian Hotspot	Nazca	139	-224.614	30.507	107.809
Hawaiian Hotspot	Nazca	140	-224.922	29.670	108.525
Hawaiian Hotspot	Nazca	141	-225.113	28.958	109.417
Hawaiian Hotspot	Nazca	142	-225.207	28.360	110.437
Hawaiian Hotspot	Nazca	143	-225.220	27.865	111.536
Hawaiian Hotspot	Nazca	144	-225.165	27.459	112.662
Hawaiian Hotspot	Nazca	145	-225.056	27.126	113.765
Hawaiian Hotspot	Nazca	146	-224.903	26.851	114.791
Hawaiian Hotspot	Nazca	147	-224.718	26.618	115.685
Hawaiian Hotspot	Nazca	148	-224.508	26.408	116.401
Hawaiian Hotspot	Nazca	149	-224.277	26.201	116.906
Hawaiian Hotspot	Nazca	150	-224.030	25.981	117.181

Table 3. Nazca-Hotspot Parameters - 0 - 150 Ma, as described in text.

Figures

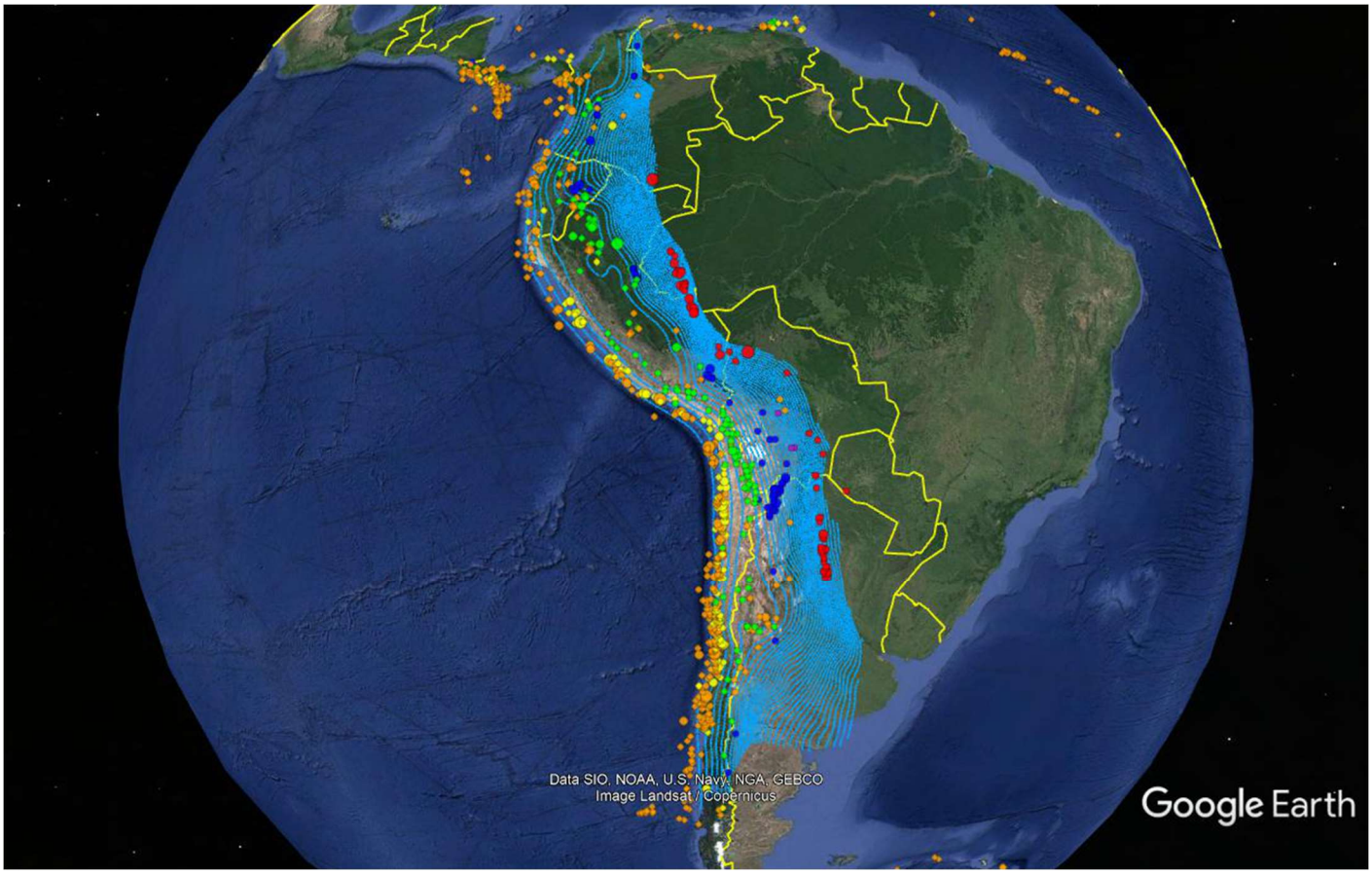

Figure 1. South American subduction zone: Surface from Hayes et al. (2012). Earthquakes from USGS (2022); circles: orange 0-33 km, yellow 33-70 km, green 70-150 km, blue 150-300 km. Red: 500-800 km. Note inferred hotspot traces in bathymetry (shown also in Figures XX-XX). All map images are in Google Earth.

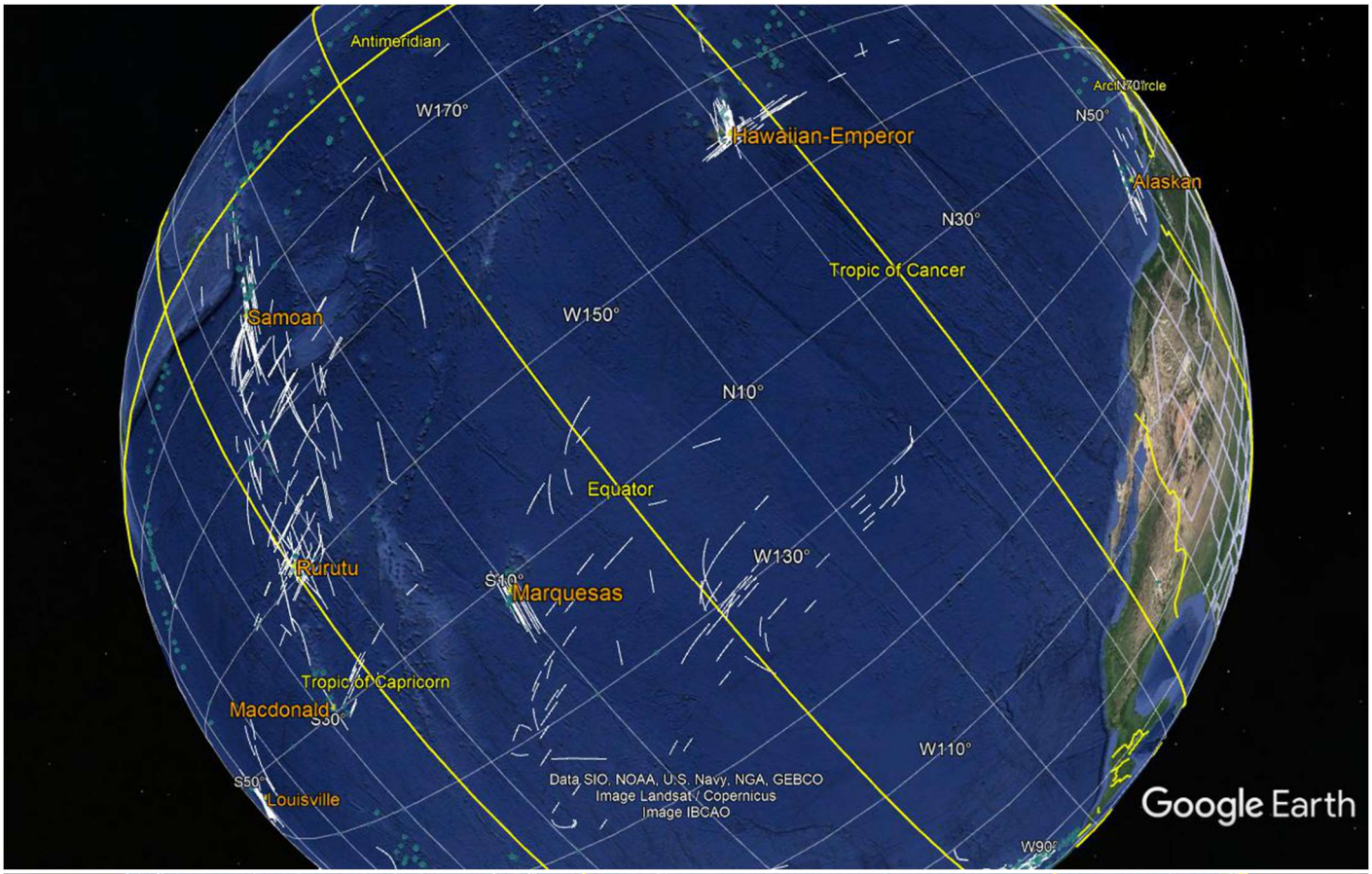
Antimeridian
W170°
Hawaiian-Emperor
Arc N70 rcle
N50°
Alaskan
N30°
Tropic of Cancer
Samoan
W150°
N10°
Equator
W130°
Rurutu
S10°
Marquesas
Tropic of Capricorn
Macdonald
S30°
W110°
S50°
Louisville
Data SIO, NOAA, U.S. Navy, NGA, GEBCO
Image Landsat / Copernicus
Image IBCAO
Google Earth
W90°

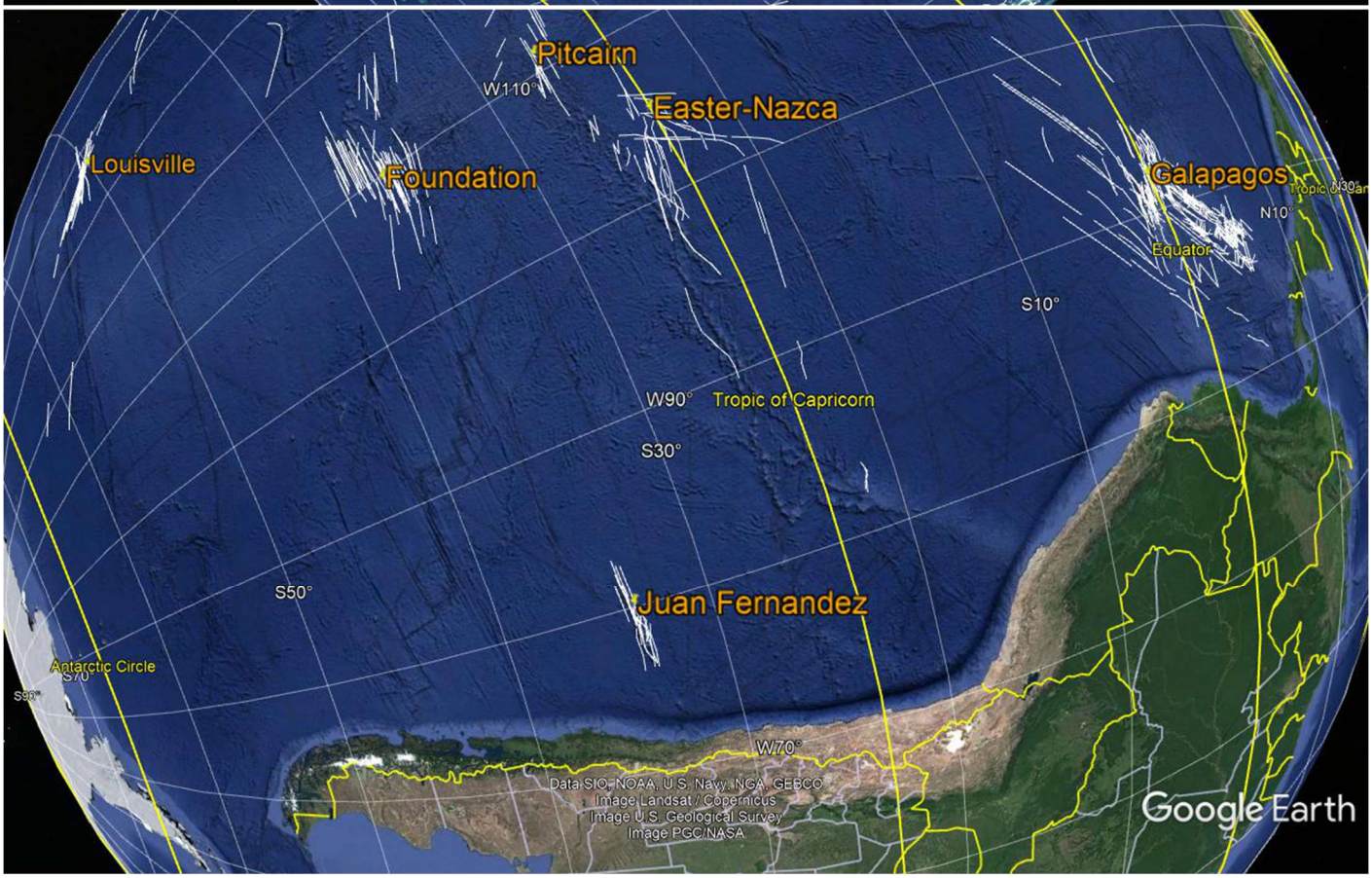
Pitcairn
W110°
Easter-Nazca
Louisville
Foundation
Galapagos
N10°
Equator
S10°
W90°
Tropic of Capricorn
S30°
S50°
Juan Fernandez
Antarctic Circle
S70°
W70°
Data SIO, NOAA, U.S. Navy, NGA, GEBCO
Image Landsat / Copernicus
Image U.S. Geological Survey
Image PGC/NASA
Google Earth

Figure 2. Two views of Pacific Ocean island-seamount volcanic rock locations rotated back by isotopic age, +/- 2.5 m.y., producing loci, according to the model of Gaastra et al. (2022) and extended to the Nazca and Cocos plates by plate-pair reconstructions as described in text. Names apply to loci clusters and inferred hotspots or hotspot groups. Google Earth format (*.kml) file is accessible in Supplementary Data files.

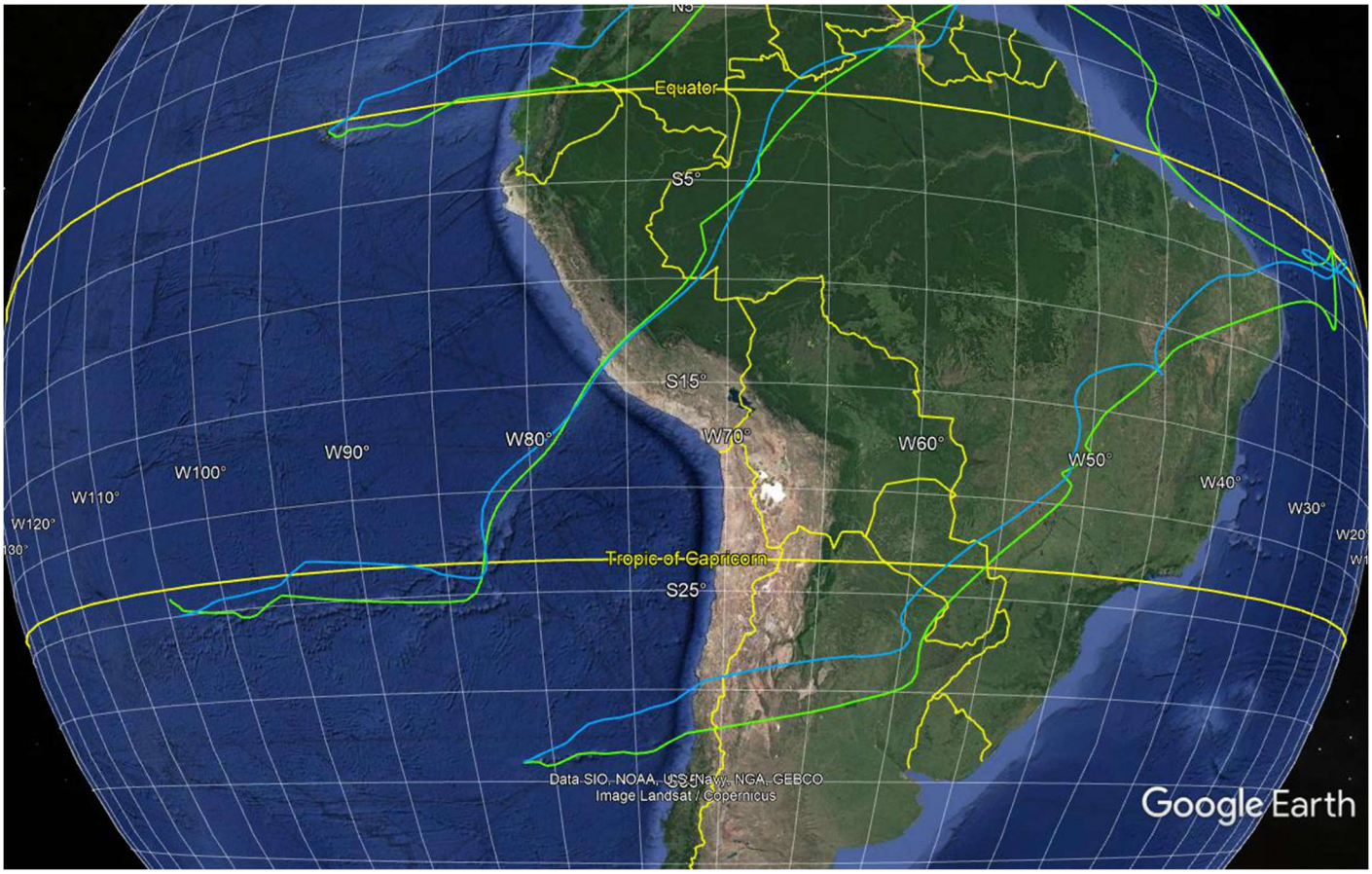

Figure 3. Hotspot loci for (south to north) Juan Fernandez, Easter, and Galapagos hotspots relative to Nazca plate. Blue: Wessel and Kroenke (2008) Pacific hotspot model, 140-0 Ma. Green: Gaastra et al. (2022) Pacific-hotspot model for 80-0 Ma, Wessel and Kroenke (2008) for 140-80 Ma; (Loci are not “deformed” onto the subducting surface.) Note that the inferred location of the Easter hotspot differs between the two models so as to visually fit the Easter-Nazca trace. .Google Earth format (*.kml) files are accessible in Supplementary Data files.

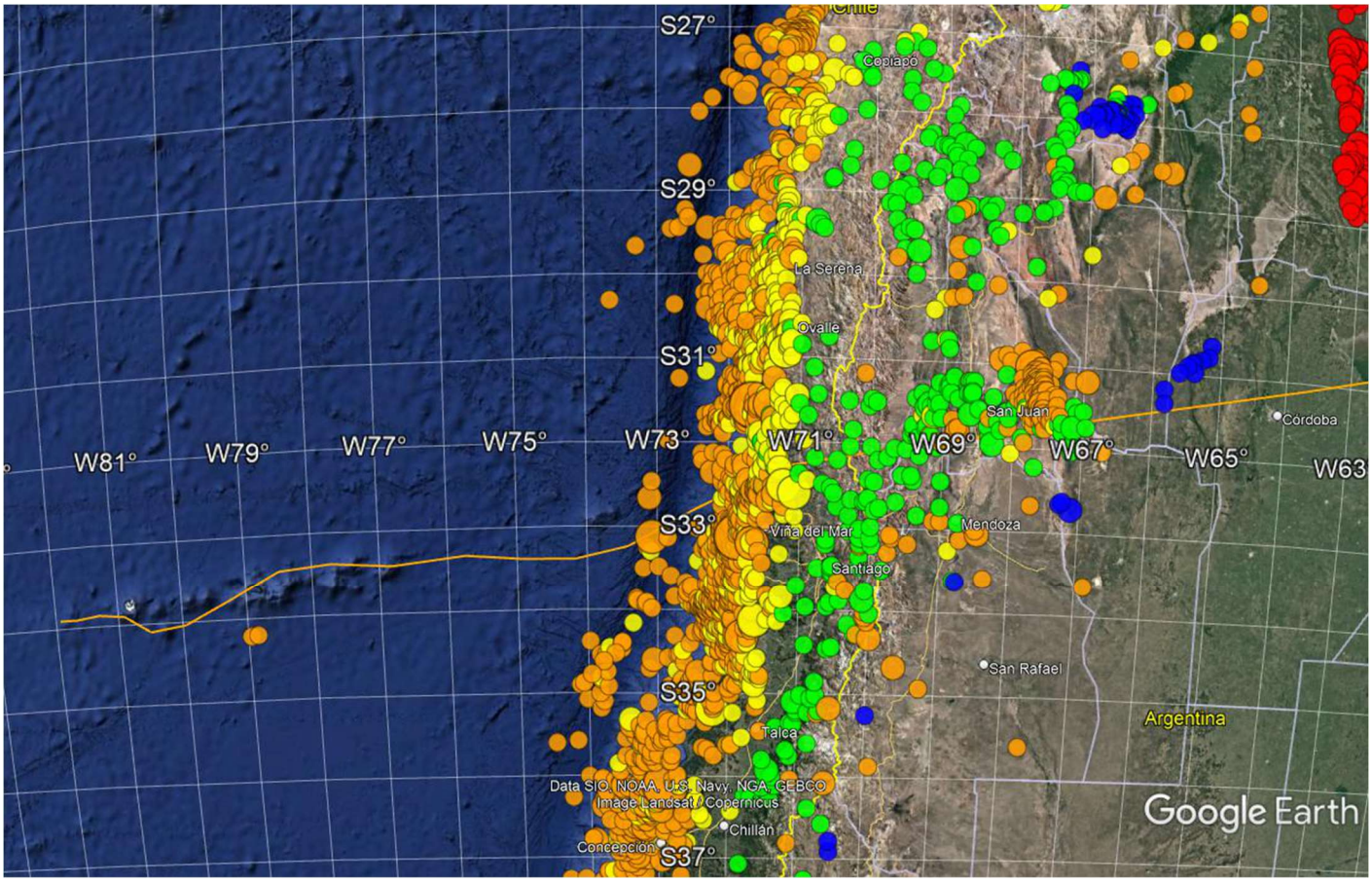

Figure 4. Calculated loci for Juan Fernandez hotspot relative to Nazca plate. Blue: based on Wessel and Kroenke (2008) Pacific hotspot model. Green (preferred), based on Gaastra et al. (2022) Pacific-hotspot model; Earthquakes from USGS (2022); circles: orange 0-33 km, yellow 33-70 km, green 70-150 km, blue 150-300 km. (Loci are not “deformed” onto the subducting surface.) Image in Google Earth. Google Earth format (*.kml) files are accessible in Supplementary Data files.

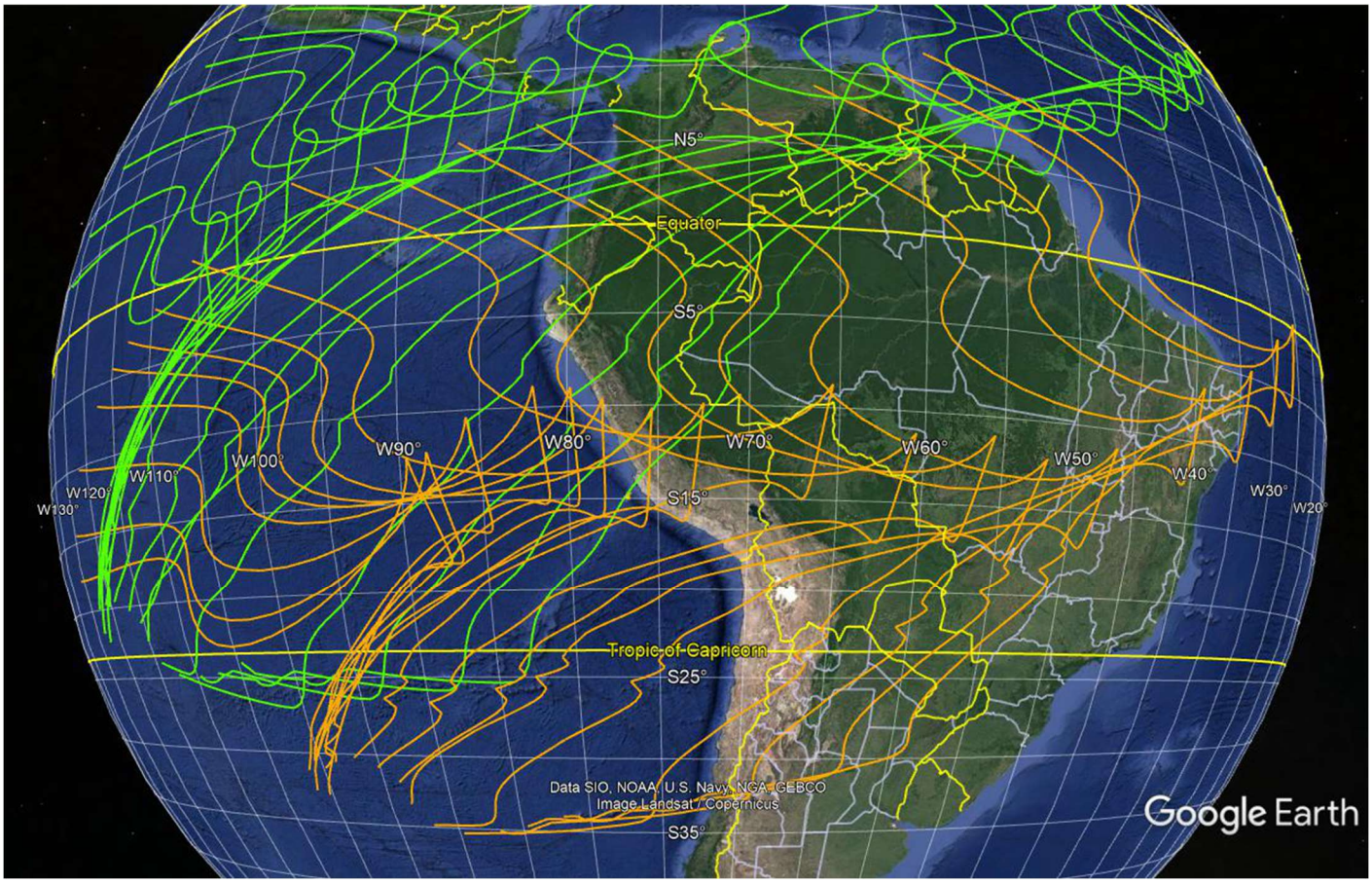

Figure 5. Calculated loci based on Gaastra et al. (2022) Pacific-hotspot model, extended to the Nazca plate, and reconstructed relative to (fixed) South America, at 5 m.y. Intervals: Juan Fernandez (gold) and Easter (green) hotspot traces on Nazca/Farallon plate, reconstructed relative to (fixed) South American plate. Present position is the most easterly Apparent first contact, relative to the current continental boundary occurred for: Juan Fernandez trace, ~65 Ma; Easter trace, ~43 Ma. The western end of each locus is the apparent location of the hotspot relative to South America. Comparison of features in each locus with adjacent positions provides insight into the relative motion of the Nazca plate to South America over that interval. Thus, from 25-0 Ma, the Nazca plate was moving east-northeast across the trench relative to South America, 50-25 Ma, eastward, and northeastward from 80-50 Ma. Also, note rapid convergence between 20-15 Ma and 50-40 Ma, and very slow convergence 70-55 and 80-75 Ma. The proximity of the Juan Fernandez locus to the Andean bend (e.g., Isacks, 1988) at Latitude ~18° S is suggestive of possible influence on the formation of the bend between 35 to 20 Ma; enhanced convergence at that latitude could have induced shortening of the shallow crust between 25 to 18° S during that period of time. See Figure 13 for higher resolution portrayal of convergence rates. Google Earth format (*.kml) files are accessible in Supplementary Data files.

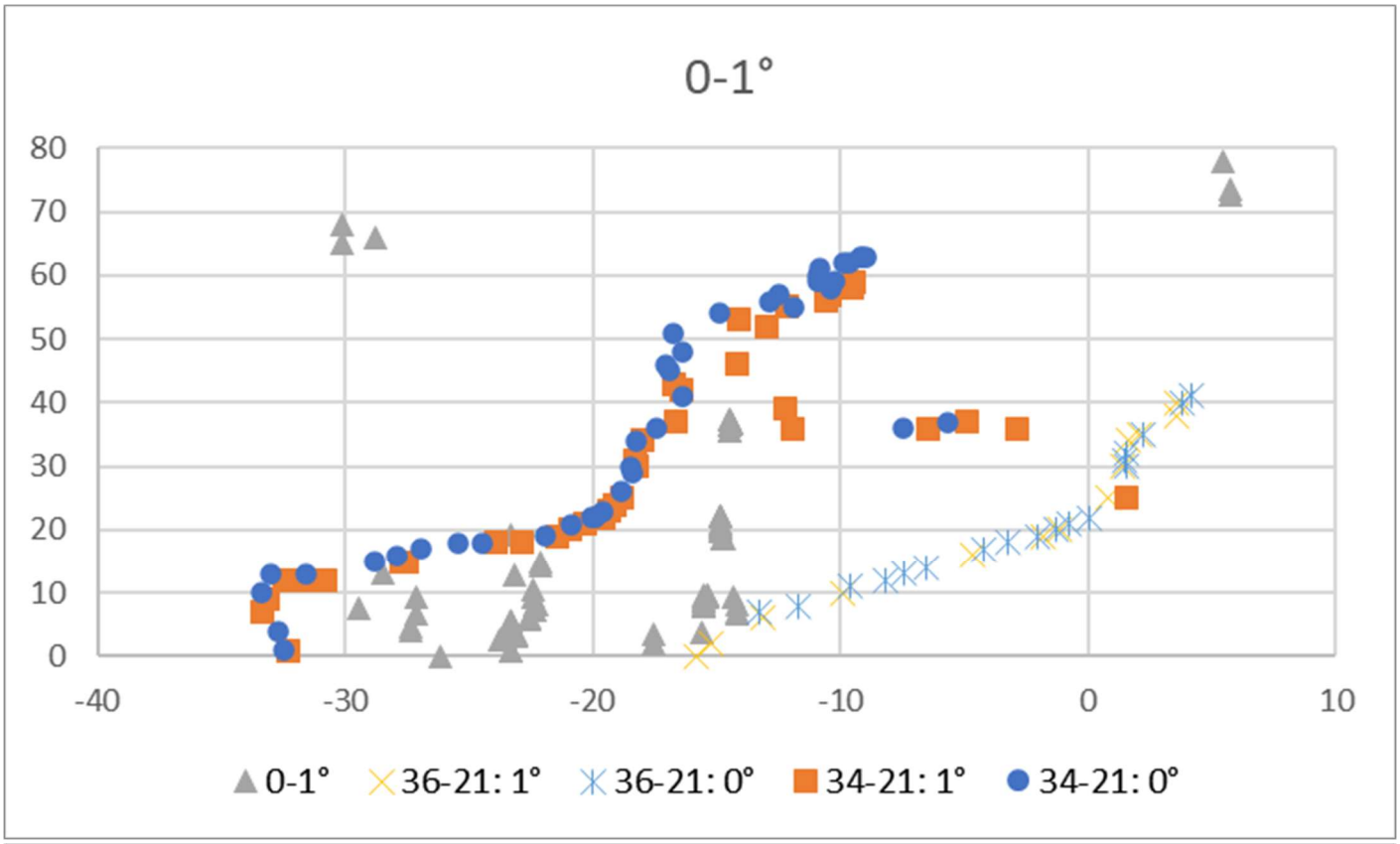
0-1°
80
70
60
50
40
30
20
10
0
-40
-30
-20
-10
0
10
0-1°
36-21: 1°
36-21: 0°
34-21: 1°
34-21: 0°

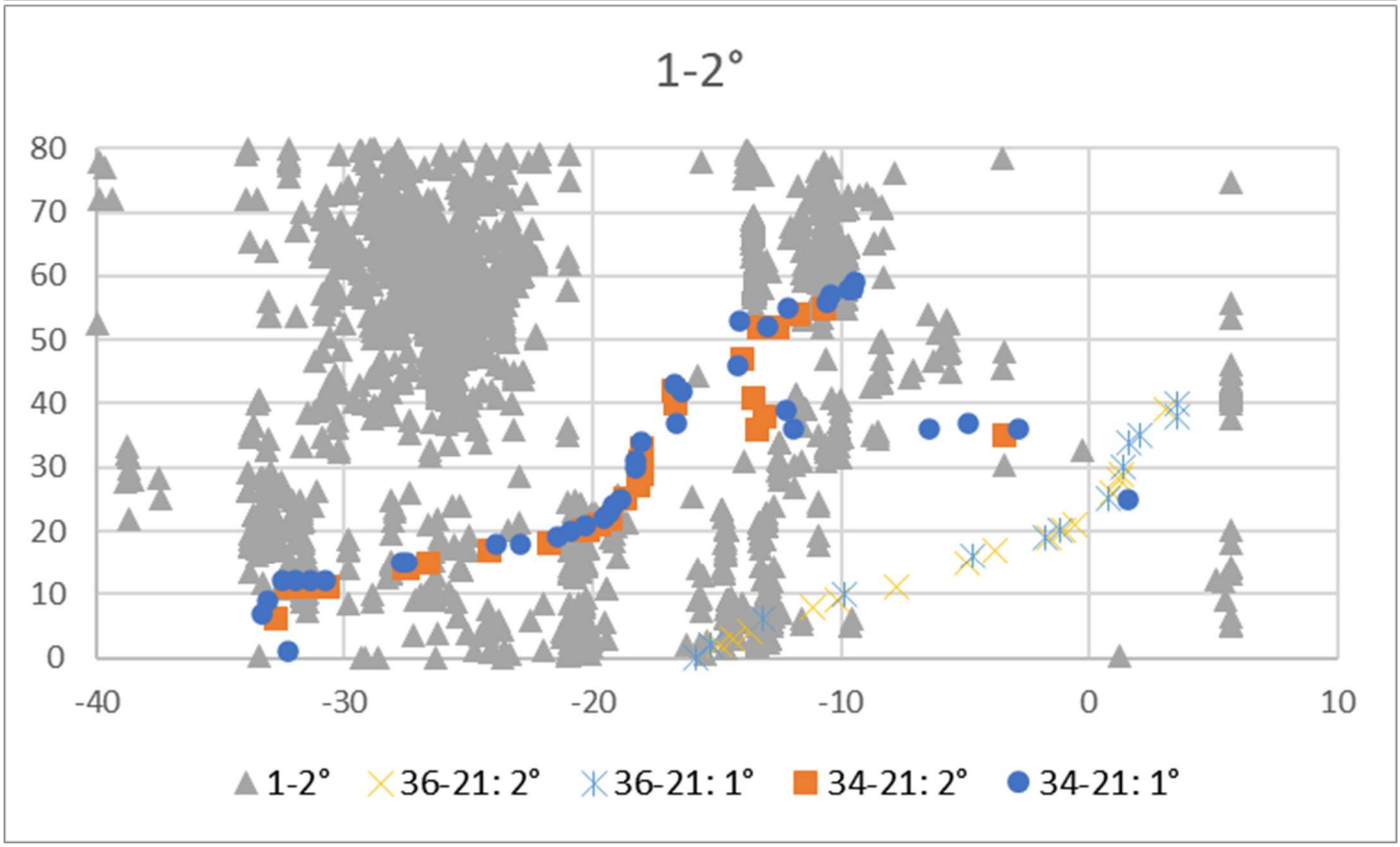
1-2°
80
70
60
50
40
30
20
10
0
-40
-30
-20
-10
0
10
1-2°
36-21: 2°
36-21: 1°
34-21: 2°
34-21: 1°

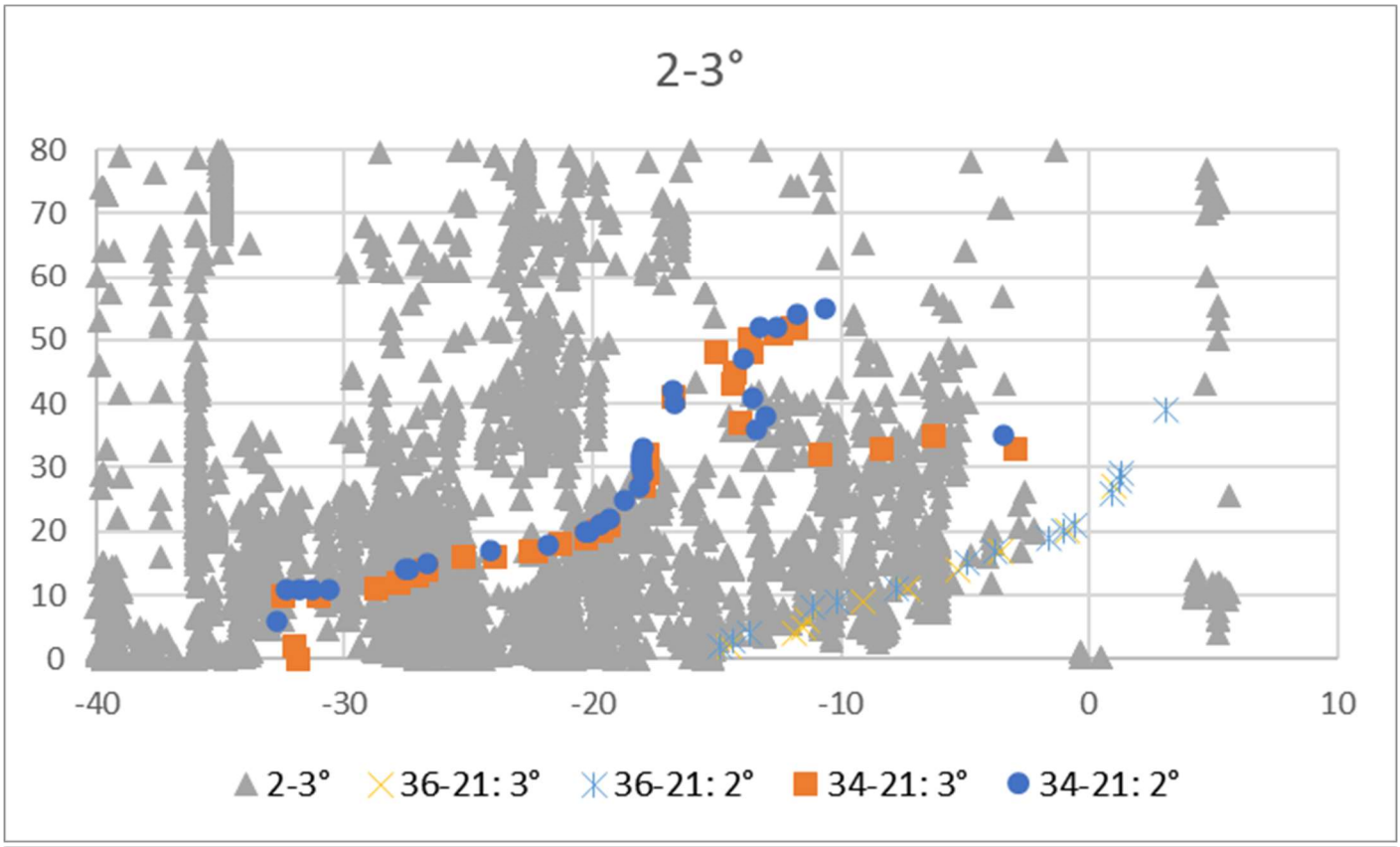
2-3°
80
70
60
50
40
30
20
10
0
-40
-30
-20
-10
0
10
2-3°
36-21: 3°
36-21: 2°
34-21: 3°
34-21: 2°

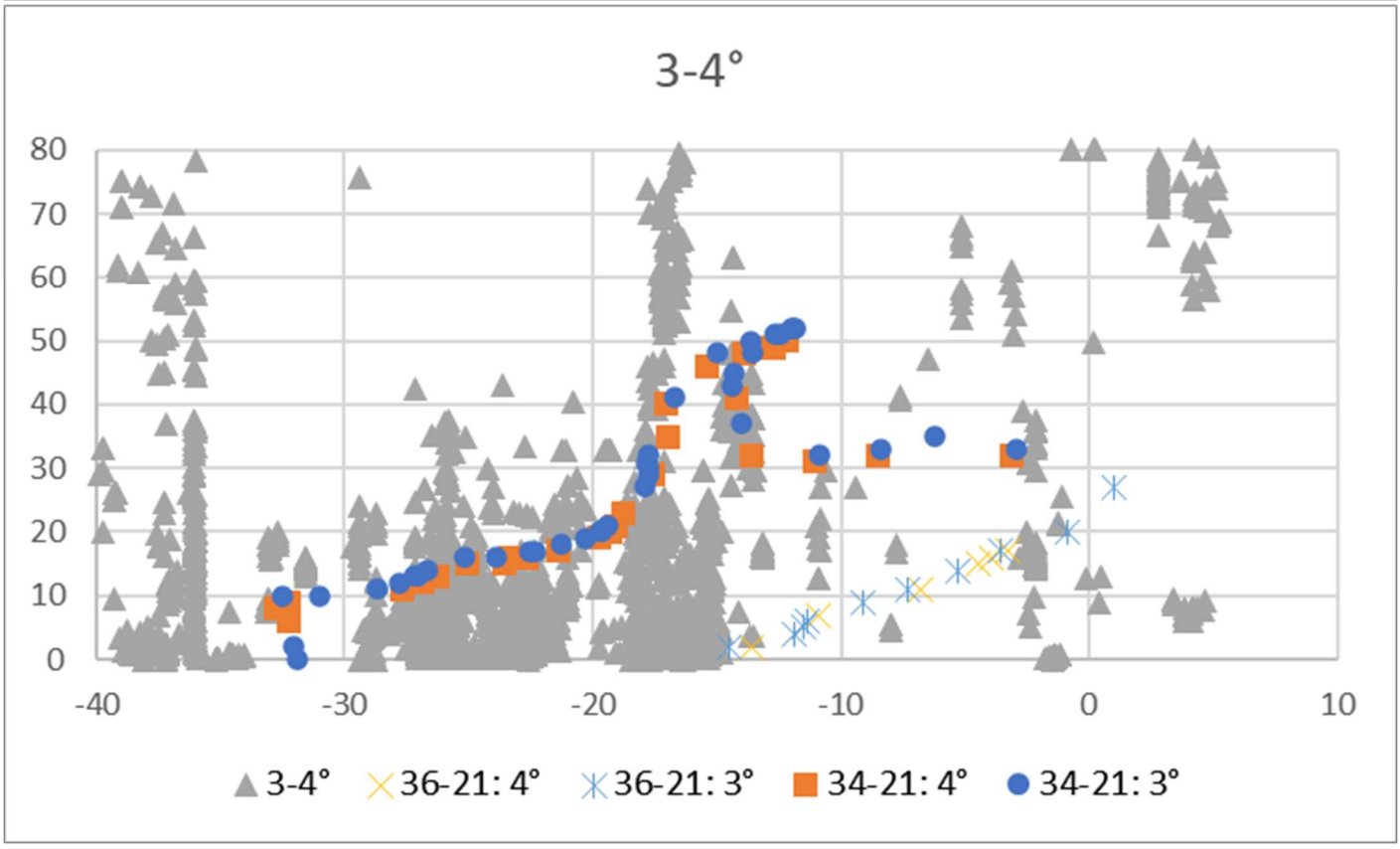
3-4°
80
70
60
50
40
30
20
10
0
-40
-30
-20
-10
0
10
3-4°
36-21: 4°
36-21: 3°
34-21: 4°
34-21: 3°

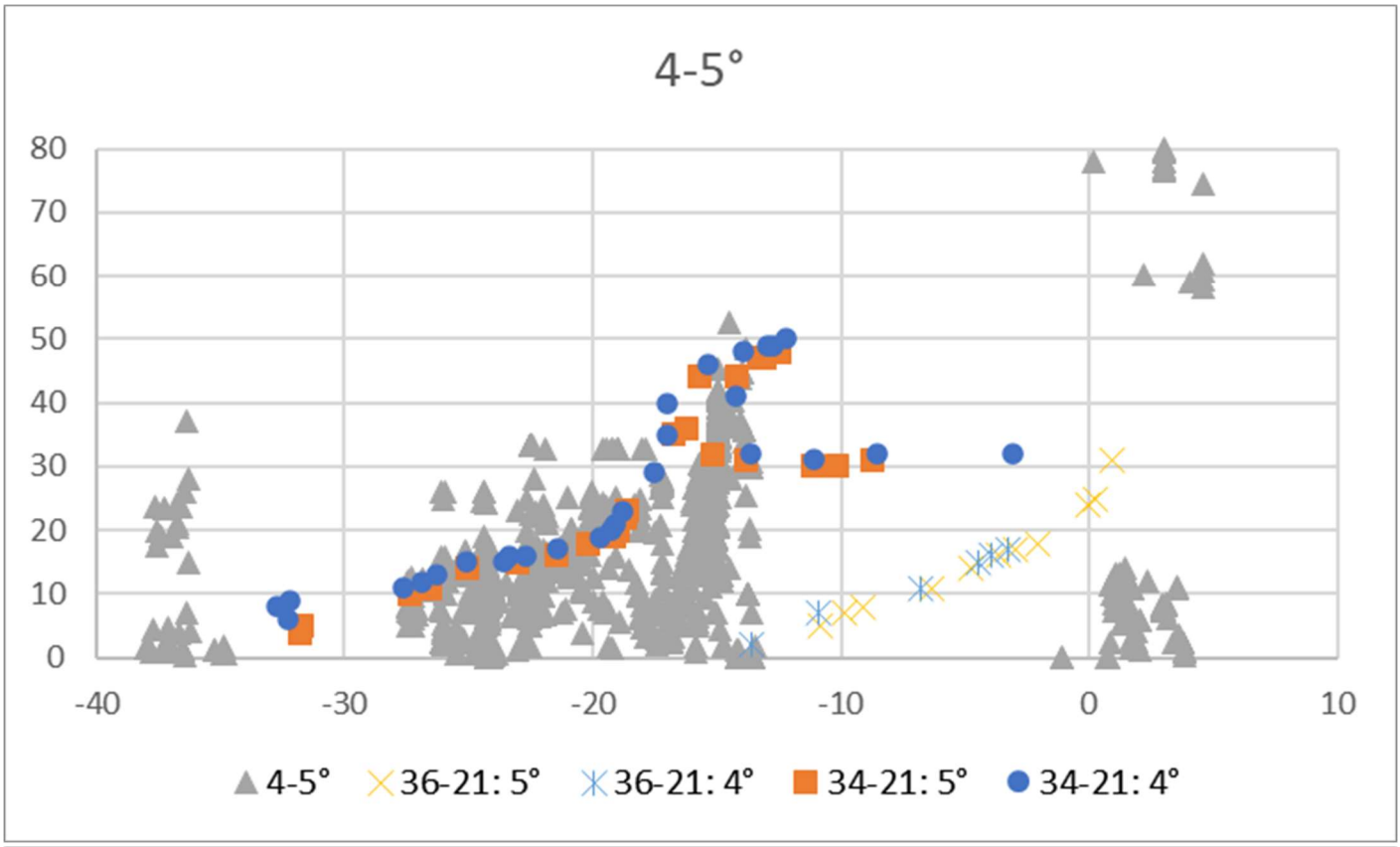
4-5°
80
70
60
50
40
30
20
10
0
-40
-30
-20
-10
0
10
4-5°
36-21: 5°
36-21: 4°
34-21: 5°
34-21: 4°

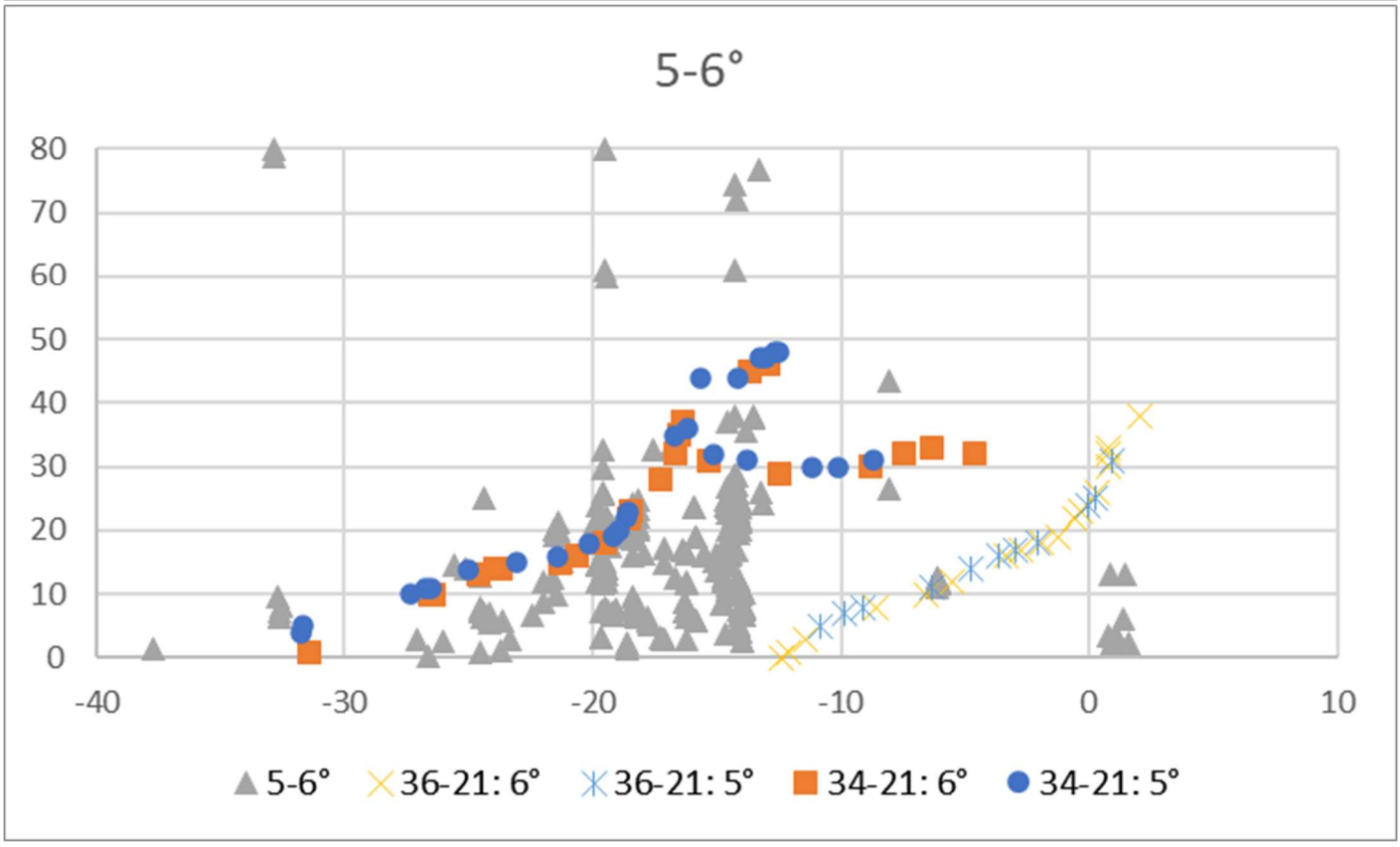
5-6°
80
70
60
50
40
30
20
10
0
-40
-30
-20
-10
0
10
5-6°
36-21: 6°
36-21: 5°
34-21: 6°
34-21: 5°

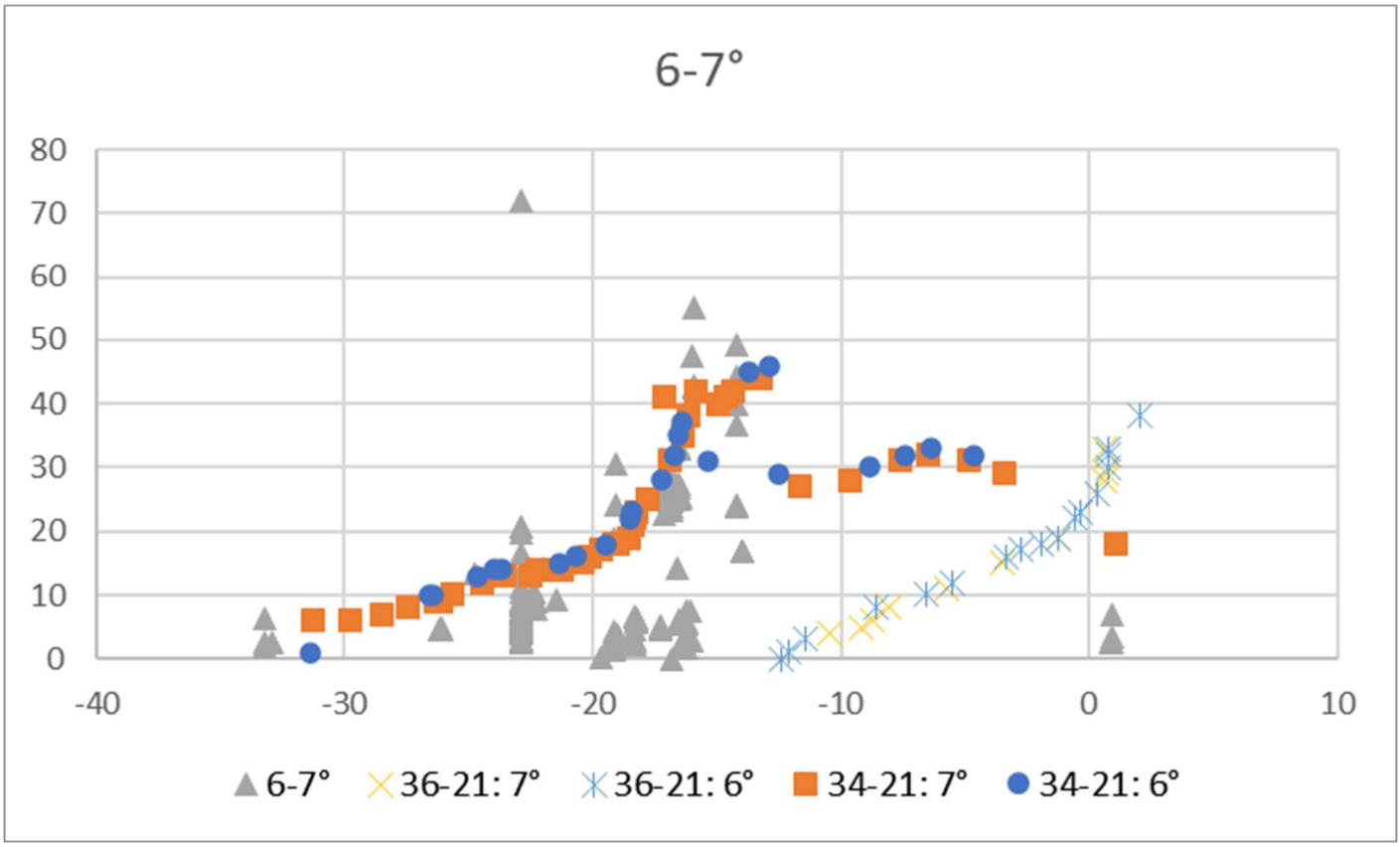

Figure 6a. Andes isotopic dates and calculated intersections of Easter (#34) and Juan Fernandez (#36) hotspot traces with trench-parallel lines, top to bottom: A. 0-1º of arc (0 to ~111 km) from trench. B: 1-2º; C: 2-3º, D: 3-4º; E: 4-5º F. 5-6º, G. 6-7º. Note especially B and C in which cessation of magmatism parallels the Easter hotspot loci intersections, and most graphs in which onset or increase in magmatism is paralleled by Juan Fernandez hotspot loci intersections. Spreadsheets are accessible in Supplementary Data files.

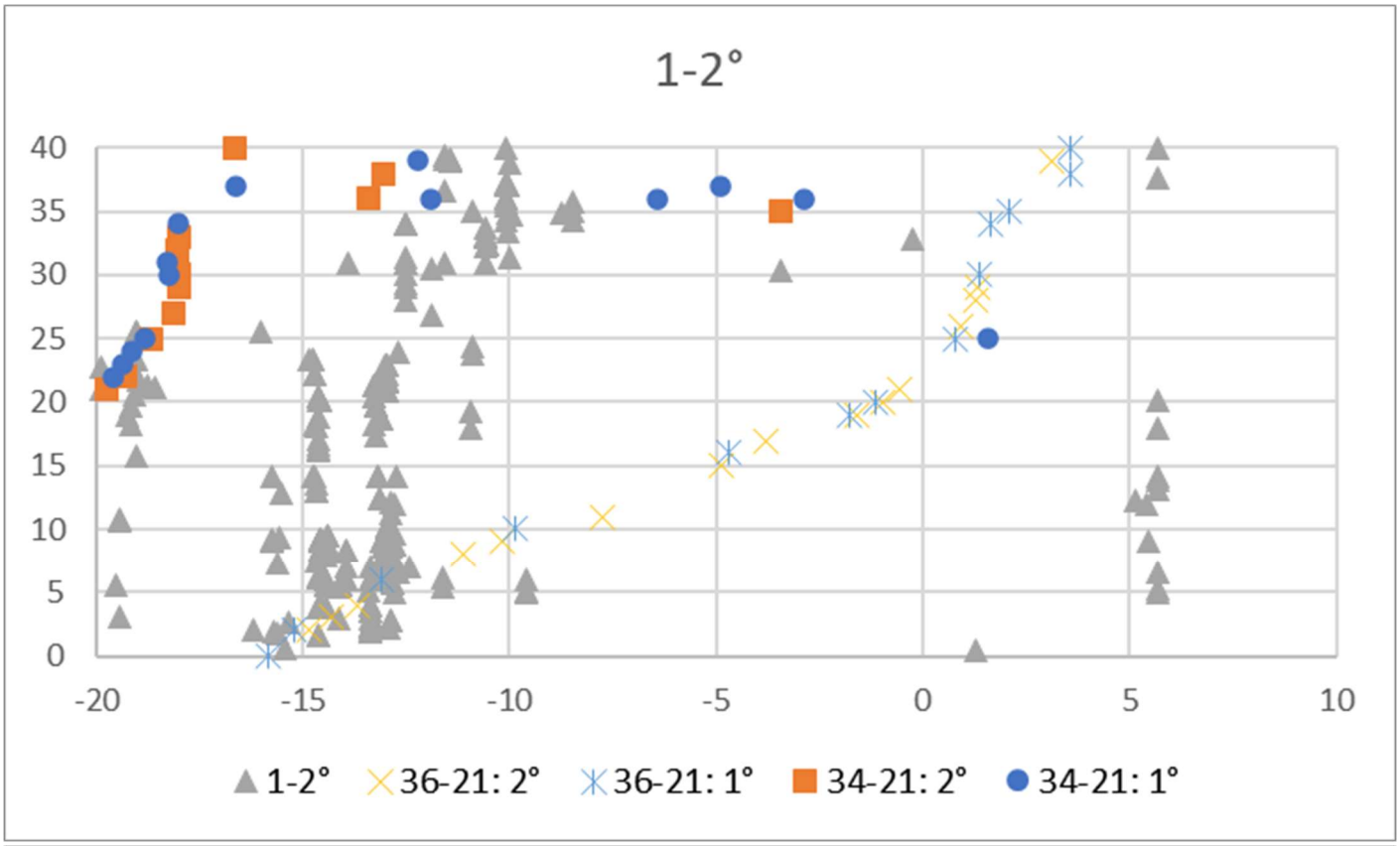
1-2°
40
35
30
25
20
15
10
5
0
-20
-15
-10
-5
0
5
10
1-2°
36-21: 2°
36-21: 1°
34-21: 2°
34-21: 1°

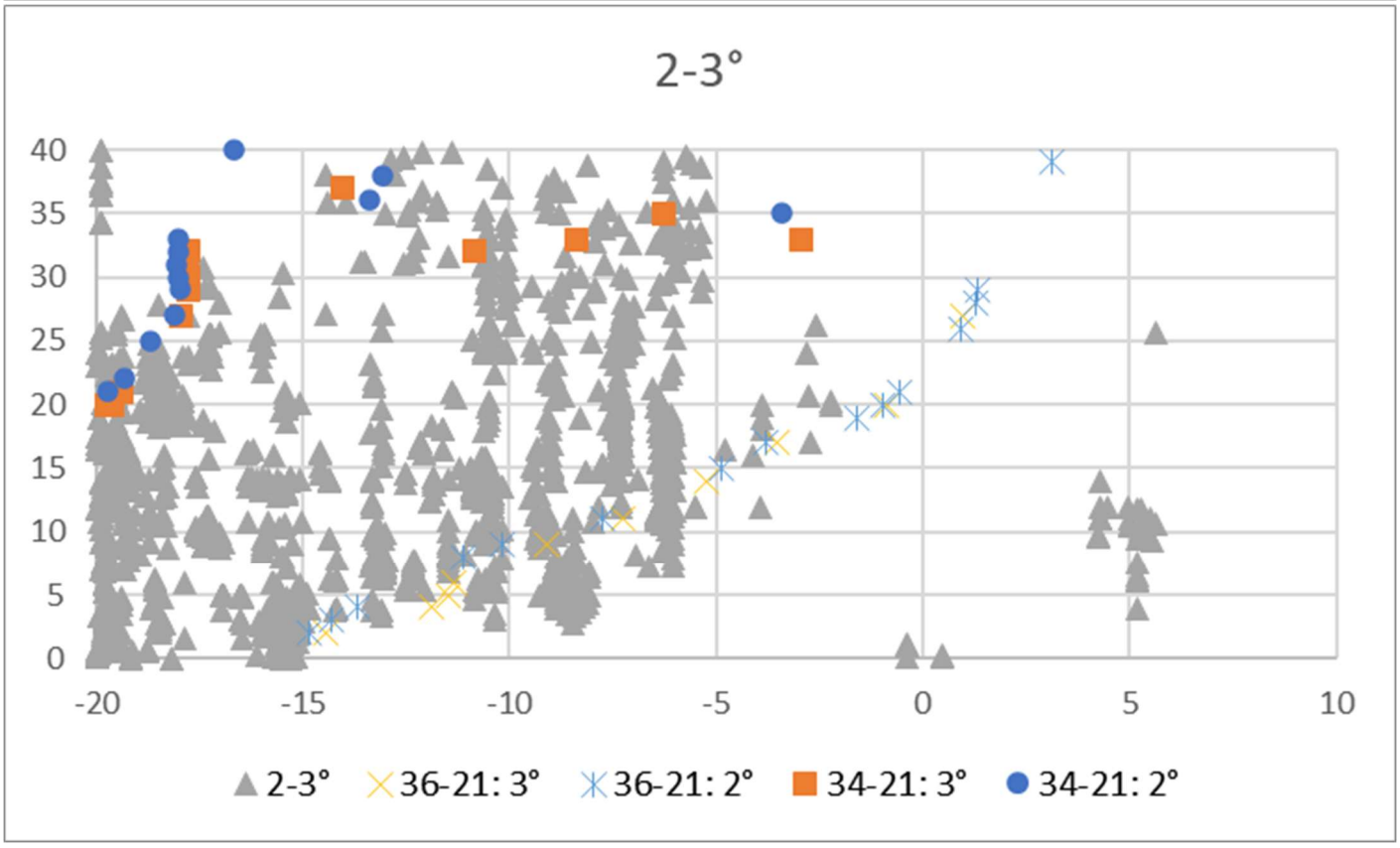
2-3°
40
35
30
25
20
15
10
5
0
-20
-15
-10
-5
0
5
10
2-3°
36-21: 3°
36-21: 2°
34-21: 3°
34-21: 2°

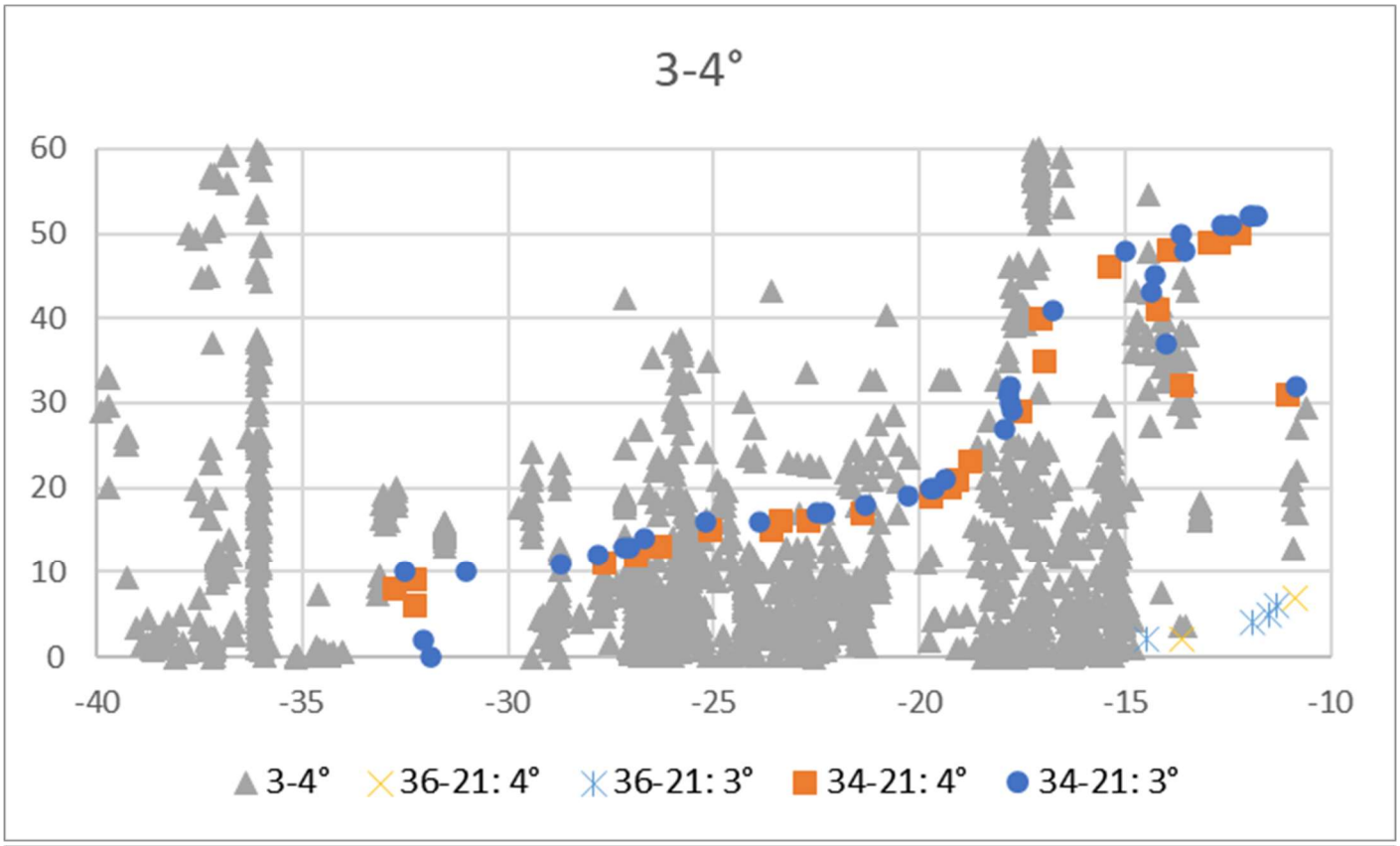
3-4°
60
50
40
30
20
10
0
-40
-35
-30
-25
-20
-15
-10
3-4°
36-21: 4°
36-21: 3°
34-21: 4°
34-21: 3°

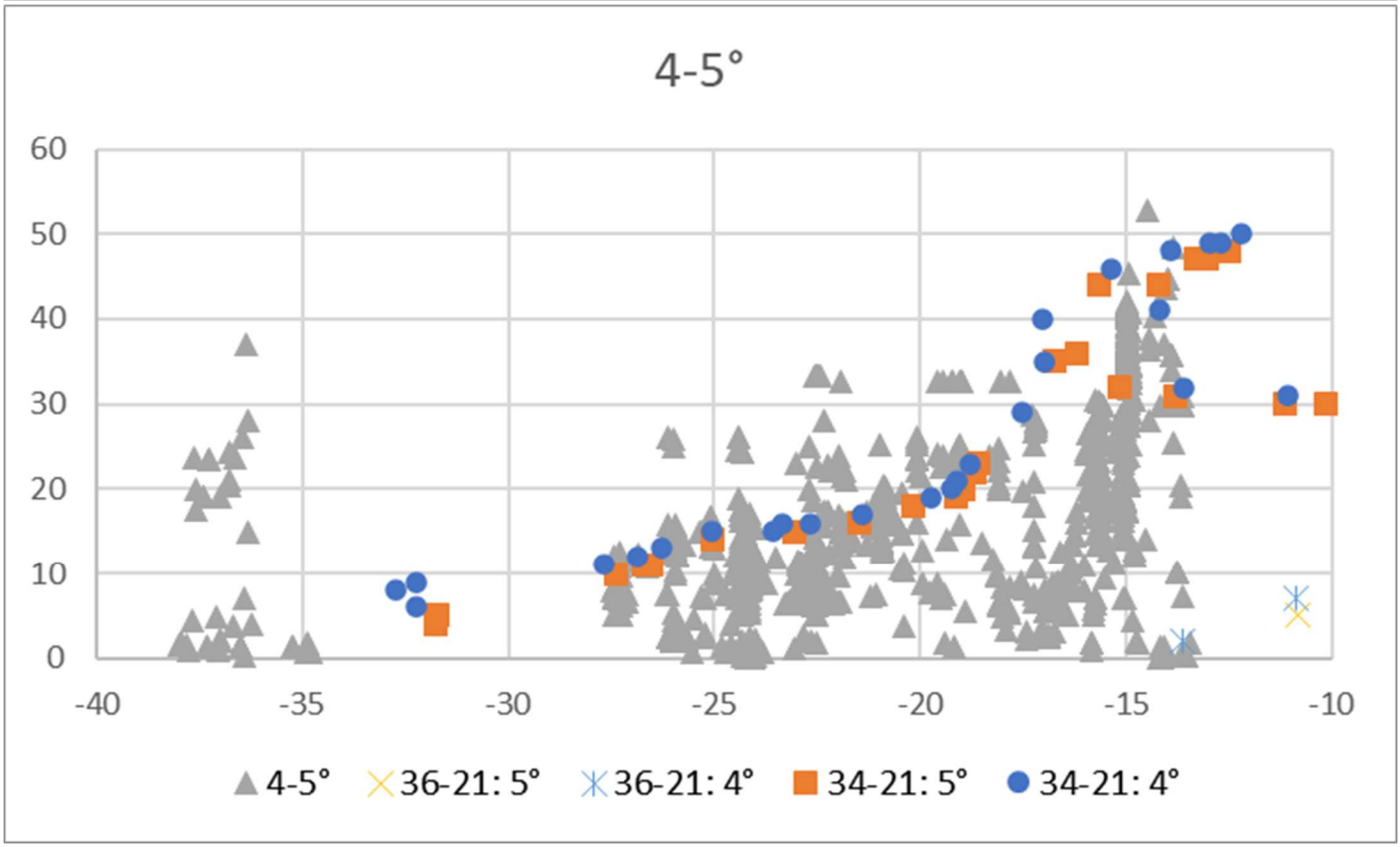
4-5°
60
50
40
30
20
10
0
-40
-35
-30
-25
-20
-15
-10
4-5°
36-21: 5°
36-21: 4°
34-21: 5°
34-21: 4°

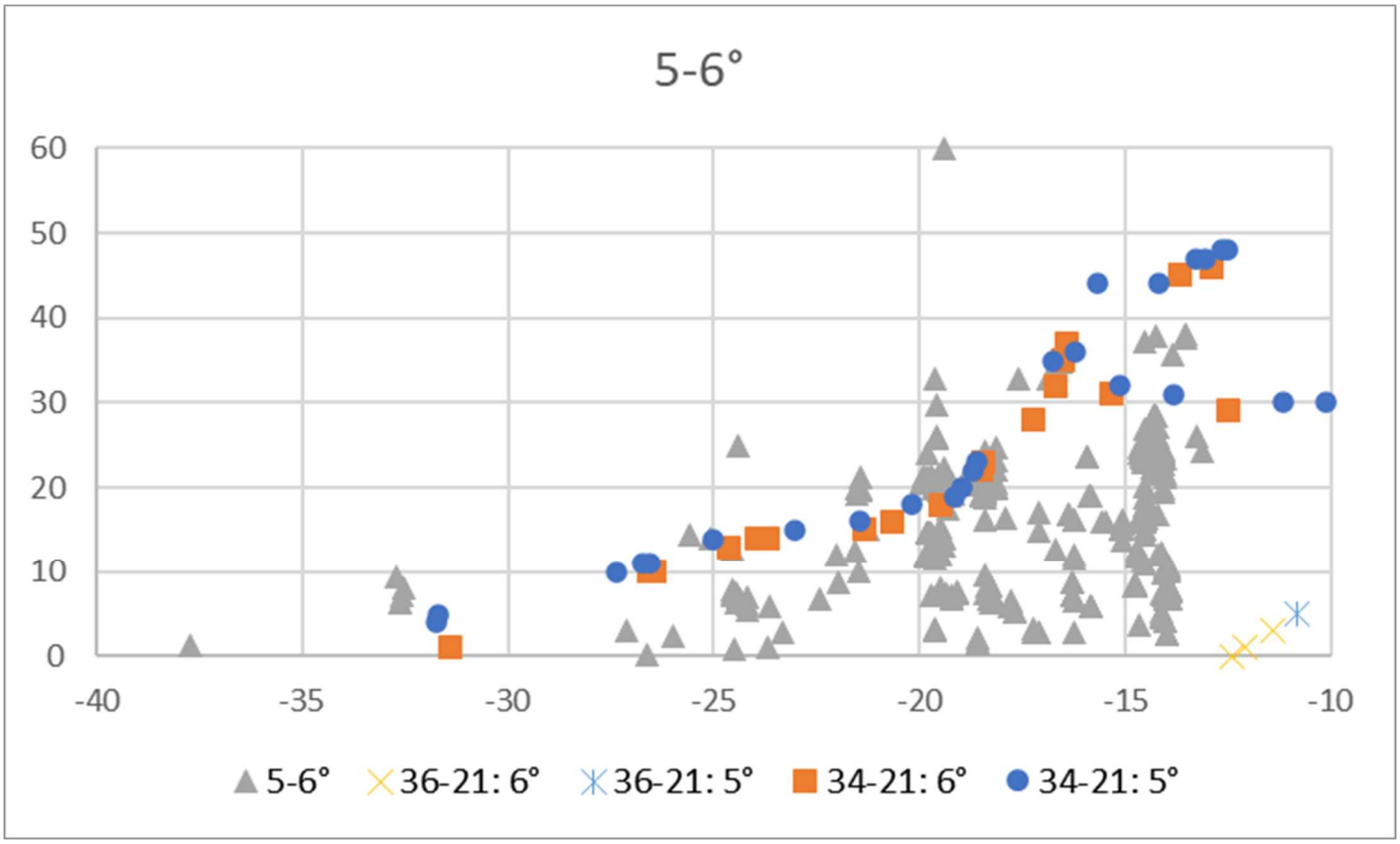

Figure 6b. Close-up graphs as in Figure 6a, showing magmatic patterns and hospot loci intersections. A & B: Easter hotspot. Note apparent cessation of magmatism and predicted trace. C-E: Juan Fernandez . hotspot trace: Note apparent parallelism of onset of mamatism and predicted trace. Might this imply the modeled trace might be a few million years older? See Figures 7 and 8.

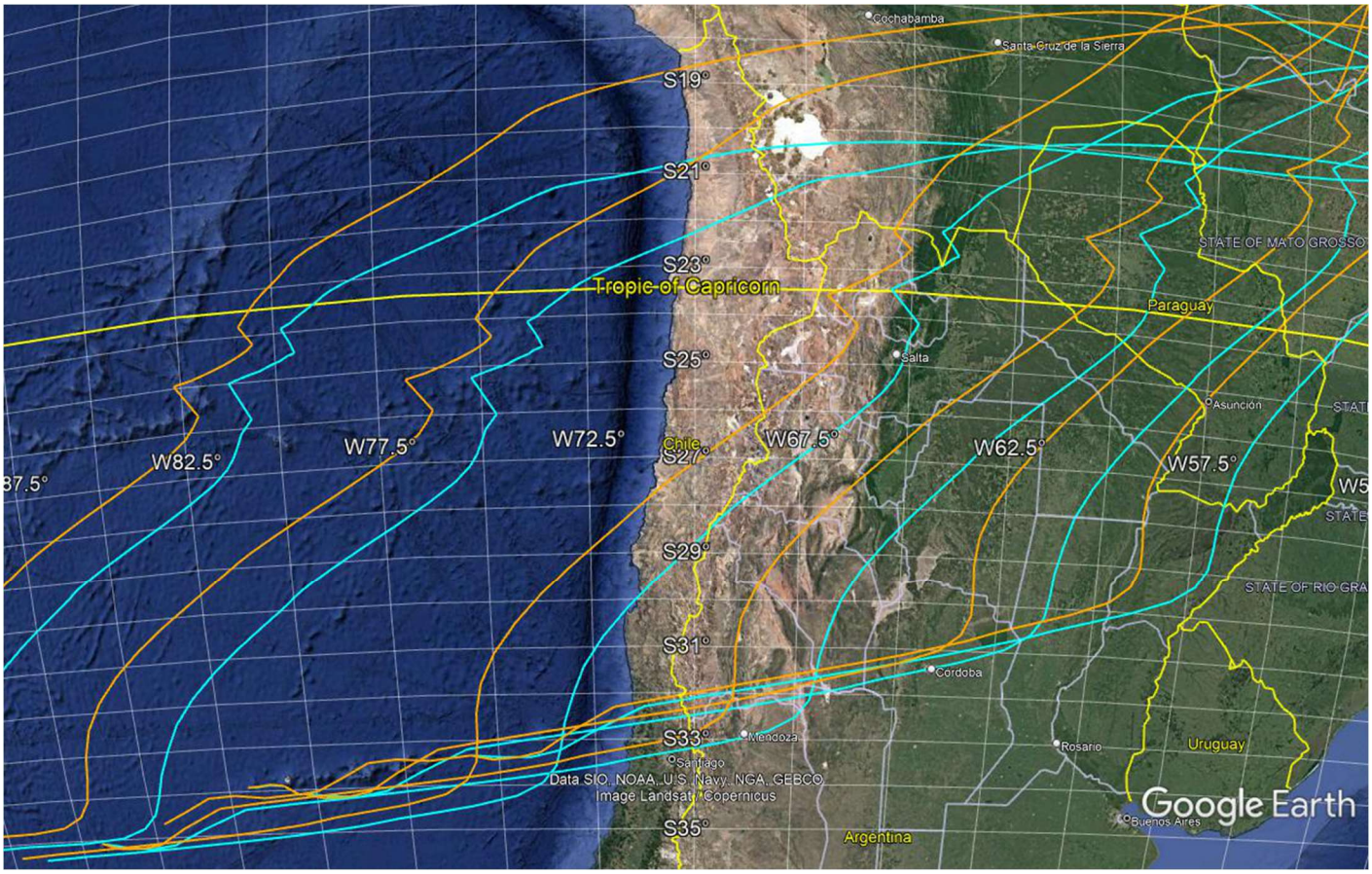

Figure 7. Alternate timing of Juan Fernandez trace loci at 5 m.y. Intervals (youngest to the east), based on older Hawaiian-Emperor bend (2 m.y. older, to 50 Ma - teal; 48 Ma, bend in orange) and older end (85 instead of 80 Ma), resulting in earlier trench-trace intersection between 18 to 30° S Latitude. Parameters of the Pacific traces are the same; only the timing has been modified resulting in 2-3 m.y. earlier intersection of the trace and trench 22-30° S (relative to contemporary trench location). Loci have not been adjusted to conform to the subduction zone configuration. Google Earth format (*.kml) files are accessible in Supplementary Data files.

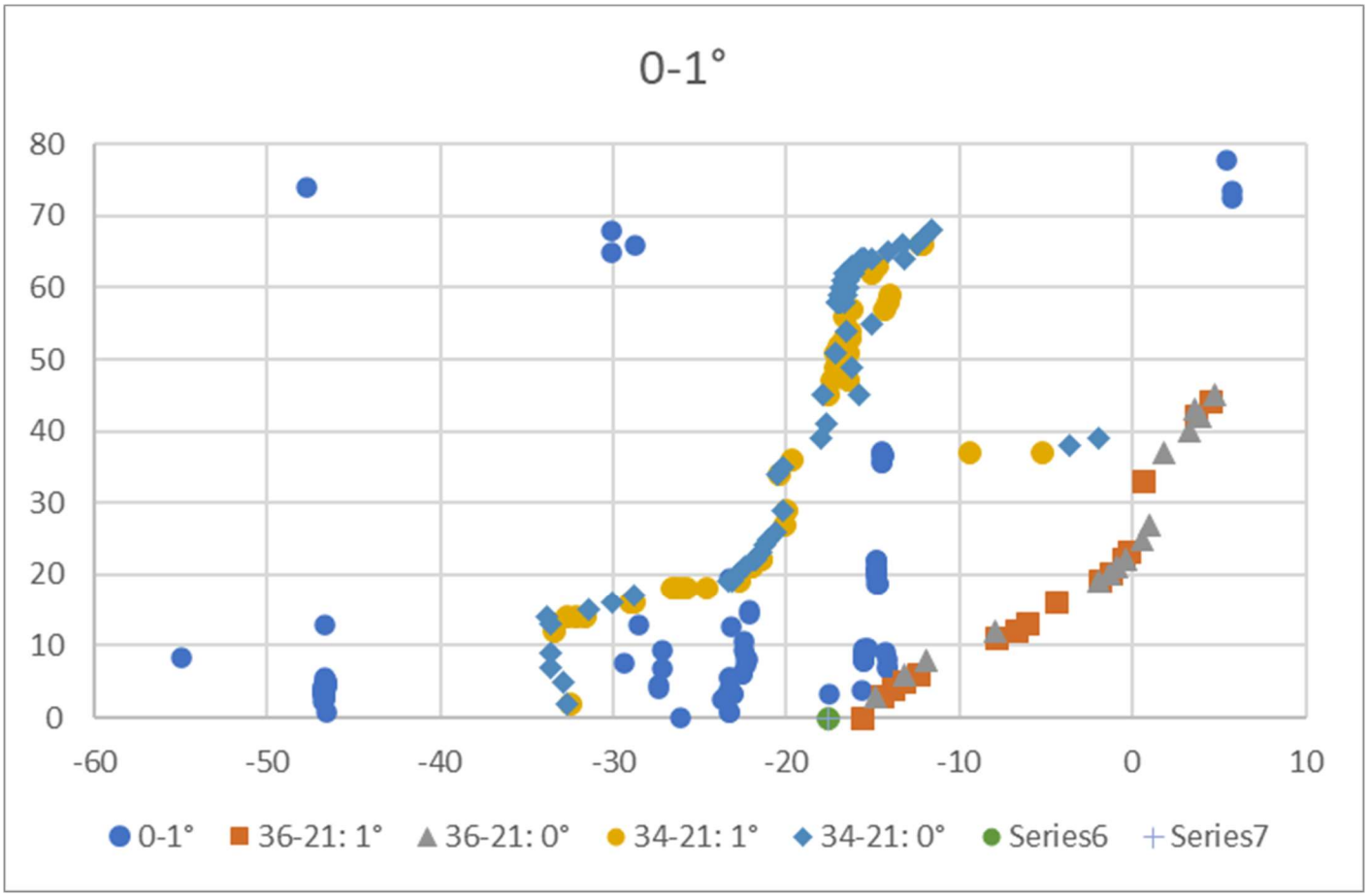
0-1°
80
70
60
50
40
30
20
10
0
-60
-50
-40
-30
-20
-10
0
10
0-1°
36-21: 1°
36-21: 0°
34-21: 1°
34-21: 0°
Series6
Series7

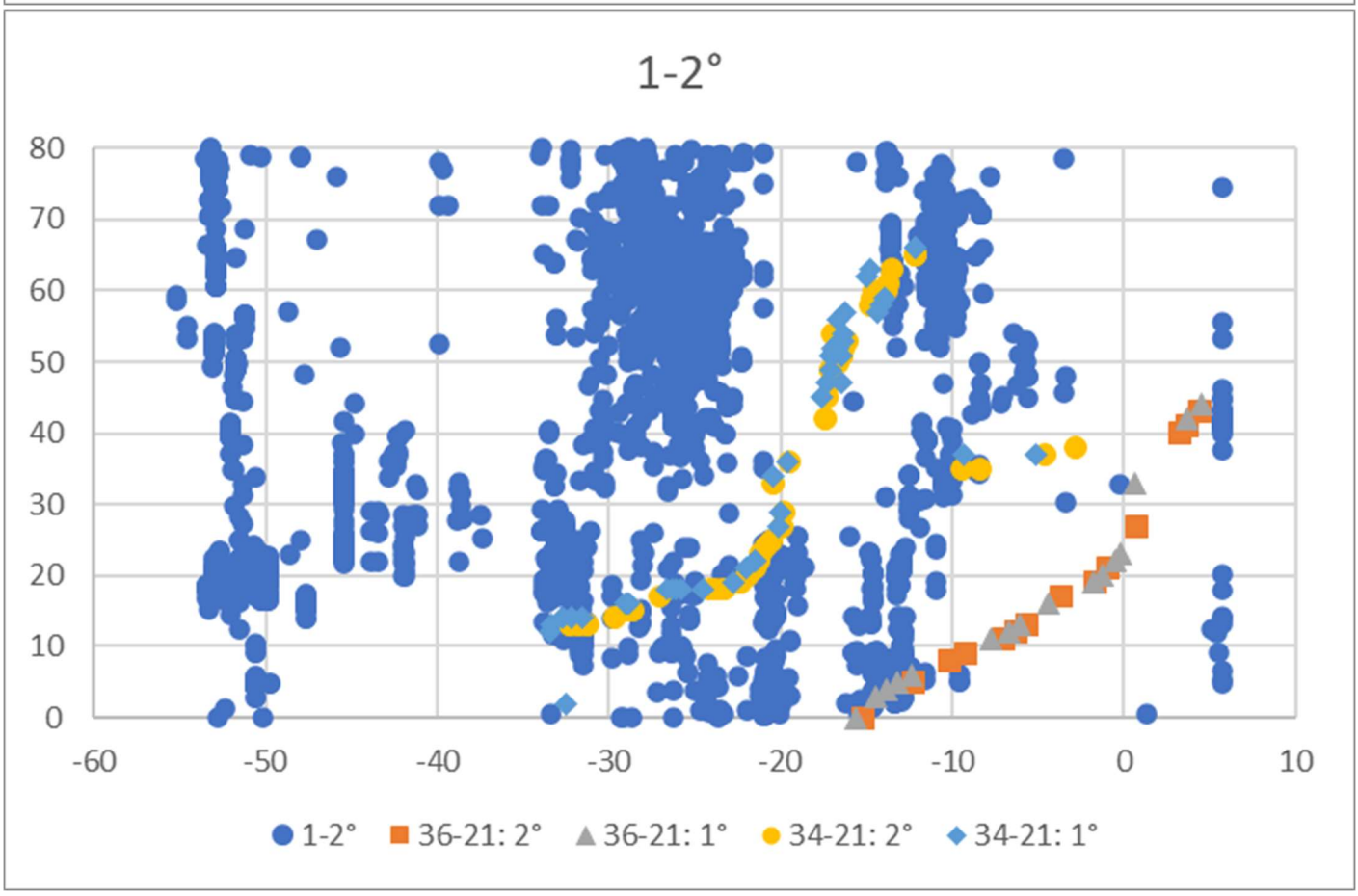
1-2°
80
70
60
50
40
30
20
10
0
-60
-50
-40
-30
-20
-10
0
10
1-2°
36-21: 2°
36-21: 1°
34-21: 2°
34-21: 1°

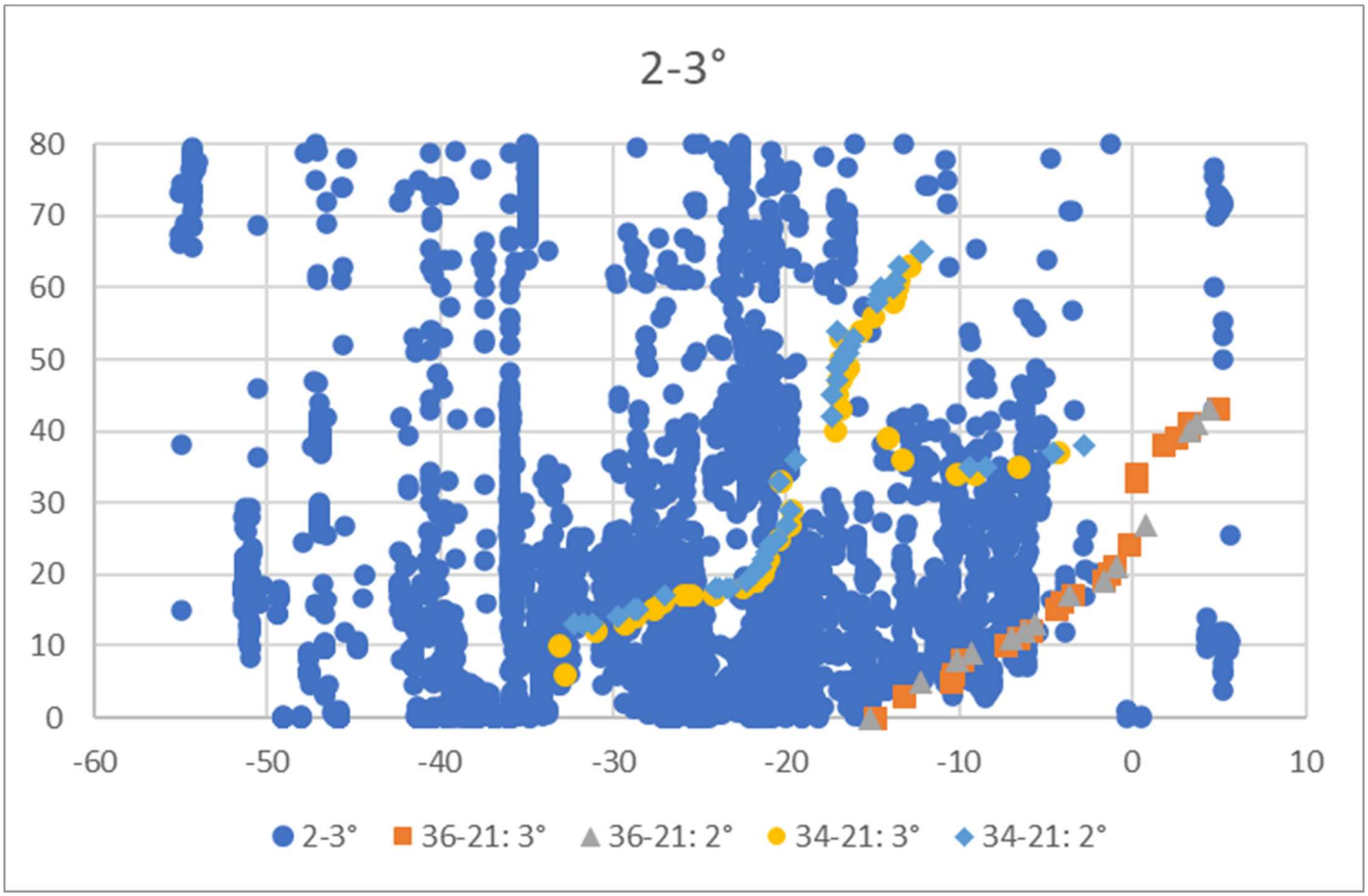
2-3°
80
70
60
50
40
30
20
10
0
-60
-50
-40
-30
-20
-10
0
10
2-3°
36-21: 3°
36-21: 2°
34-21: 3°
34-21: 2°

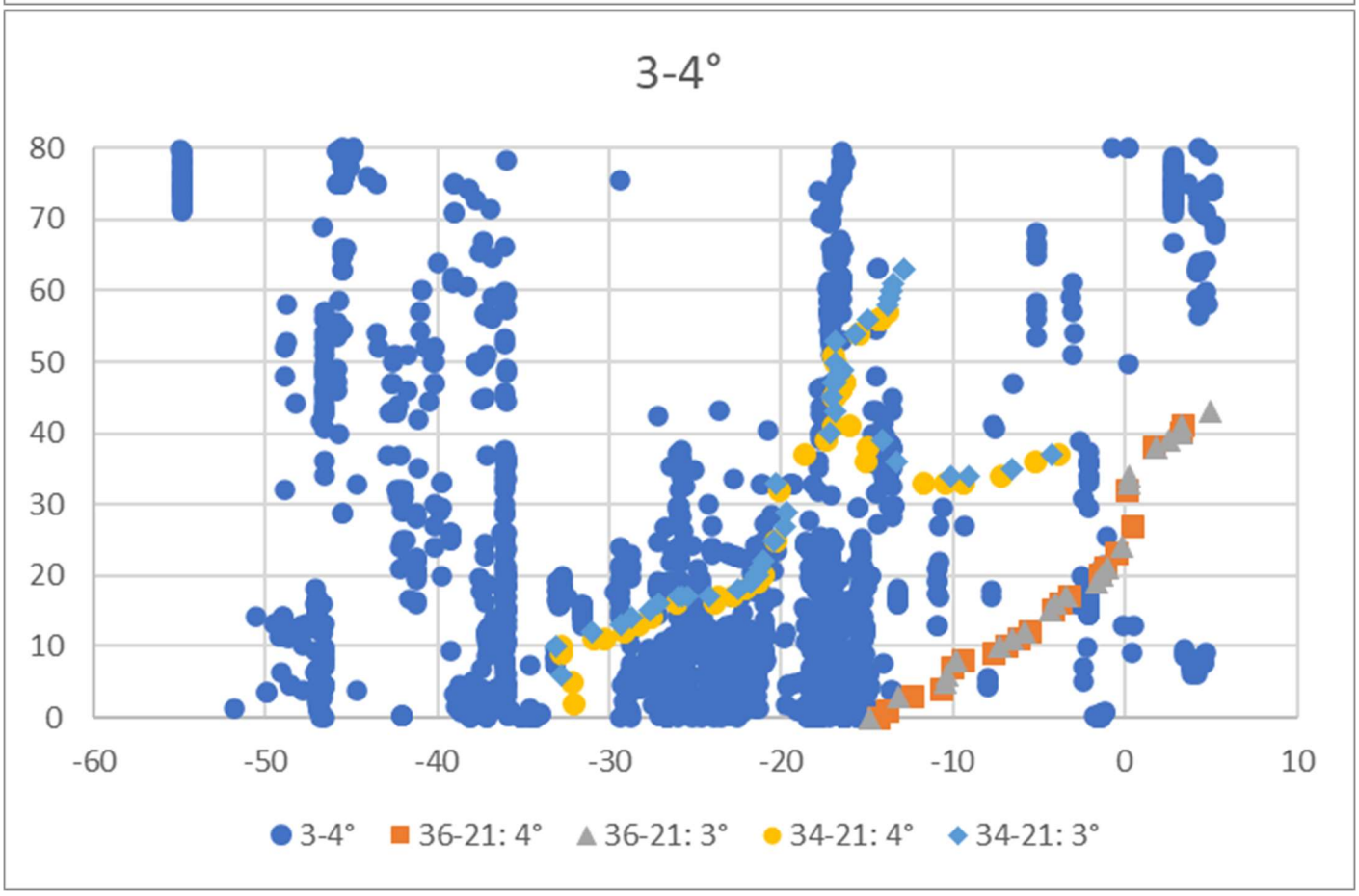
3-4°
80
70
60
50
40
30
20
10
0
-60
-50
-40
-30
-20
-10
0
10
3-4°
36-21: 4°
36-21: 3°
34-21: 4°
34-21: 3°

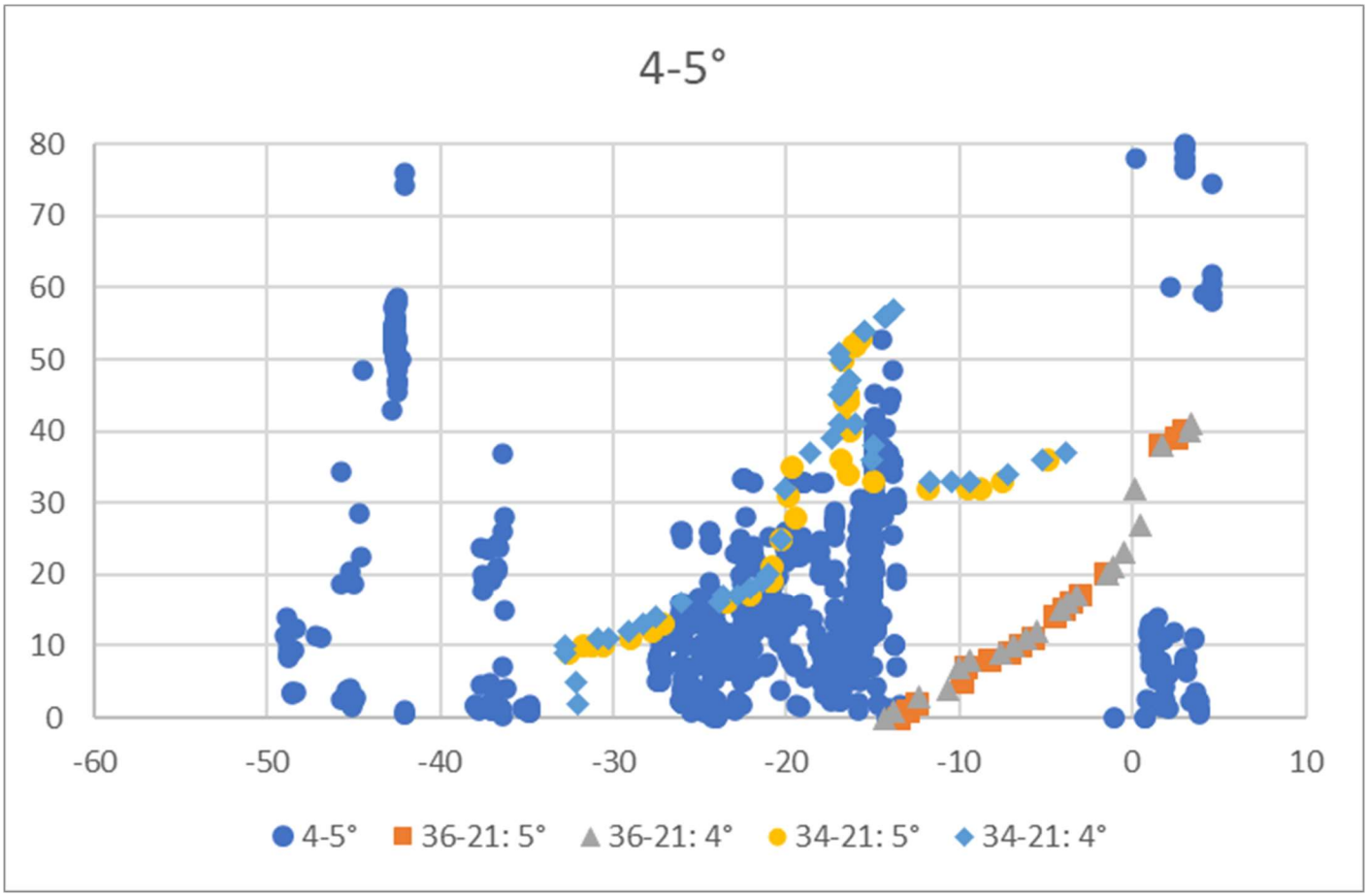
4-5°
80
70
60
50
40
30
20
10
0
-60
-50
-40
-30
-20
-10
0
10
4-5°
36-21: 5°
36-21: 4°
34-21: 5°
34-21: 4°

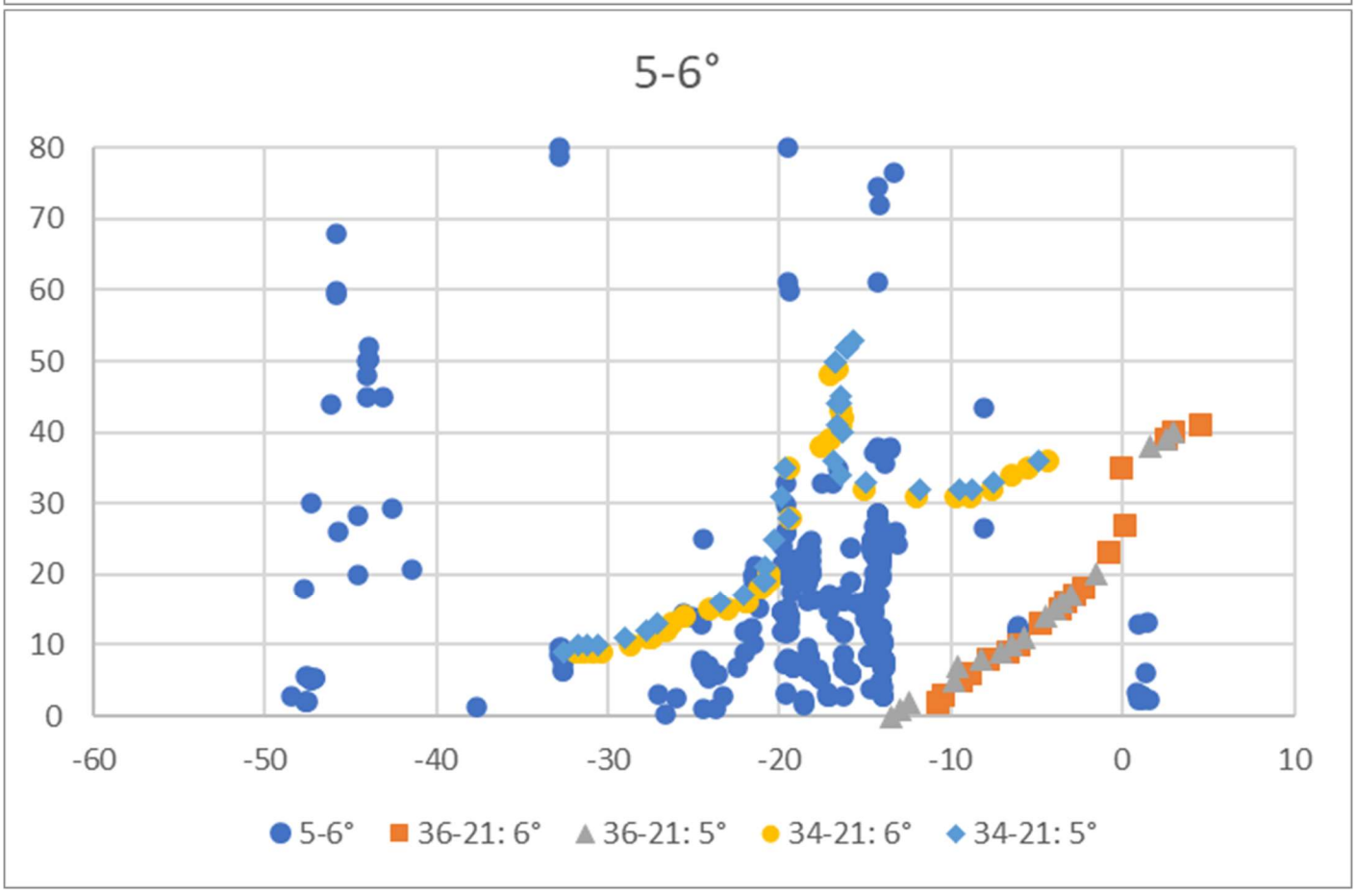
5-6°
80
70
60
50
40
30
20
10
0
-60
-50
-40
-30
-20
-10
0
10
5-6°
36-21: 6°
36-21: 5°
34-21: 6°
34-21: 5°

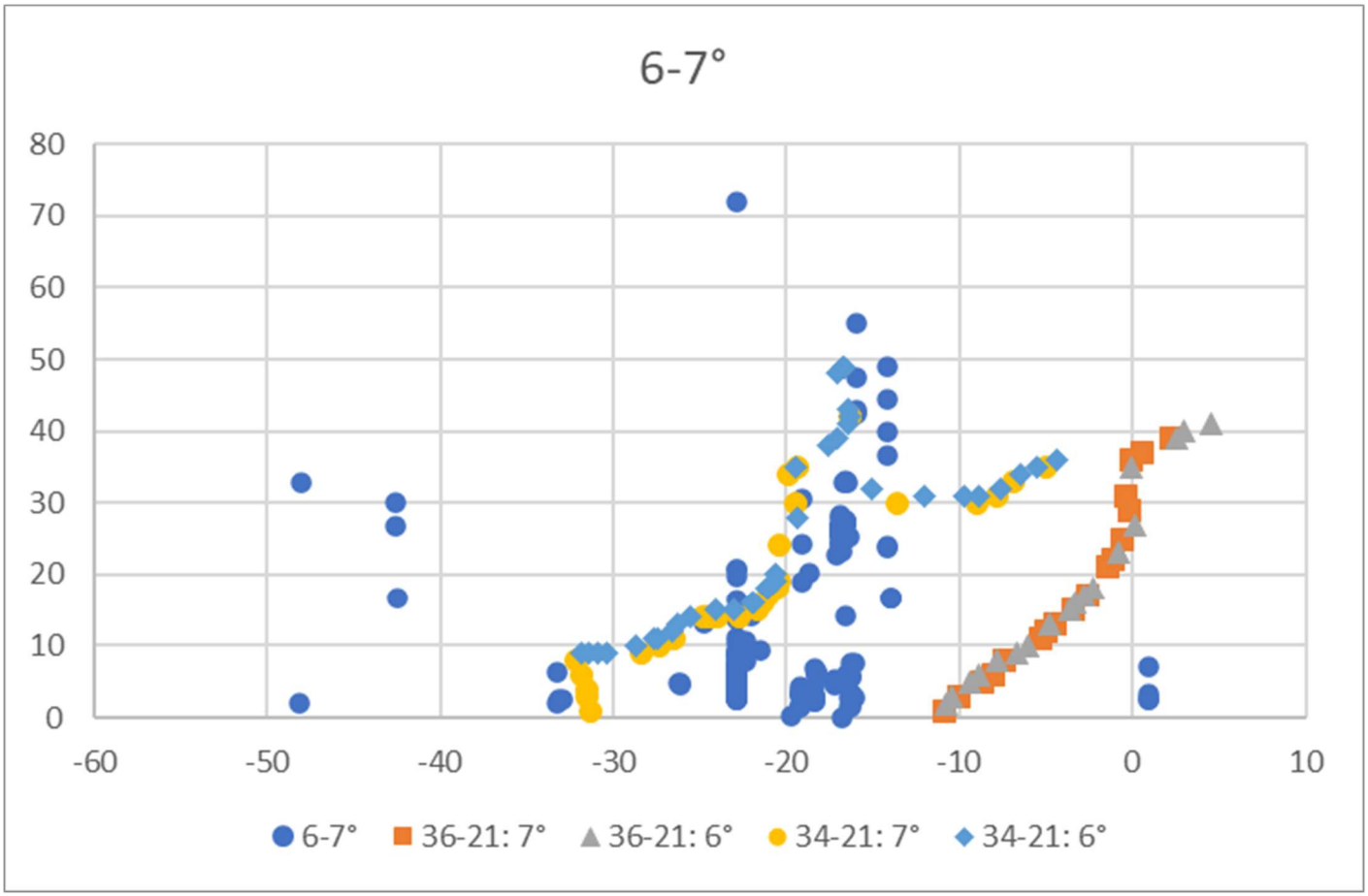
6-7°
80
70
60
50
40
30
20
10
0
-60
-50
-40
-30
-20
-10
0
10
6-7°
36-21: 7°
36-21: 6°
34-21: 7°
34-21: 6°

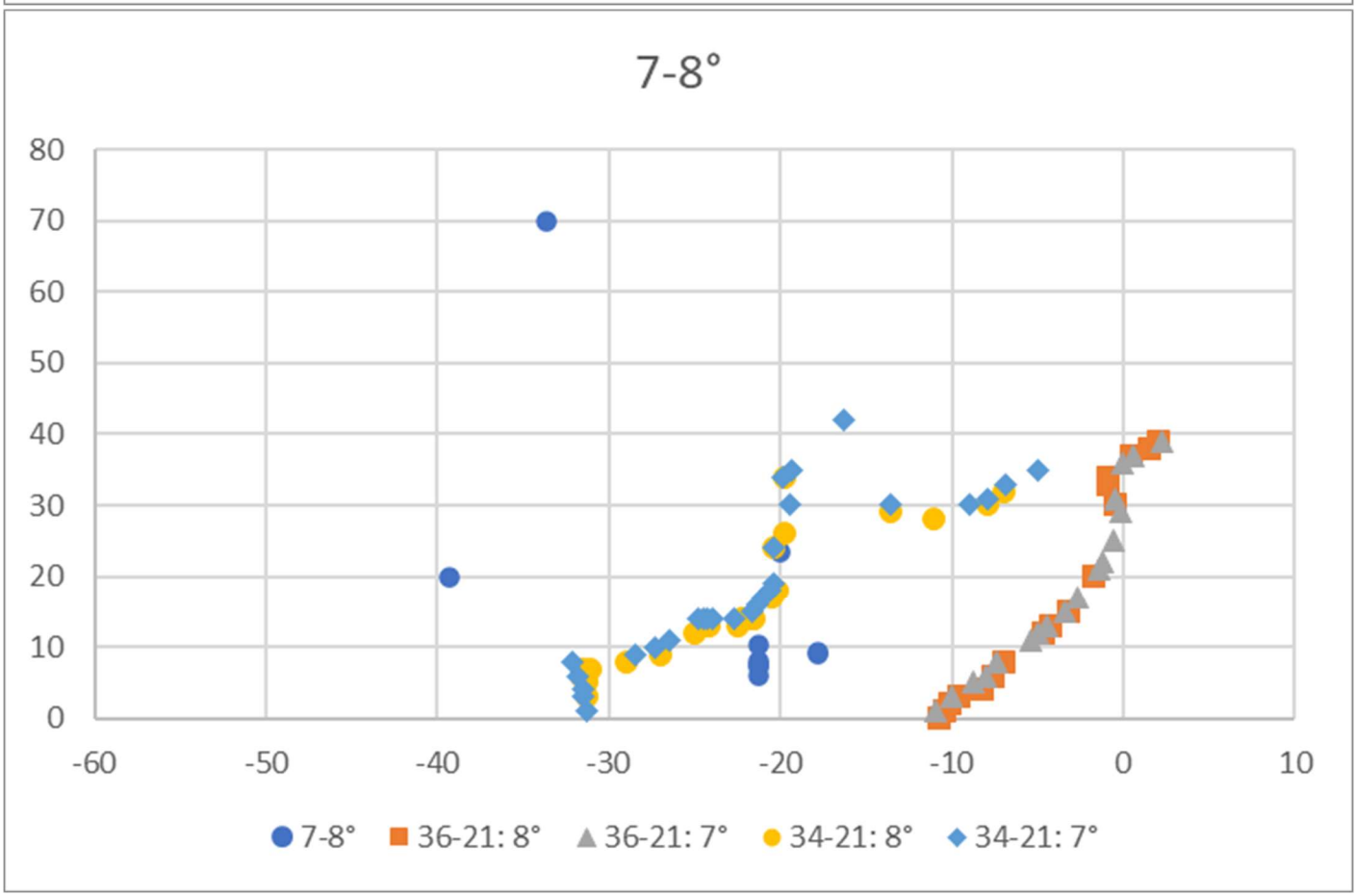
7-8°
80
70
60
50
40
30
20
10
0
-60
-50
-40
-30
-20
-10
0
10
7-8°
36-21: 8°
36-21: 7°
34-21: 8°
34-21: 7°

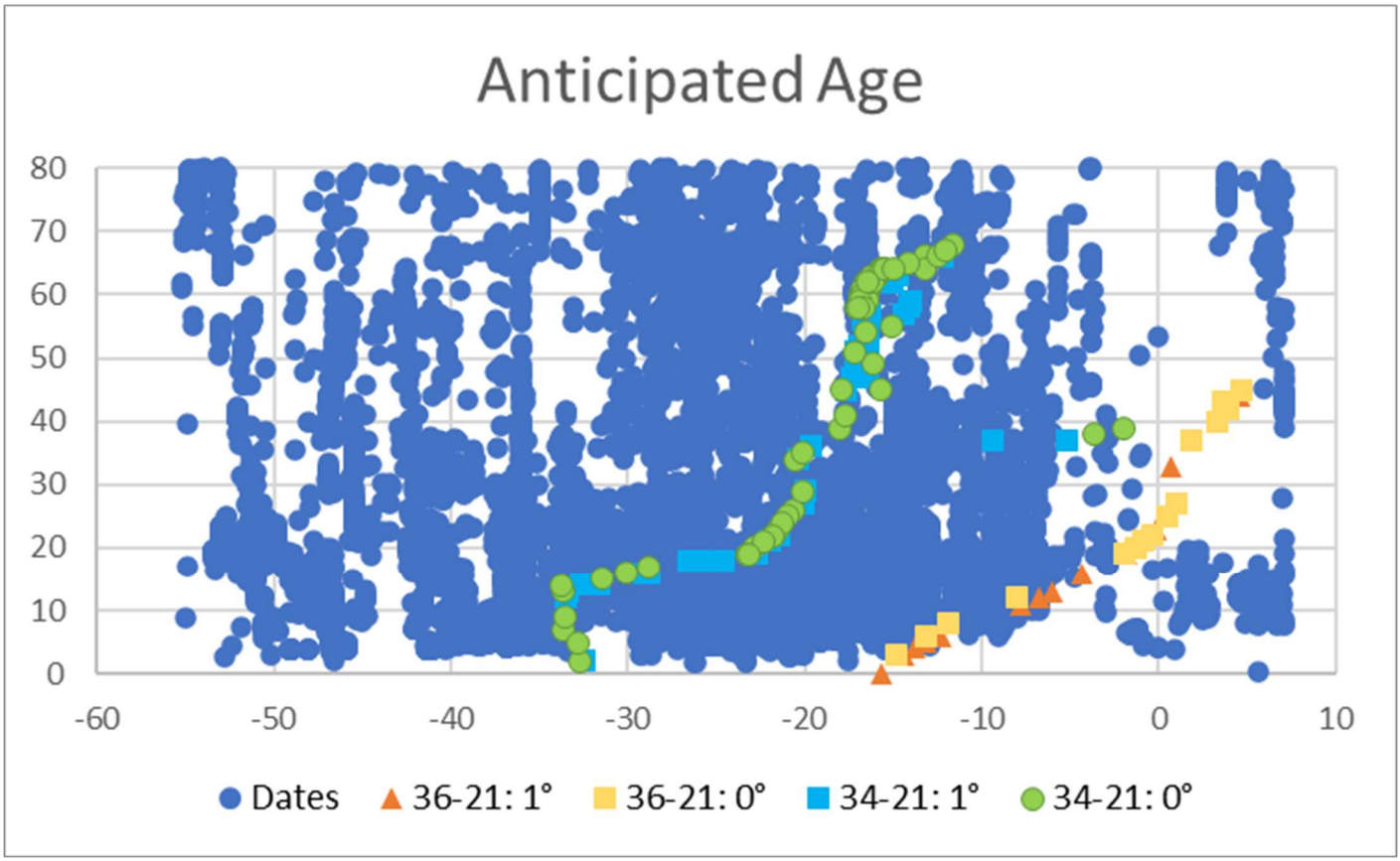

Figure 8. Central Andes isotopic dates in 1° segments from trench with calculated Juan Fernandez loci for older GWB22-older bend (50 Ma) and end (85 Ma) model, at increments of 1° distance from trench. All data are shown in the last diagram, projected to the trench at estimated time of encounter. The similarity in extent of magmatic dates with that of the calculated loci in the segments 8A, C-E, and G is striking. The influence of the hotspot trace may have been comparable to the width of the current low-angle segment. Also, the older part of the trace may be older than Wessel and Kroenke's (2008) initial estimate as the oldest dates in the segments exceed those of the oldest points on the loci. (As noted in Figure 6E, above, there are young dates, < 10 Ma, on igneous rocks from the Pampean Ranges, 4-5° from the trench, that have been reported within the contemporary low-angle subduction zone, but their precise locations are unknown.) Spreadsheet is accessible in Supplementary Data files.

Figure 9. Isotopic dates of silicic to intermediate igneous rocks younger than 5.0 Ma, central and southern Andes. Magmatism from the coast inland into northwestern Argentina extends over 500 km while the central zone of concentrated magmatism along the Andean crest typically exceeds 125 km in width.The western margins of the central zone correspond with the inferred first contact of the subducting Nazca plate with the asthenosphere (compare with Figure 3). Google Earth format (*.kml) files is accessible in Supplementary Data files.

Figure 10. Reconstructed Juan Fernandez trace in (gold) Nazca plate reference frame, extended from Gaastra et al.'s (2022) Pacific-hotspot model, (violet) Atlantic hotspot frame of Müller et al. (1997), and (green) global-averaged hotspot frame of Müller et al. (2019). Google Earth format (*.kml) file is accessible in Supplementary Data files. The differences between the loci are an indirect indication of the discrepancies between the three supposed reference frames, especially comparing small scale variations, which are the same ages. The bend in the JF trace near 30°S, 59°W is approximately 25 Ma, near the time of the breakup of the Farallon plate into the Nazca and Cocos plates and apparent on the other two traces.The "peak" near 18°S, 52°W corresponds with the Hawaiian-Emperor bend, near 50 Ma. At that time there are ~5° and ~7° differences between JF and the Atlantic and JF and global, or an average of ~11 to 15 km per m.y. average displacement between hotspot frames. The calculated average rate of motion of the Nazca plate relative to the JF hotspot is approximately 90 km per m.y. over its full length; relative rates of motion between frames is 12 to 15% of the plate motion rate. And, there is a larger discrepancy between the original Atlantic-Indian frame and the global average frame.

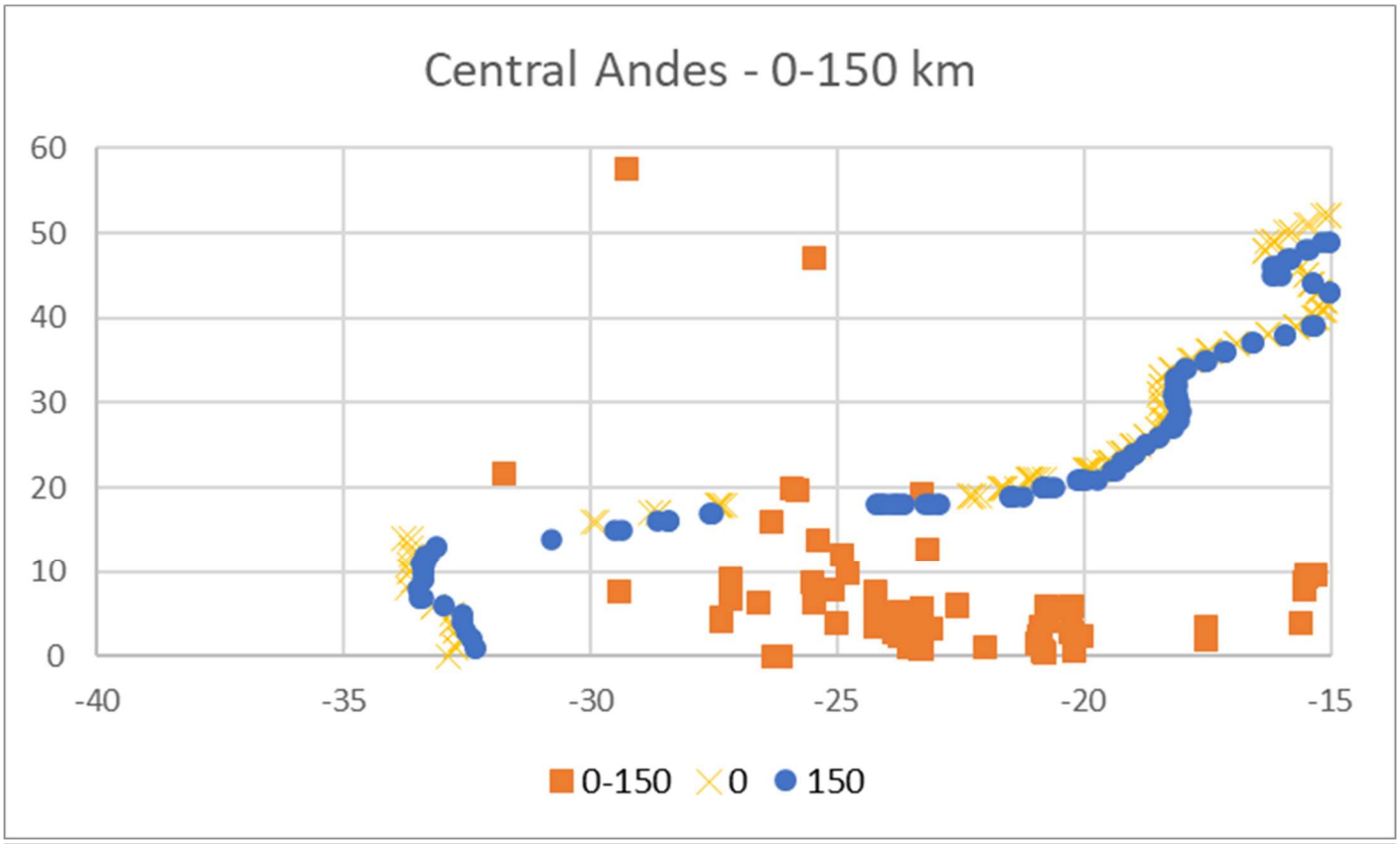
Central Andes - 0-150 km
60
50
40
30
20
10
0
-40
-35
-30
-25
-20
-15
0-150
0
150

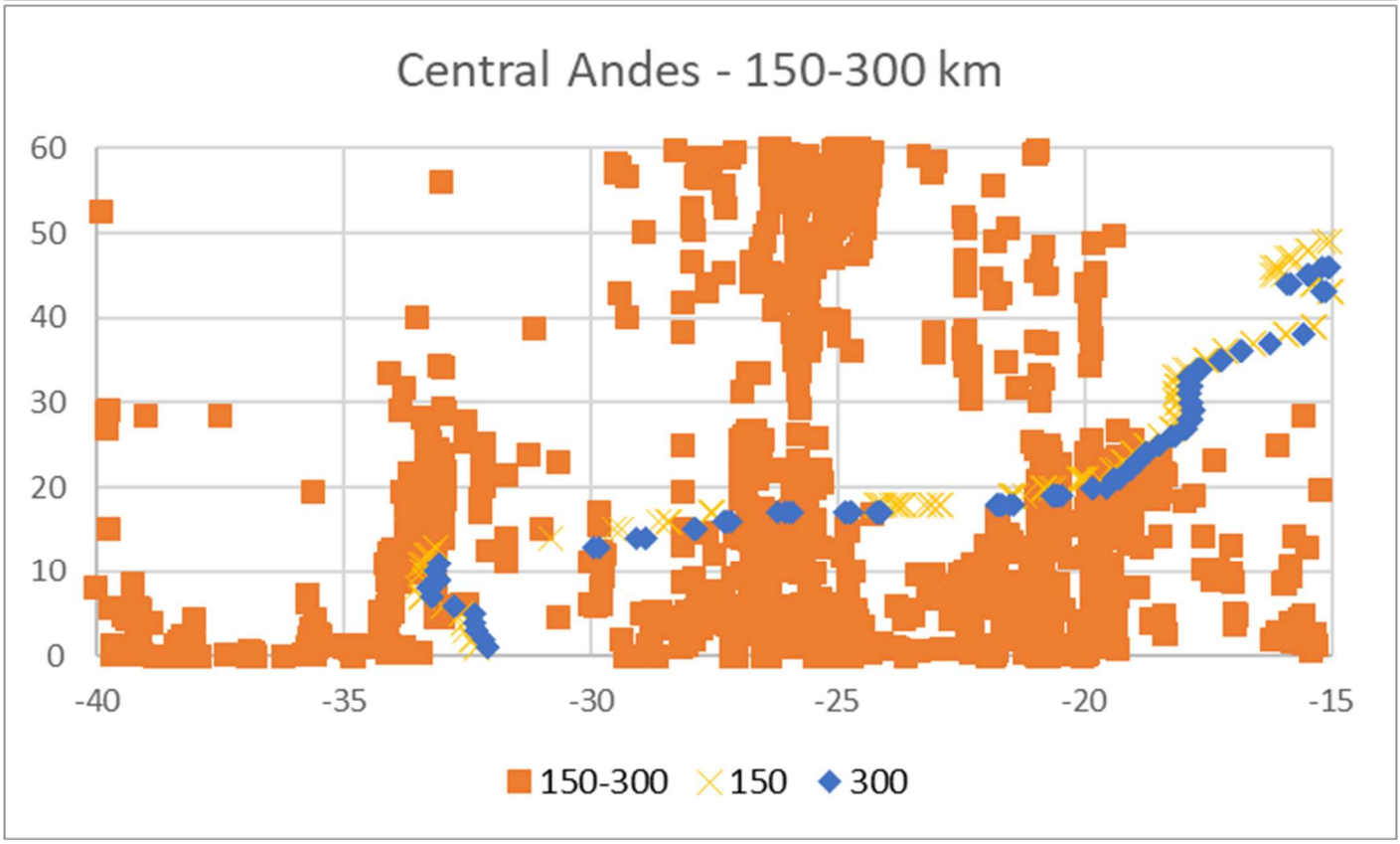
Central Andes - 150-300 km
60
50
40
30
20
10
0
-40
-35
-30
-25
-20
-15
150-300
150
300

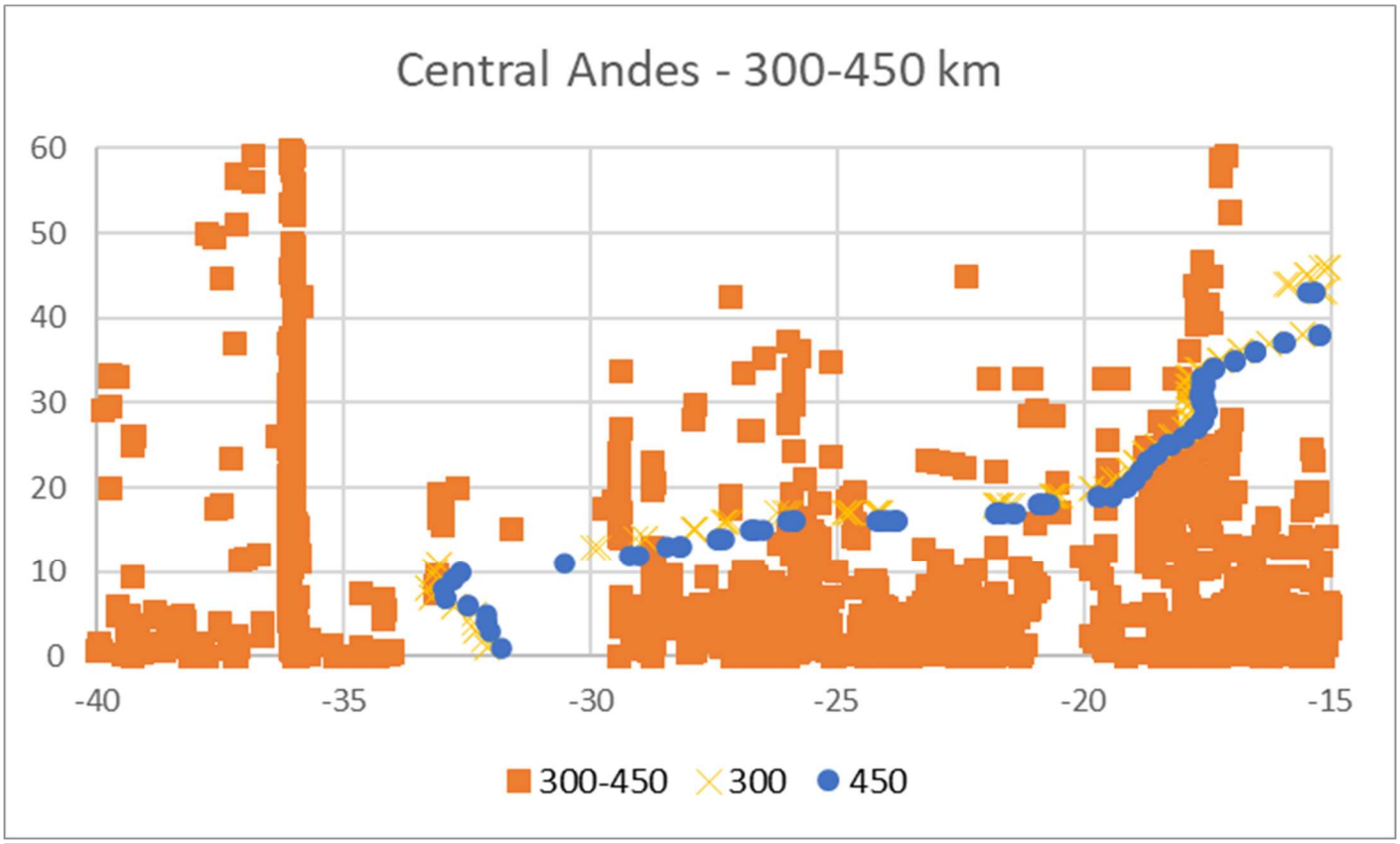
Central Andes - 300-450 km
60
50
40
30
20
10
0
-40
-35
-30
-25
-20
-15
300-450
300
450

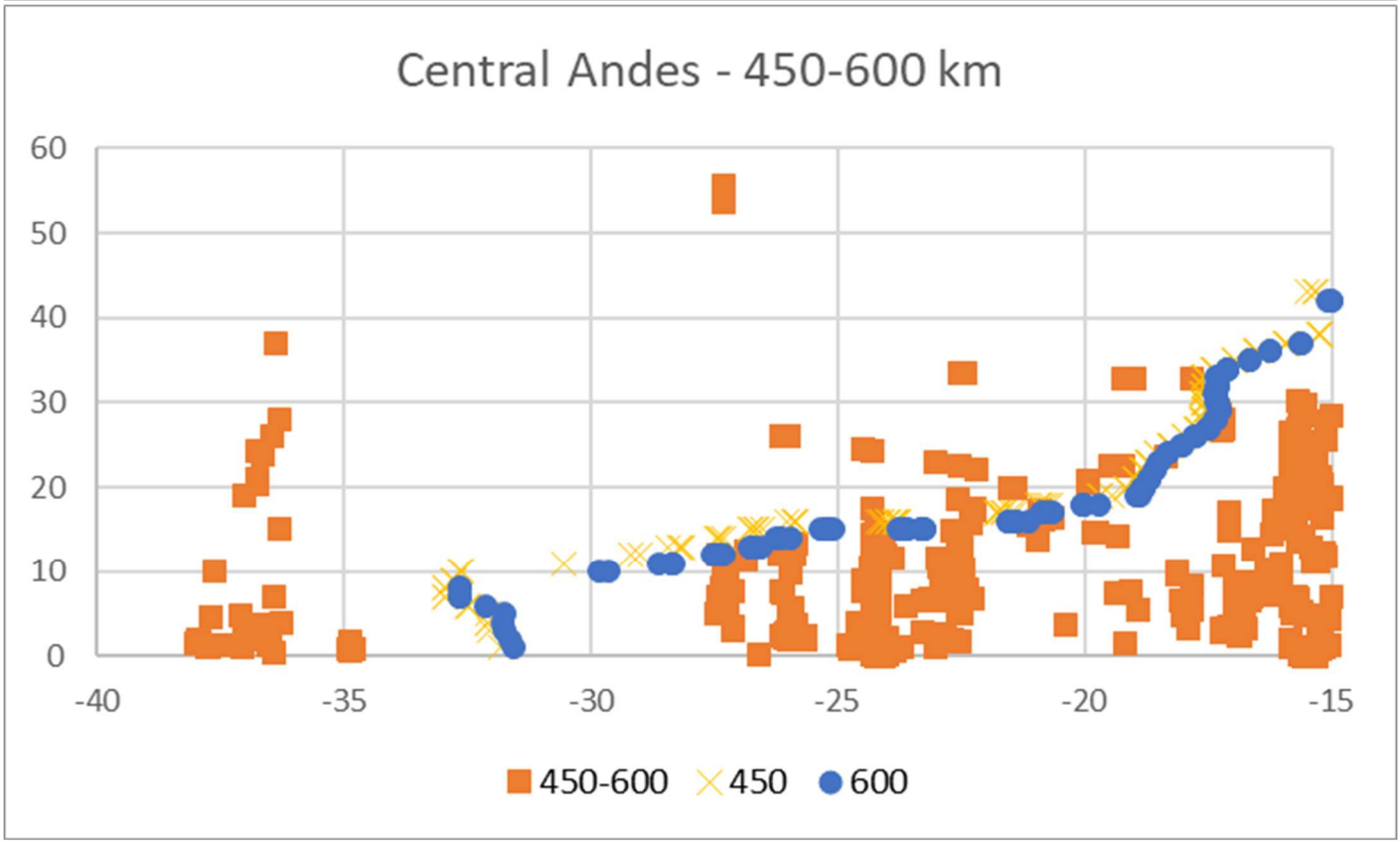
Central Andes - 450-600 km
60
50
40
30
20
10
0
-40
-35
-30
-25
-20
-15
450-600
450
600

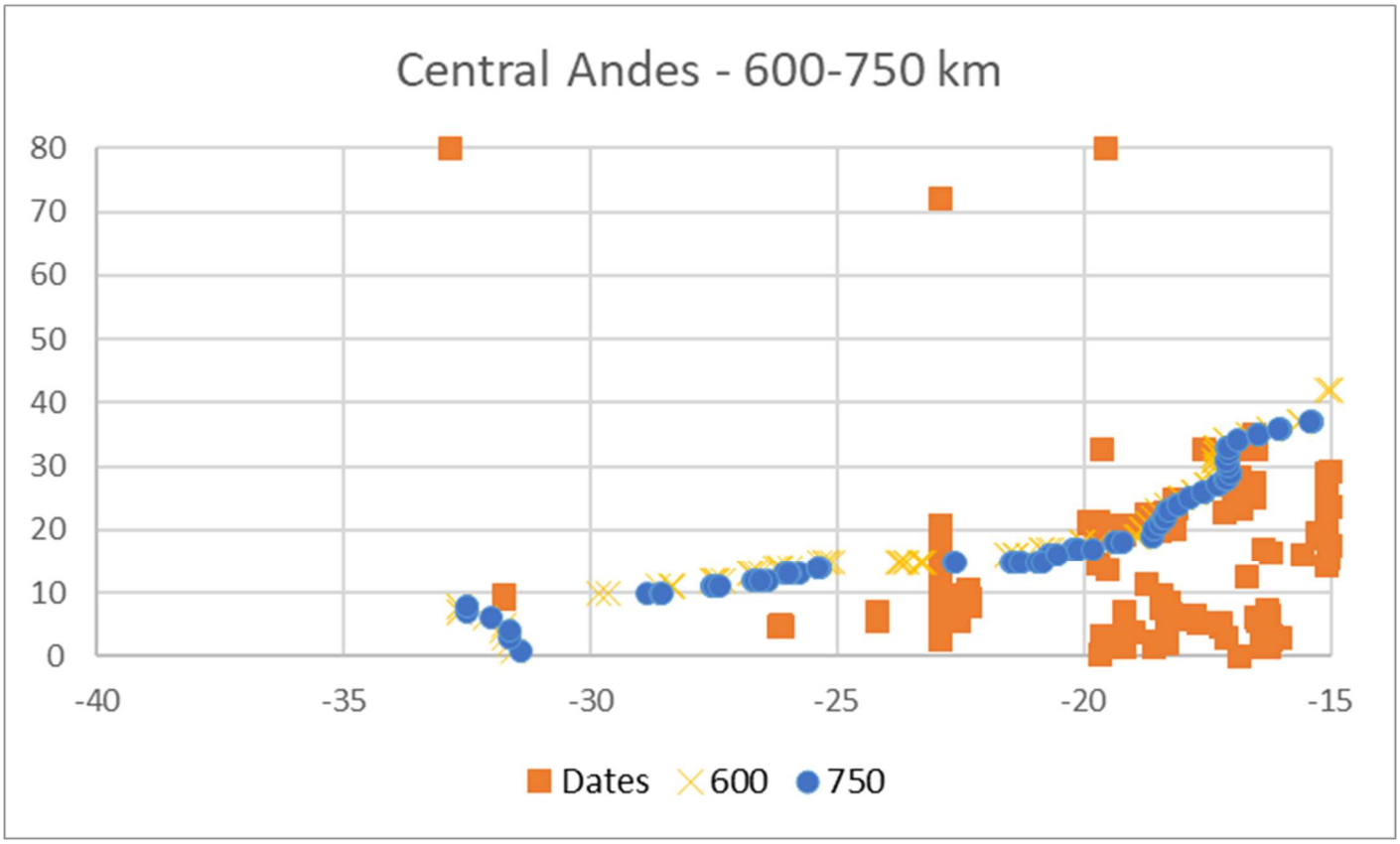

Figure 11. Central and southern Andes isotopic dates and calculated intersections of Atlantic-Indian (Tristan) model of Juan Fernandez hotspot trace (Muller et al., 1997) with trench-parallel lines, top to bottom: segments Spreadsheets are accessible in Supplementary Data files.

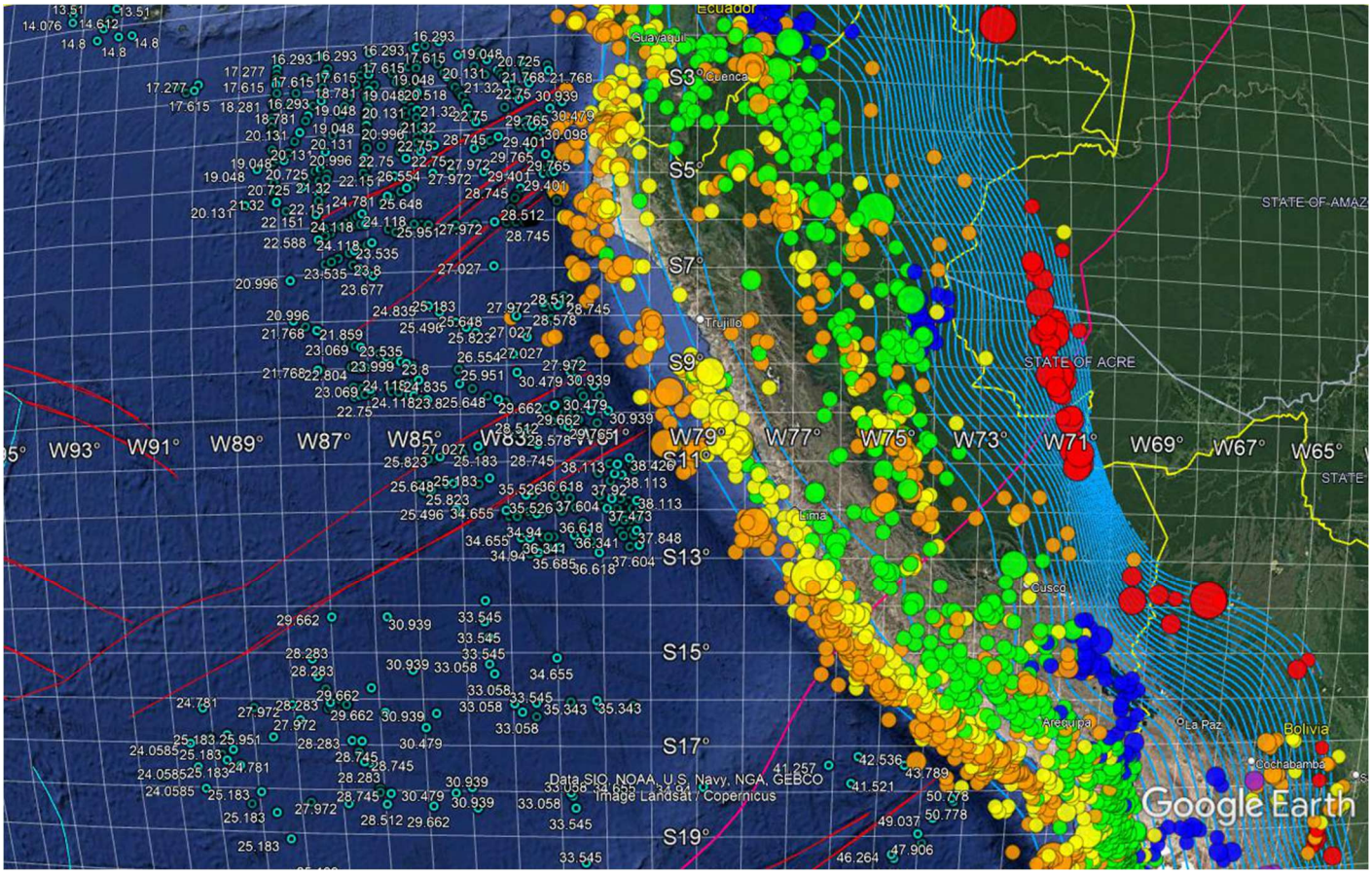

Figure 12. USGS earthquakes, SLAB configuration (Hayes et al., 2018), dated isochrons and mapped fracture zones (Seton et al., 2014, with links), and calculated locus of the Easter-Nazca ridge (this paper), Peru and adjacent areas. Note the end of the fracture zone in the trench at 10.3°S latitude. Chrons on the northwest side are ~7 m.y. Younger; and, similarly, the next fracture zone north, 9°S, separates plate ~3 m.y. younger on the north from that on the south. Younger plate subducts at lower angles than does older plate (see, e.g, southern Chile subduction zone).

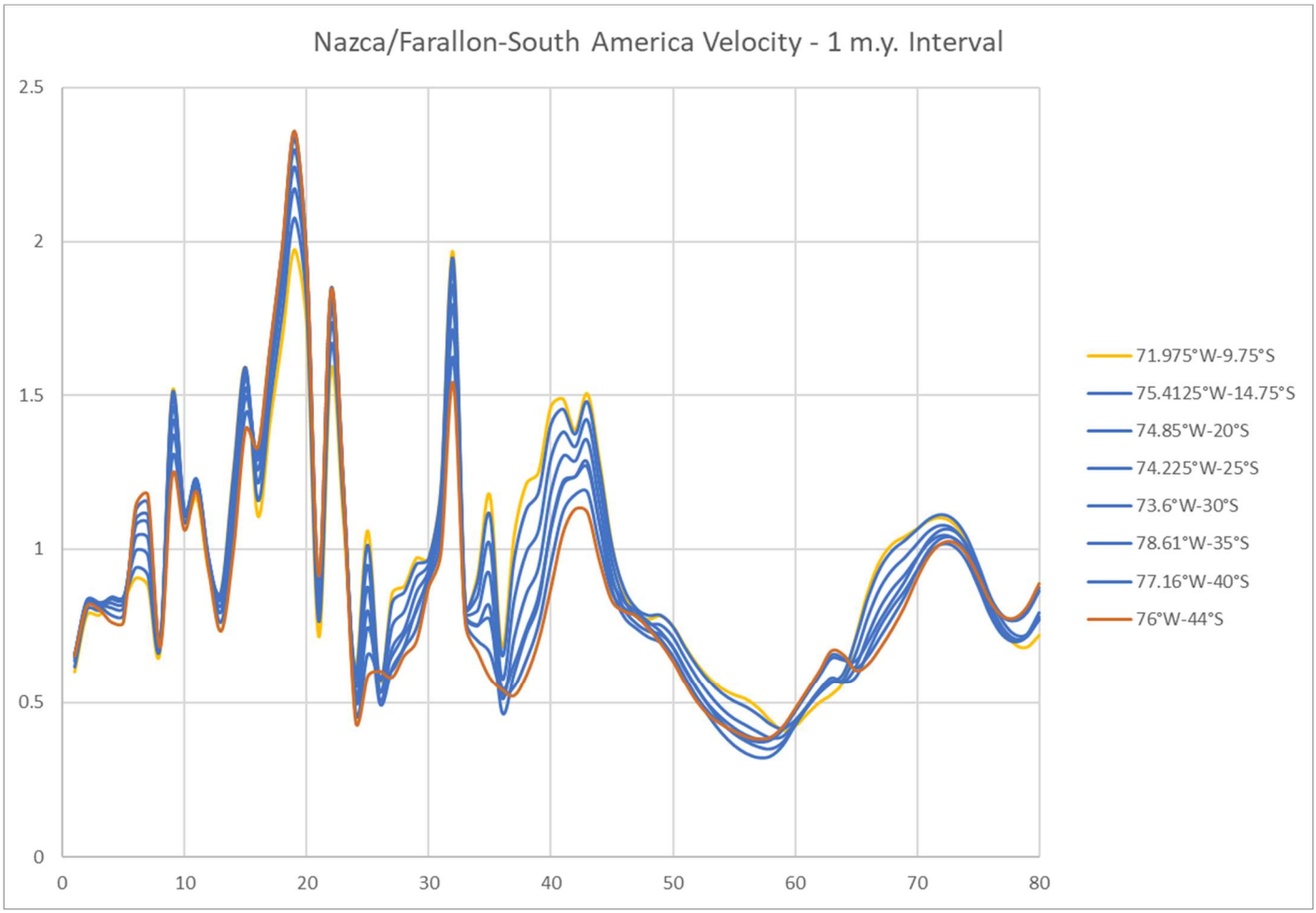
Nazca/Farallon-South America Velocity - 1 m.y. Interval
2.5
2
1.5
1
0.5
0
0
10
20
30
40
50
60
70
80
71.975°W-9.75°S
75.4125°W-14.75°S
74.85°W-20°S
74.225°W-25°S
73.6°W-30°S
78.61°W-35°S
77.16°W-40°S
76°W-44°S

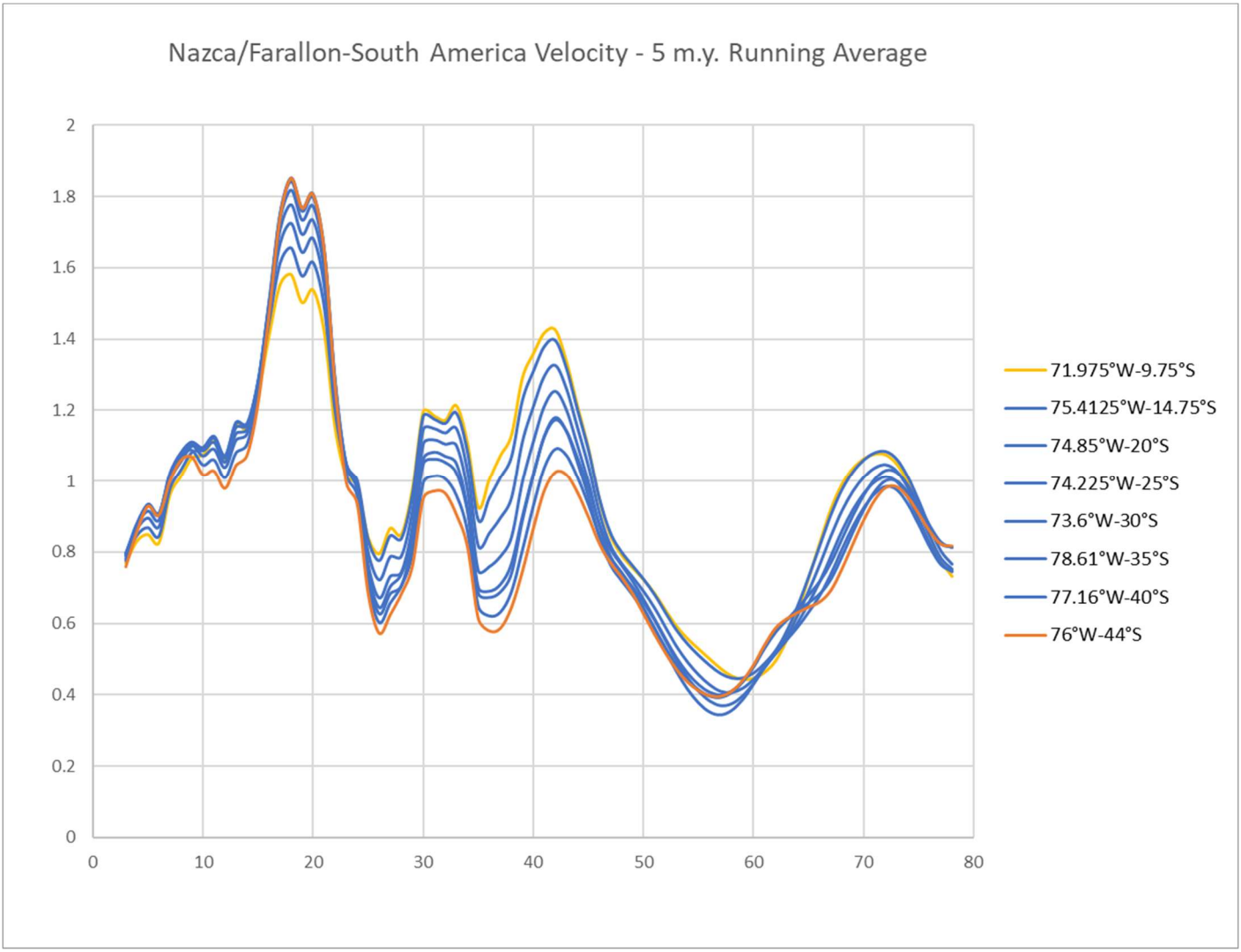

Figure 13. (Top to bottom:) a. Calculated total convergence rate, Nazca to South American plate, 80-0 Ma, calculated at 1 m.y. interval, deg of arc per m.y., at indicated points along the contemporary trench. b. Total convergence rate, as a, at 5 m.y., moving average. Spreadsheet is accessible in Supplementary Data files.

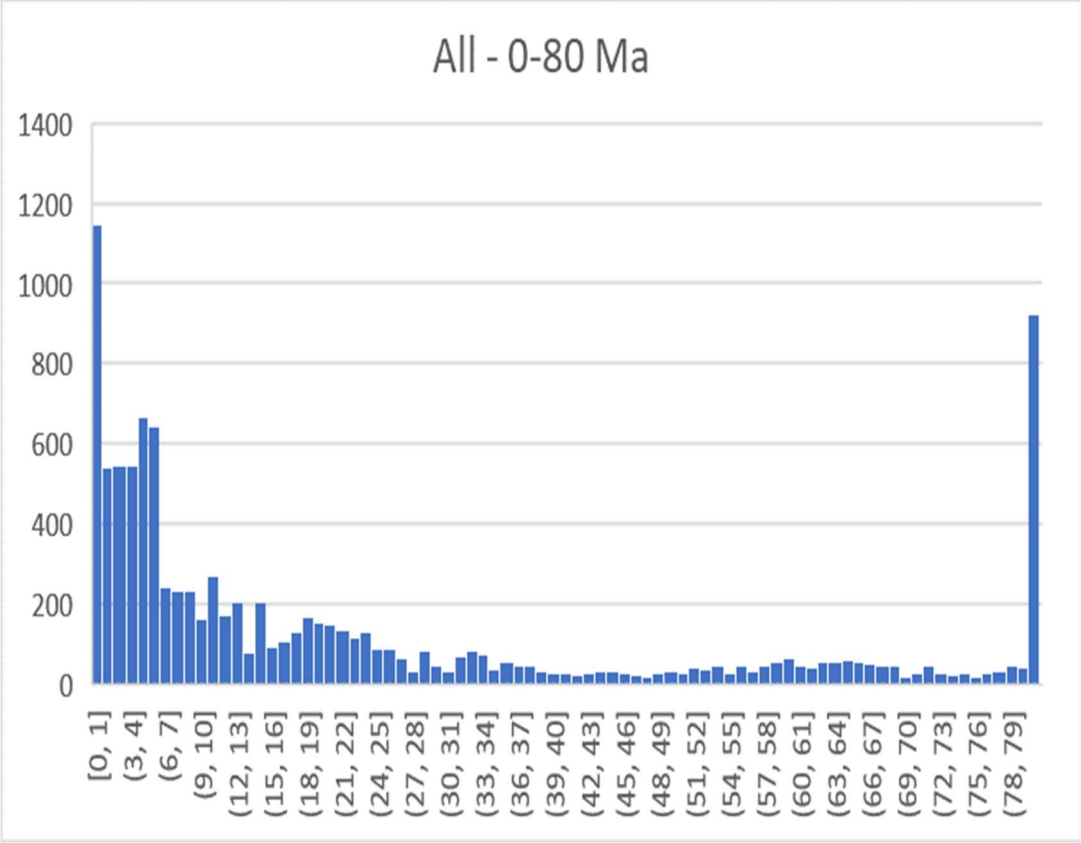
All - 0-80 Ma
1400
1200
1000
800
600
400
200
0
[0, 1]
(3, 4]
(6, 7]
(9, 10]
(12, 13]
(15, 16]
(18, 19]
(21, 22]
(24, 25]
(27, 28]
(30, 31]
(33, 34]
(36, 37]
(39, 40]
(42, 43]
(45, 46]
(48, 49]
(51, 52]
(54, 55]
(57, 58]
(60, 61]
(63, 64]
(66, 67]
(69, 70]
(72, 73]
(75, 76]
(78, 79]

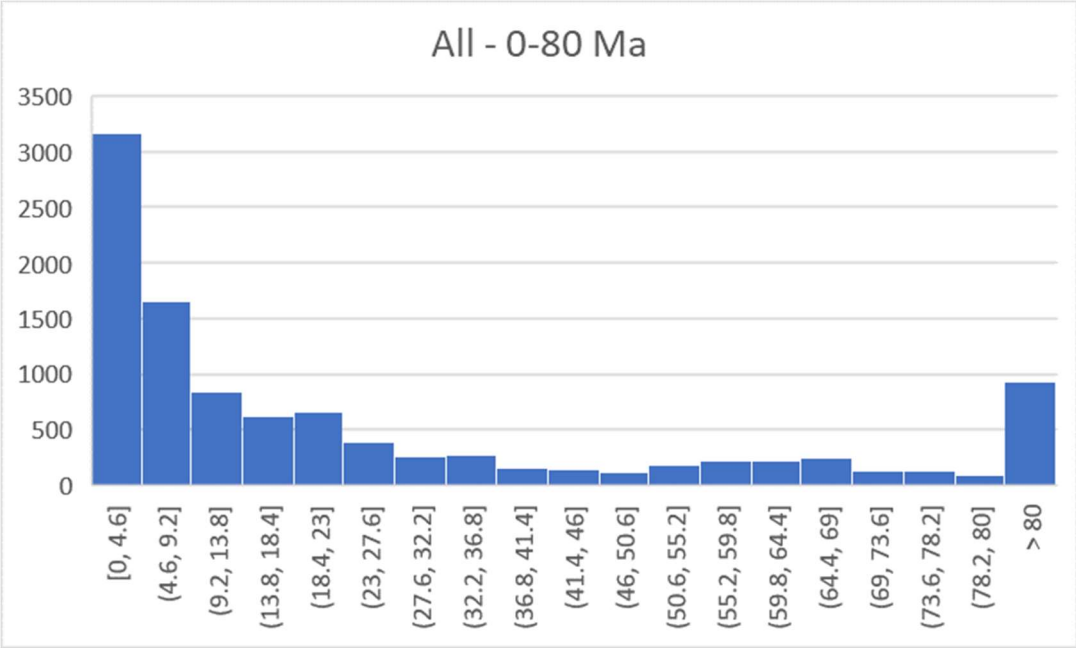
All - 0-80 Ma
3500
3000
2500
2000
1500
1000
500
0
[0, 4.6]
(4.6, 9.2]
(9.2, 13.8]
(13.8, 18.4]
(18.4, 23]
(23, 27.6]
(27.6, 32.2]
(32.2, 36.8]
(36.8, 41.4]
(41.4, 46]
(46, 50.6]
(50.6, 55.2]
(55.2, 59.8]
(59.8, 64.4]
(64.4, 69]
(69, 73.6]
(73.6, 78.2]
(78.2, 80]
> 80

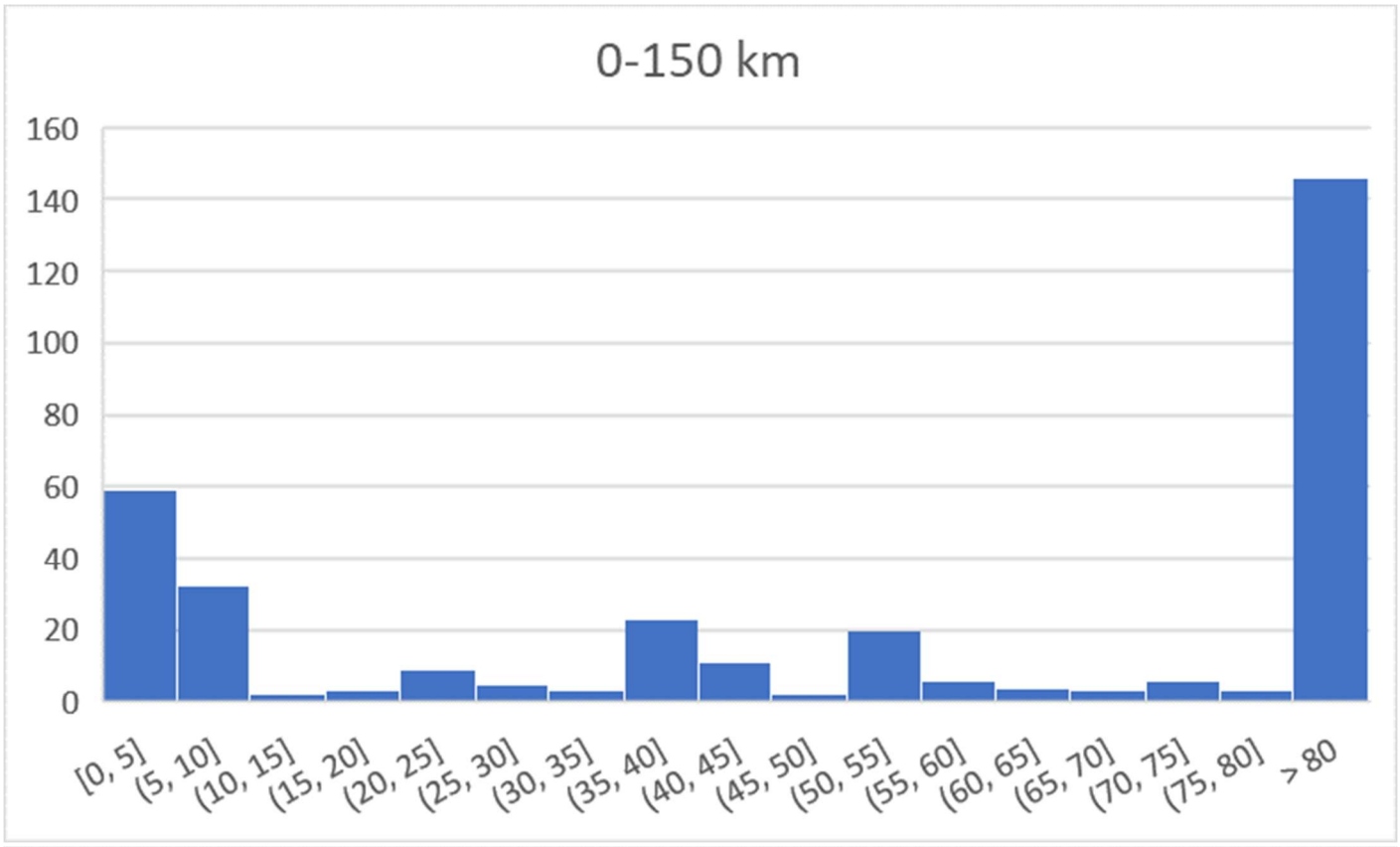
0-150 km
160
140
120
100
80
60
40
20
0
[0, 5]
(5, 10]
(10, 15]
(15, 20]
(20, 25]
(25, 30]
(30, 35]
(35, 40]
(40, 45]
(45, 50]
(50, 55]
(55, 60]
(60, 65]
(65, 70]
(70, 75]
(75, 80]
> 80

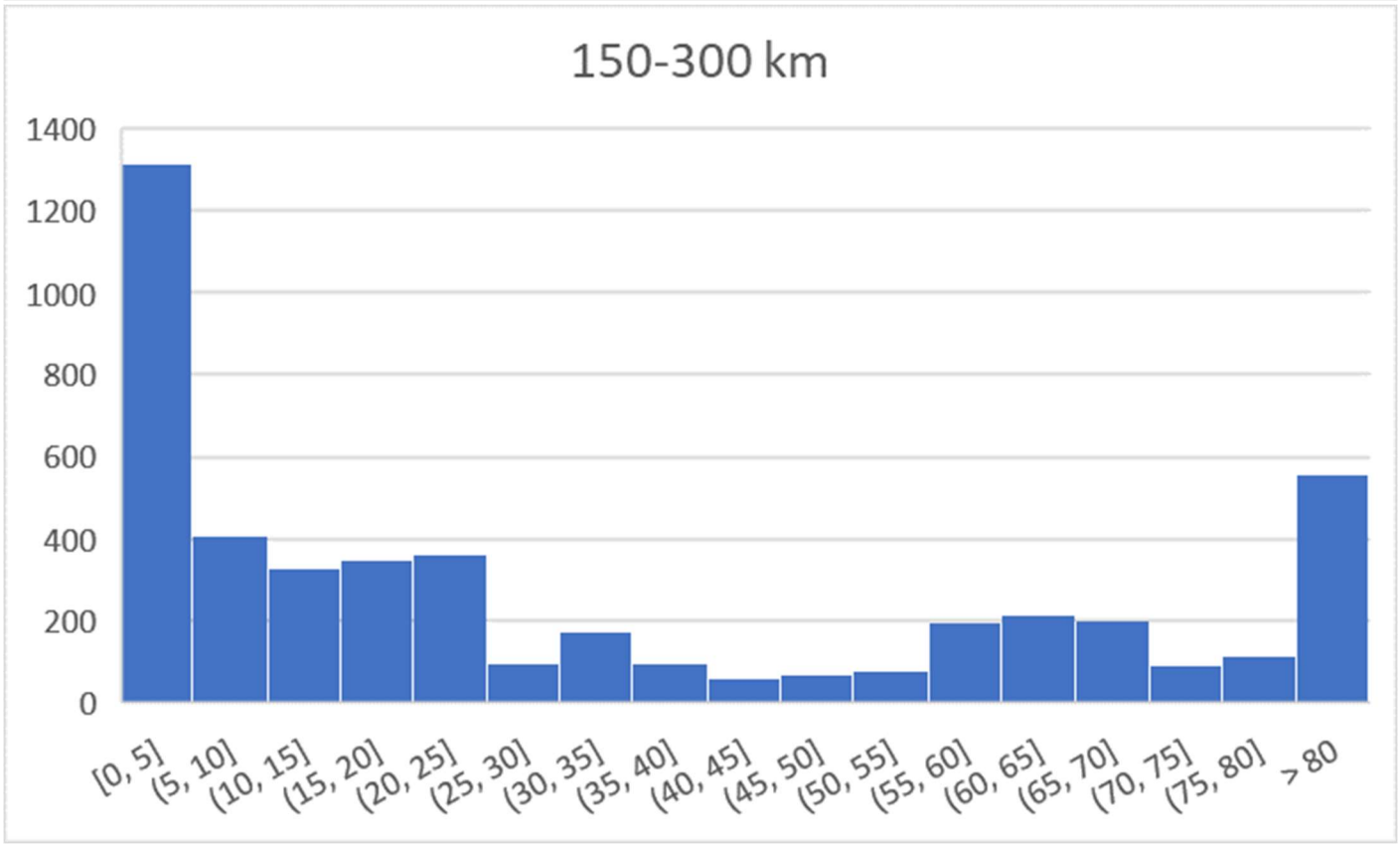
150-300 km
1400
1200
1000
800
600
400
200
0
[0, 5]
(5, 10]
(10, 15]
(15, 20]
(20, 25]
(25, 30]
(30, 35]
(35, 40]
(40, 45]
(45, 50]
(50, 55]
(55, 60]
(60, 65]
(65, 70]
(70, 75]
(75, 80]
> 80

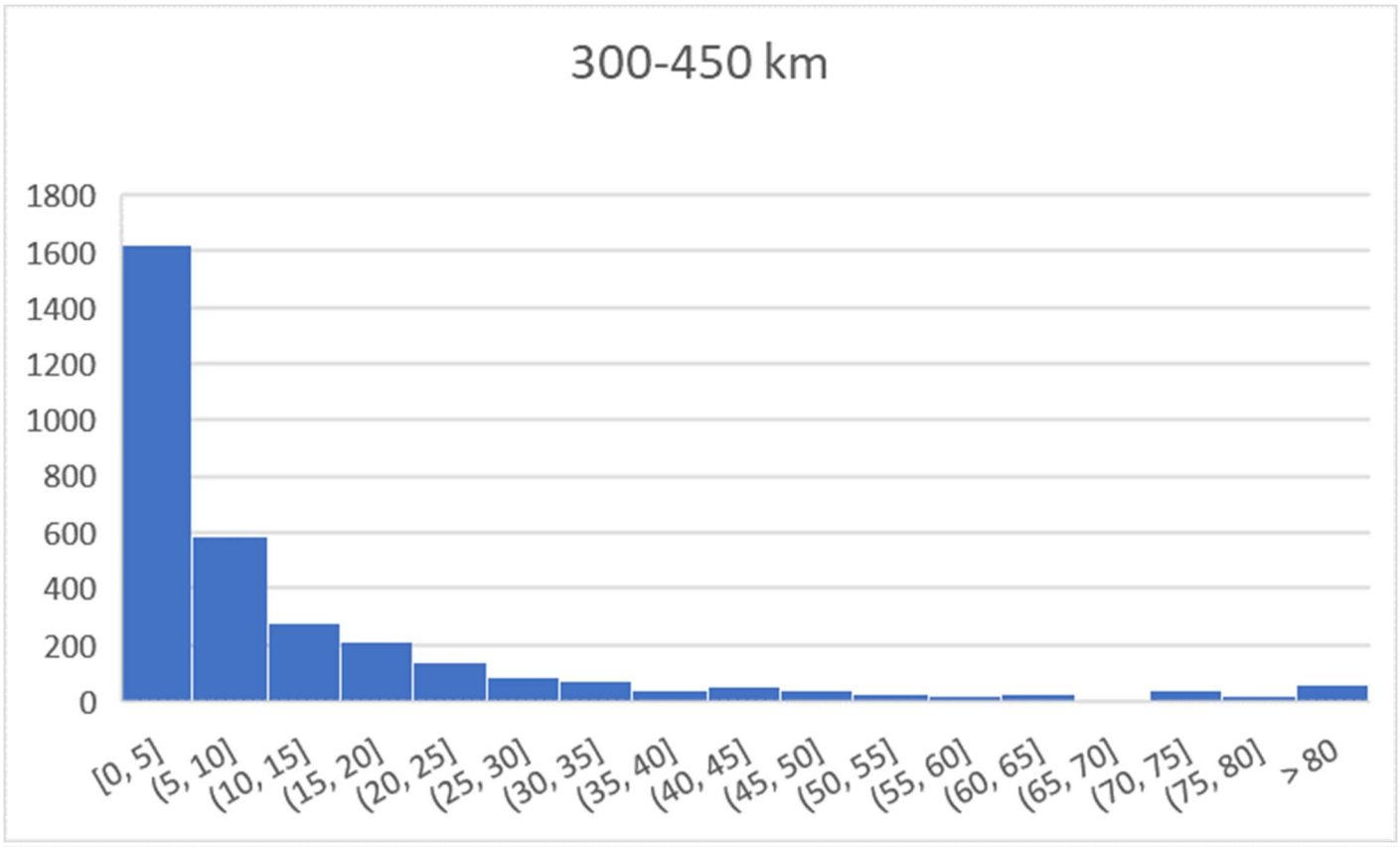
300-450 km
1800
1600
1400
1200
1000
800
600
400
200
0
[0, 5]
(5, 10]
(10, 15]
(15, 20]
(20, 25]
(25, 30]
(30, 35]
(35, 40]
(40, 45]
(45, 50]
(50, 55]
(55, 60]
(60, 65]
(65, 70]
(70, 75]
(75, 80]
> 80

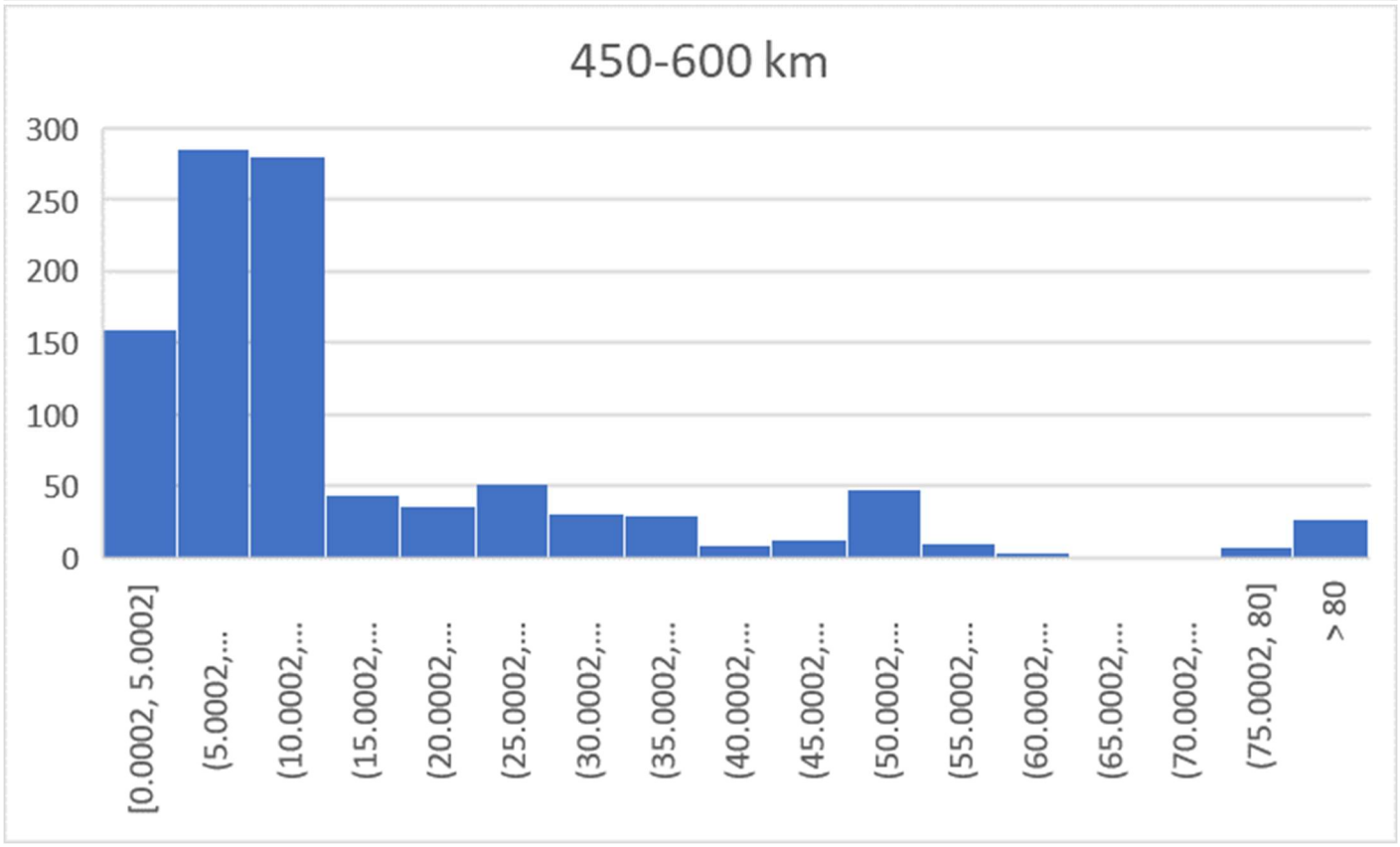
450-600 km
300
250
200
150
100
50
0
[0.0002, 5.0002]
(5.0002,...
(10.0002,...
(15.0002,...
(20.0002,...
(25.0002,...
(30.0002,...
(35.0002,...
(40.0002,...
(45.0002,...
(50.0002,...
(55.0002,...
(60.0002,...
(65.0002,...
(70.0002,...
(75.0002, 80]
> 80

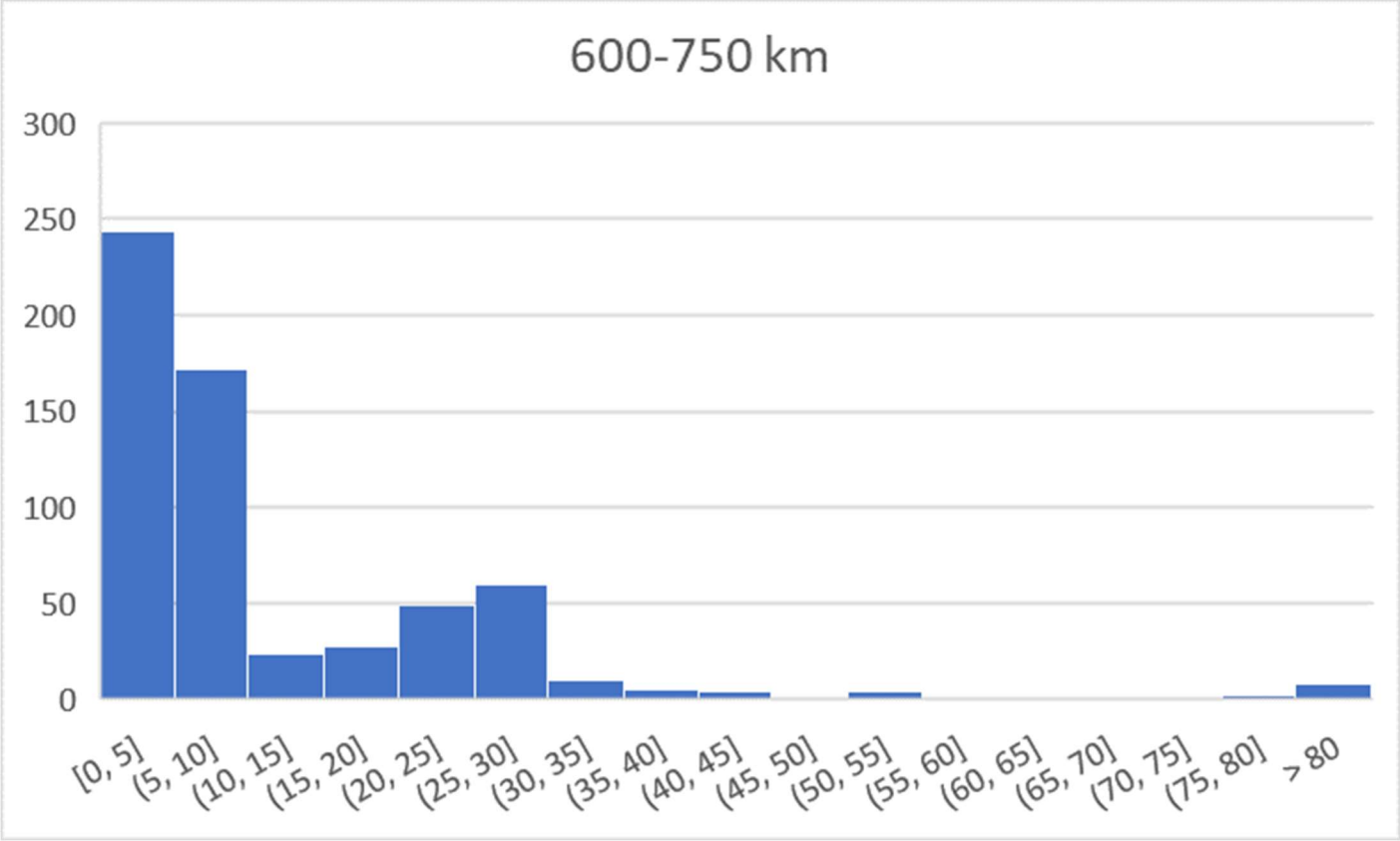

Figure 14. Histograms of igneous dates from Andes, 80-0 Ma. a. All dates 1 m.y. Bins. b. As A, 5 m.y. Bins. c. Within 0-150 km from trench. d. 150-300 km from trench. e. 300-450 km from trench. f. 450-600 km from trench. g. 600-750 km from trench.

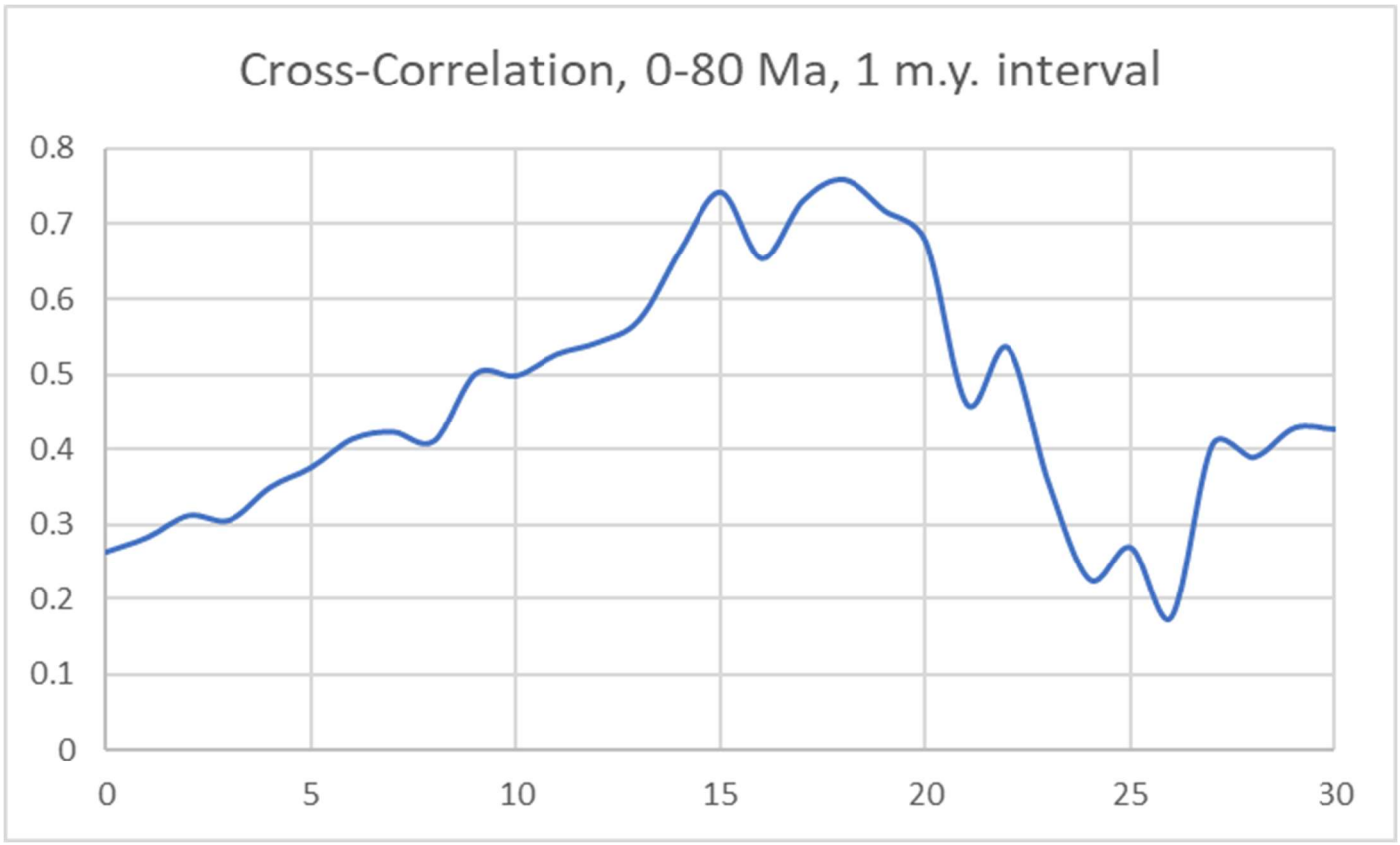

Figure 15. Normalized cross-correlation of convergence rate versus bin date size.

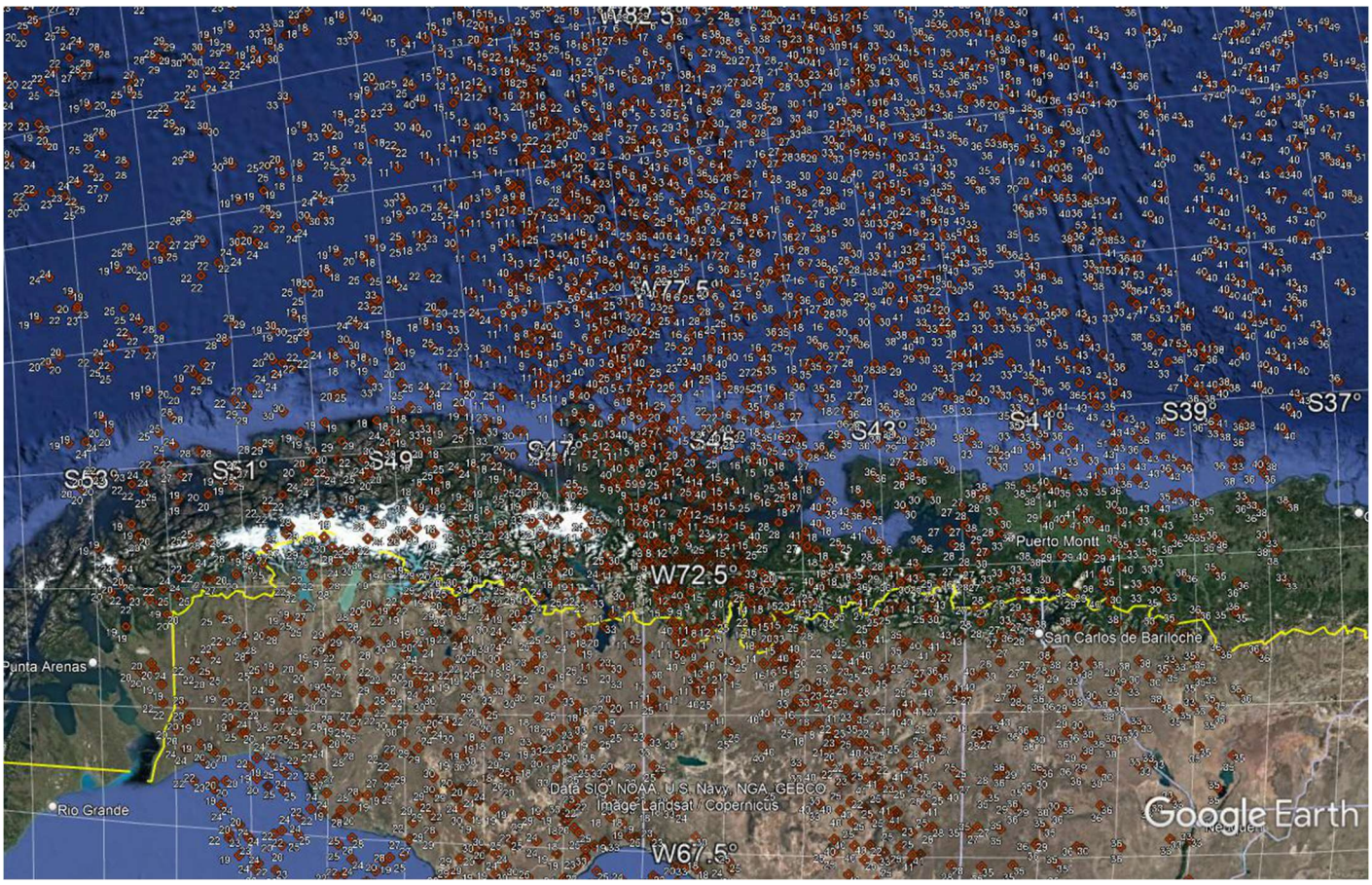

Figure 16. Reconstructed isochrons from the Antarctic plate to South America according to age via the global circuit. Google Earth format (*.kml) file is accessible in Supplementary Data files.

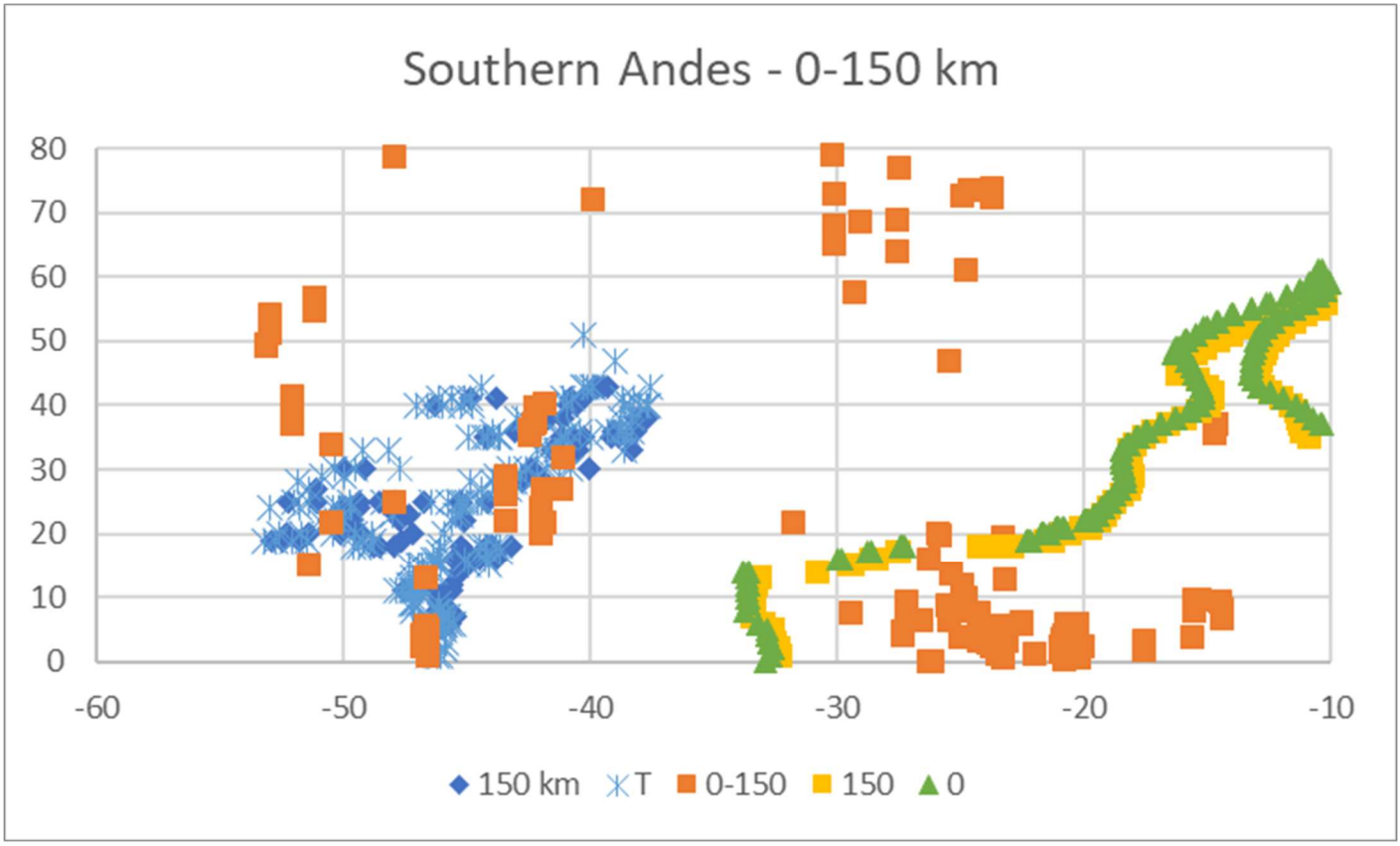

Figure 17. Projected section of igneous isotopic dates, reconstructed isochrons (from Figure 16), and Juan Fernandez trace (older Hawaiian-Emperor model), Ma, 0-150 km from trench, versus latitude.

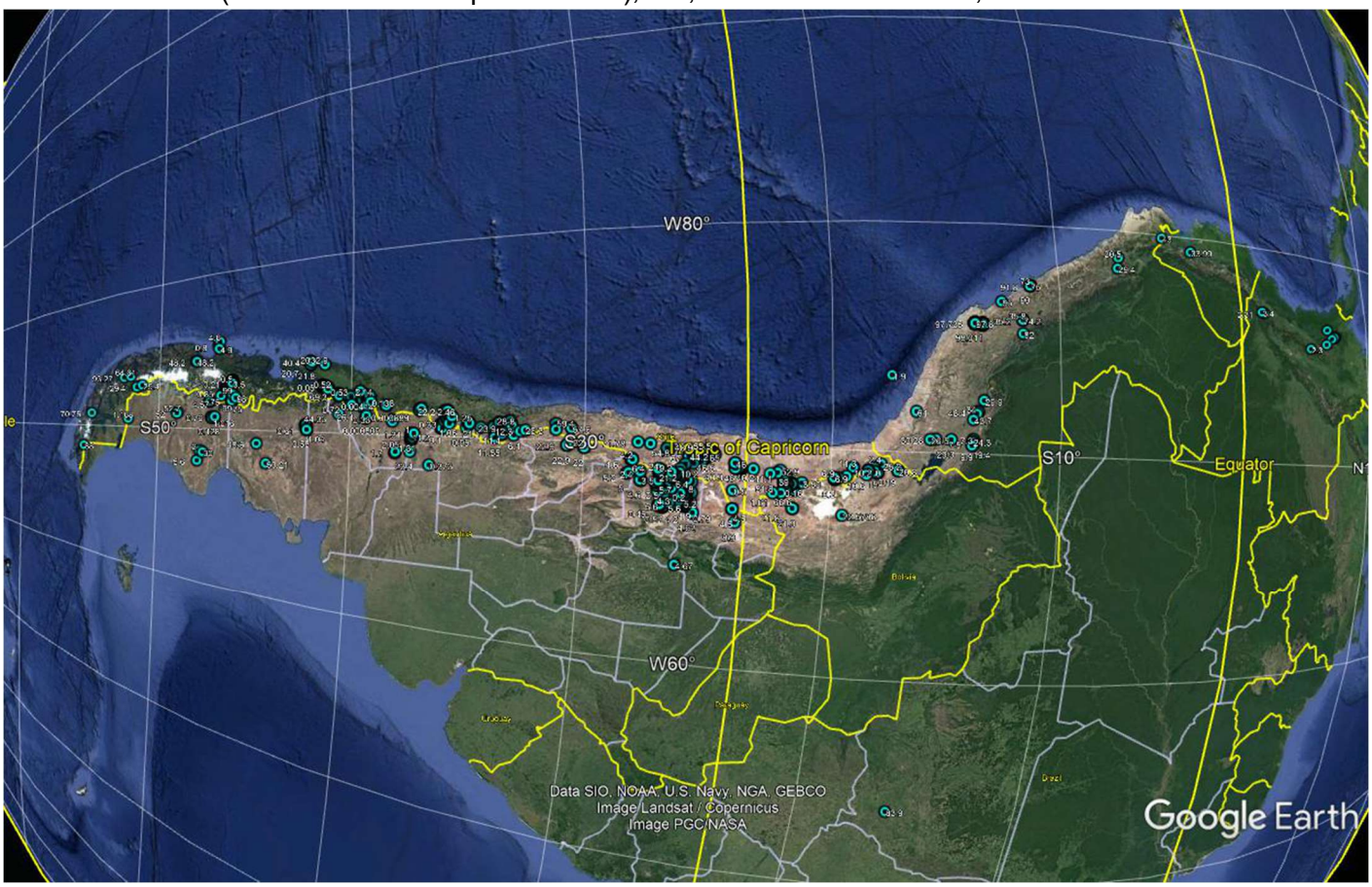

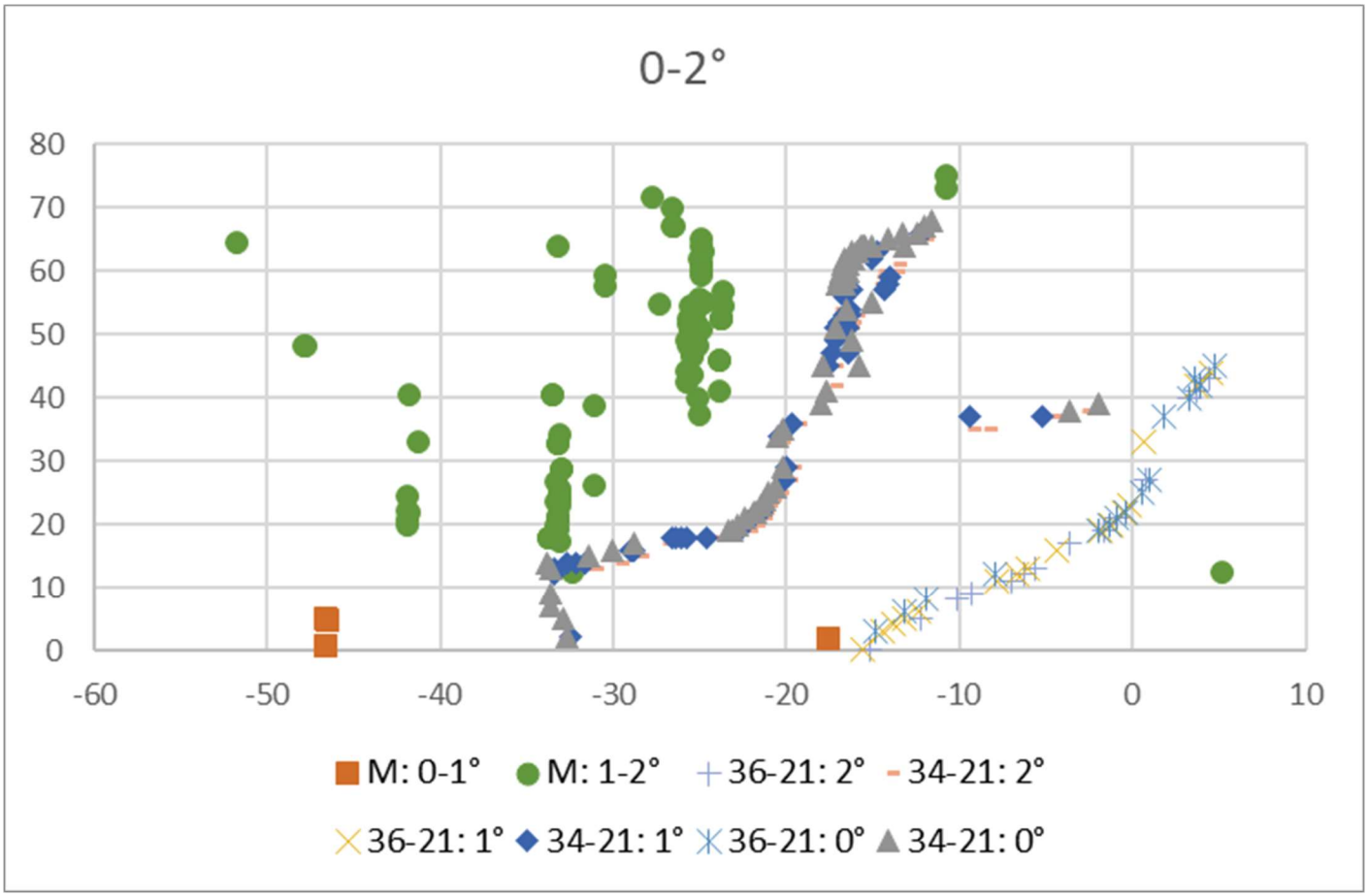
0-2°
80
70
60
50
40
30
20
10
0
-60
-50
-40
-30
-20
-10
0
10
M: 0-1°
M: 1-2°
36-21: 2°
34-21: 2°
36-21: 1°
34-21: 1°
36-21: 0°
34-21: 0°

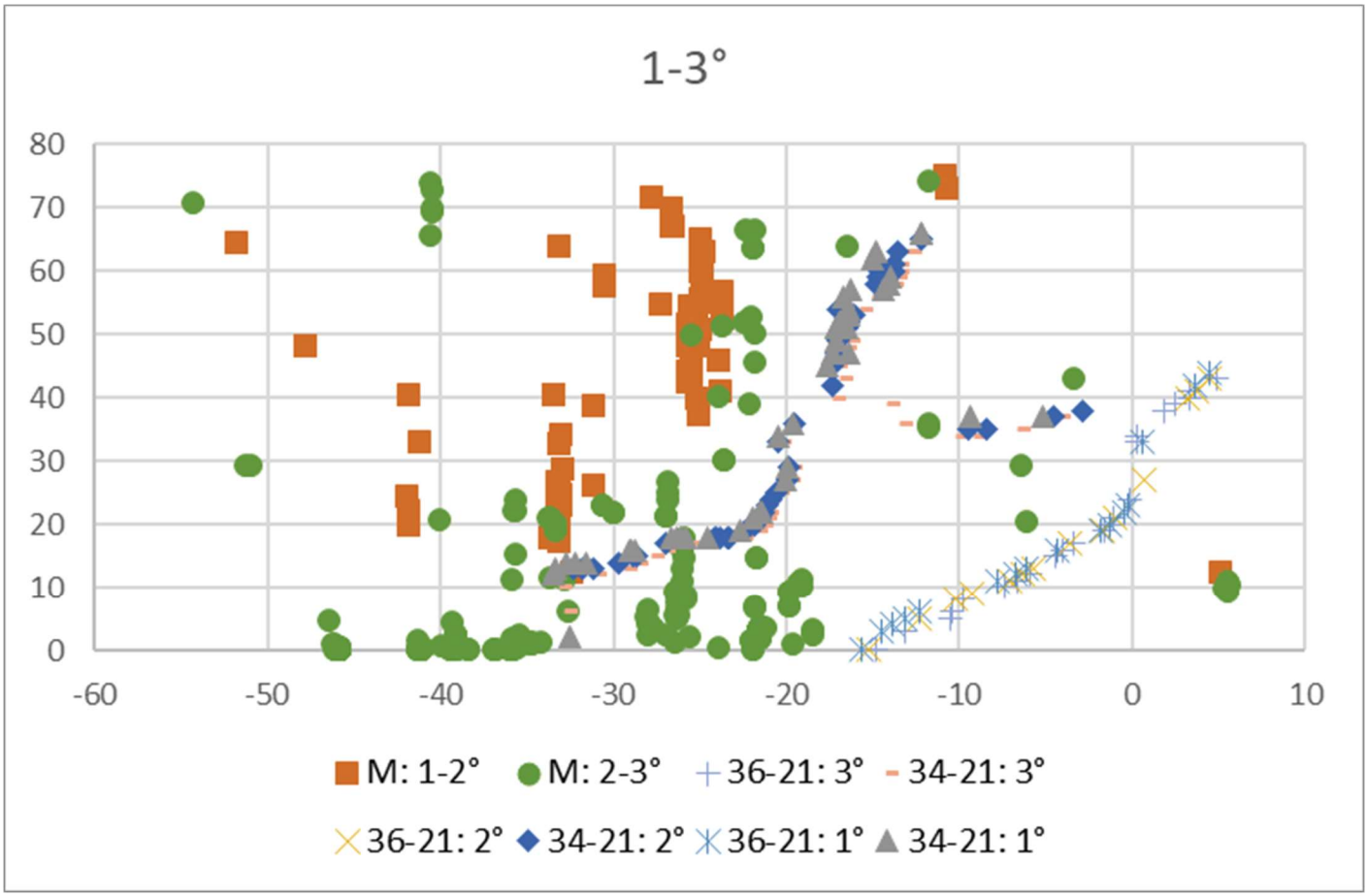
1-3°
80
70
60
50
40
30
20
10
0
-60
-50
-40
-30
-20
-10
0
10
M: 1-2°
M: 2-3°
36-21: 3°
34-21: 3°
36-21: 2°
34-21: 2°
36-21: 1°
34-21: 1°

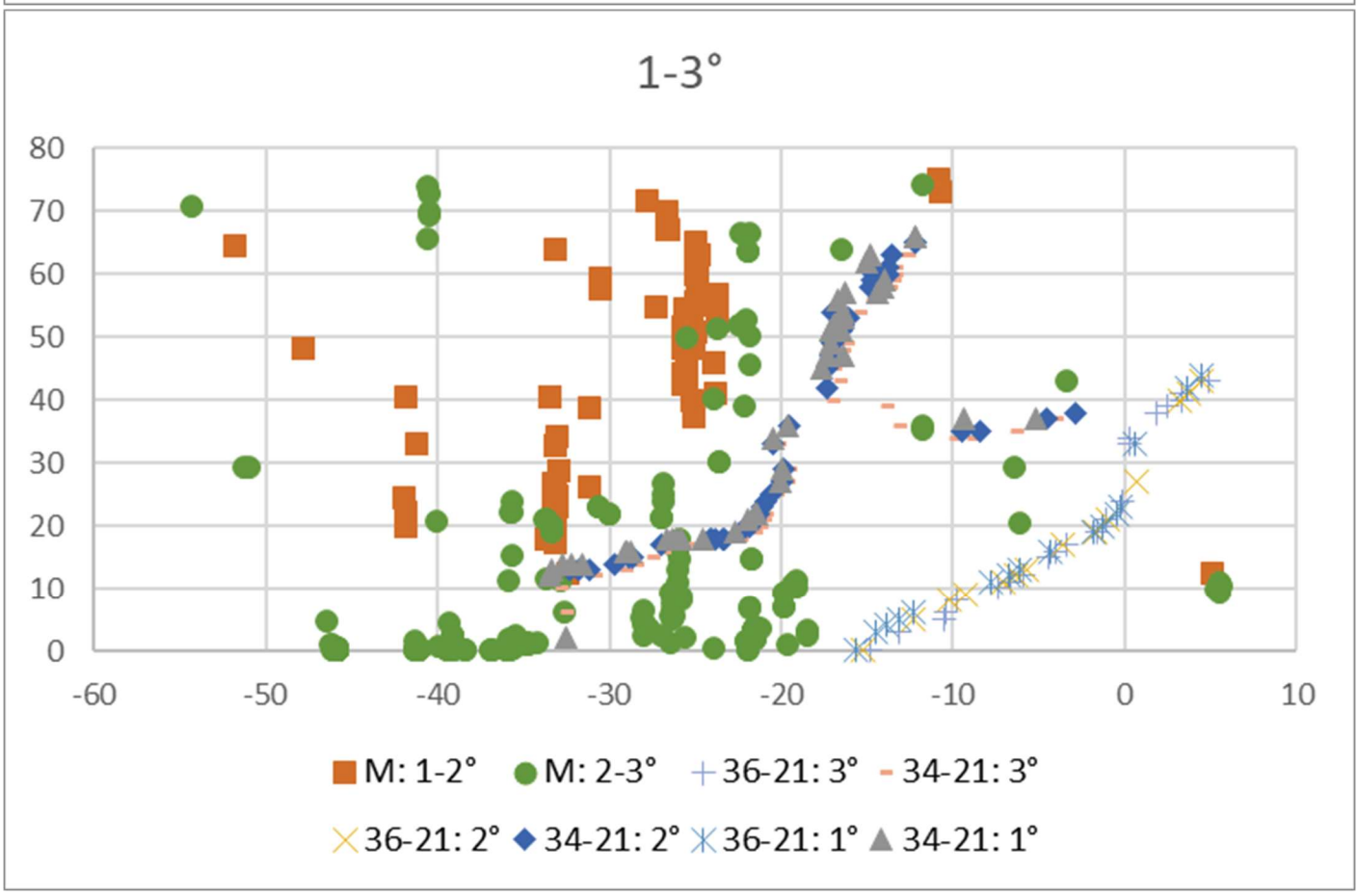
1-3°
80
70
60
50
40
30
20
10
0
-60
-50
-40
-30
-20
-10
0
10
M: 1-2°
M: 2-3°
36-21: 3°
34-21: 3°
36-21: 2°
34-21: 2°
36-21: 1°
34-21: 1°

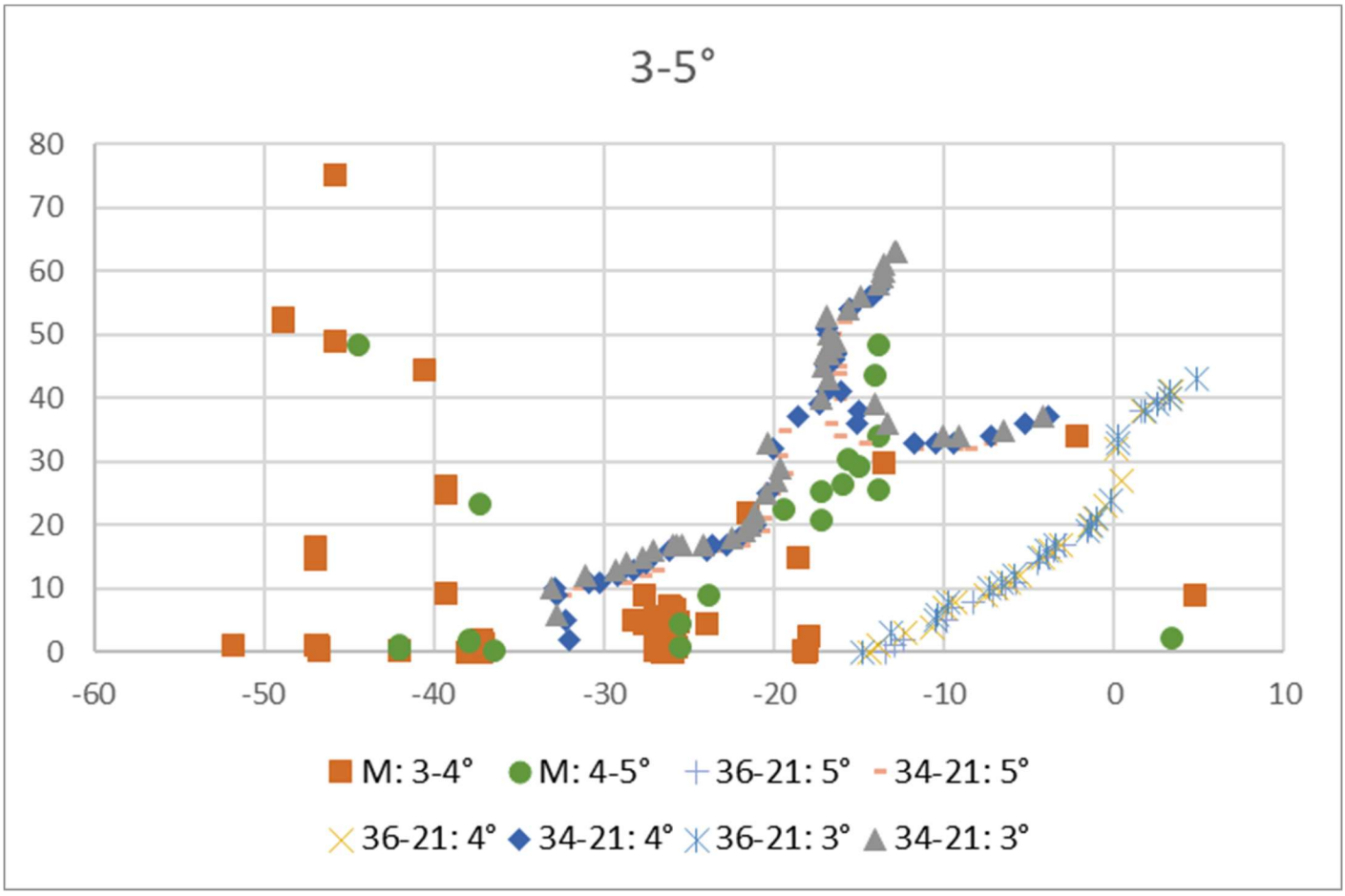
3-5°
80
70
60
50
40
30
20
10
0
-60
-50
-40
-30
-20
-10
0
10
M: 3-4°
M: 4-5°
36-21: 5°
34-21: 5°
36-21: 4°
34-21: 4°
36-21: 3°
34-21: 3°

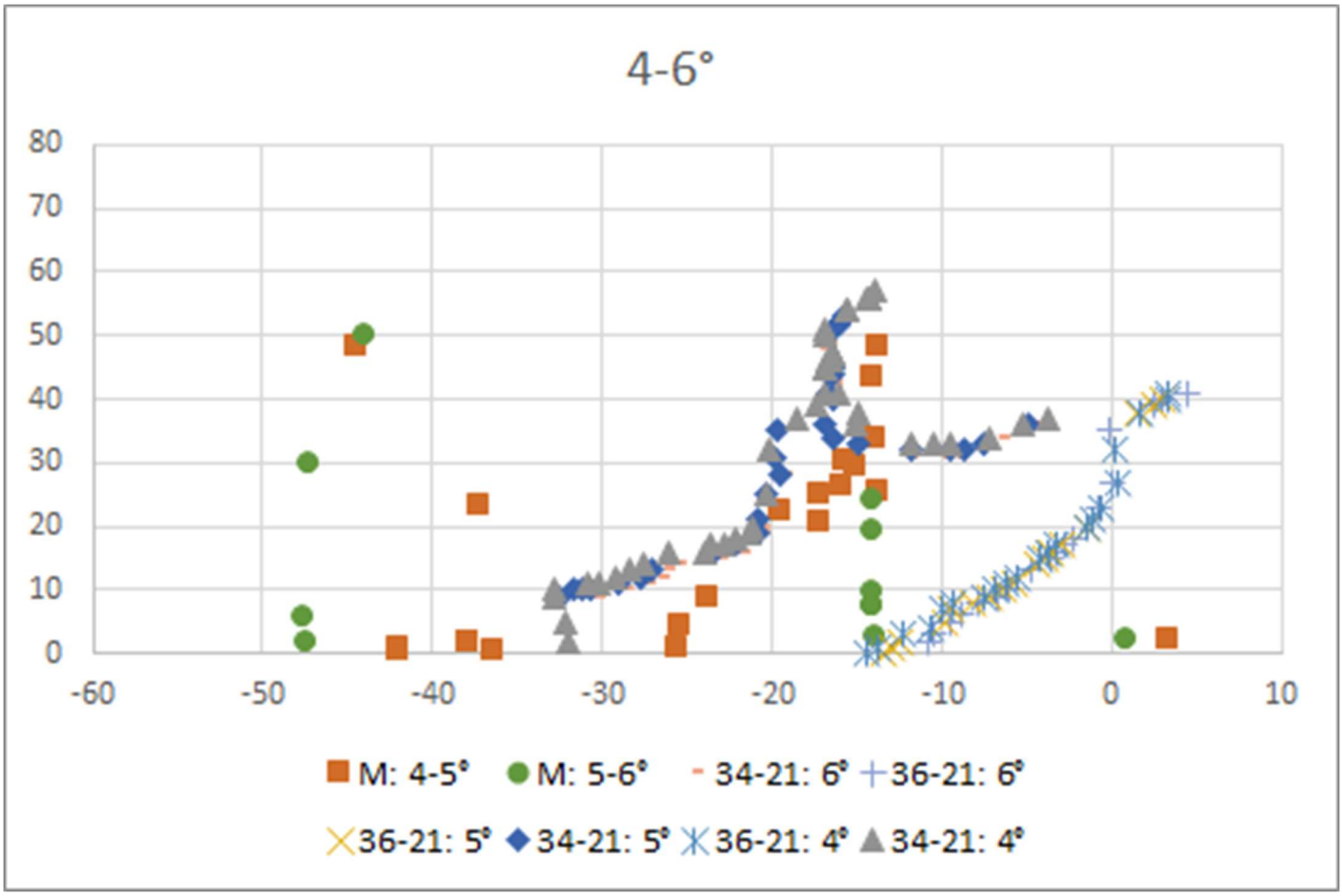
4-6°
80
70
60
50
40
30
20
10
0
-60
-50
-40
-30
-20
-10
0
10
M: 4-5°
M: 5-6°
34-21: 6°
36-21: 6°
36-21: 5°
34-21: 5°
36-21: 4°
34-21: 4°

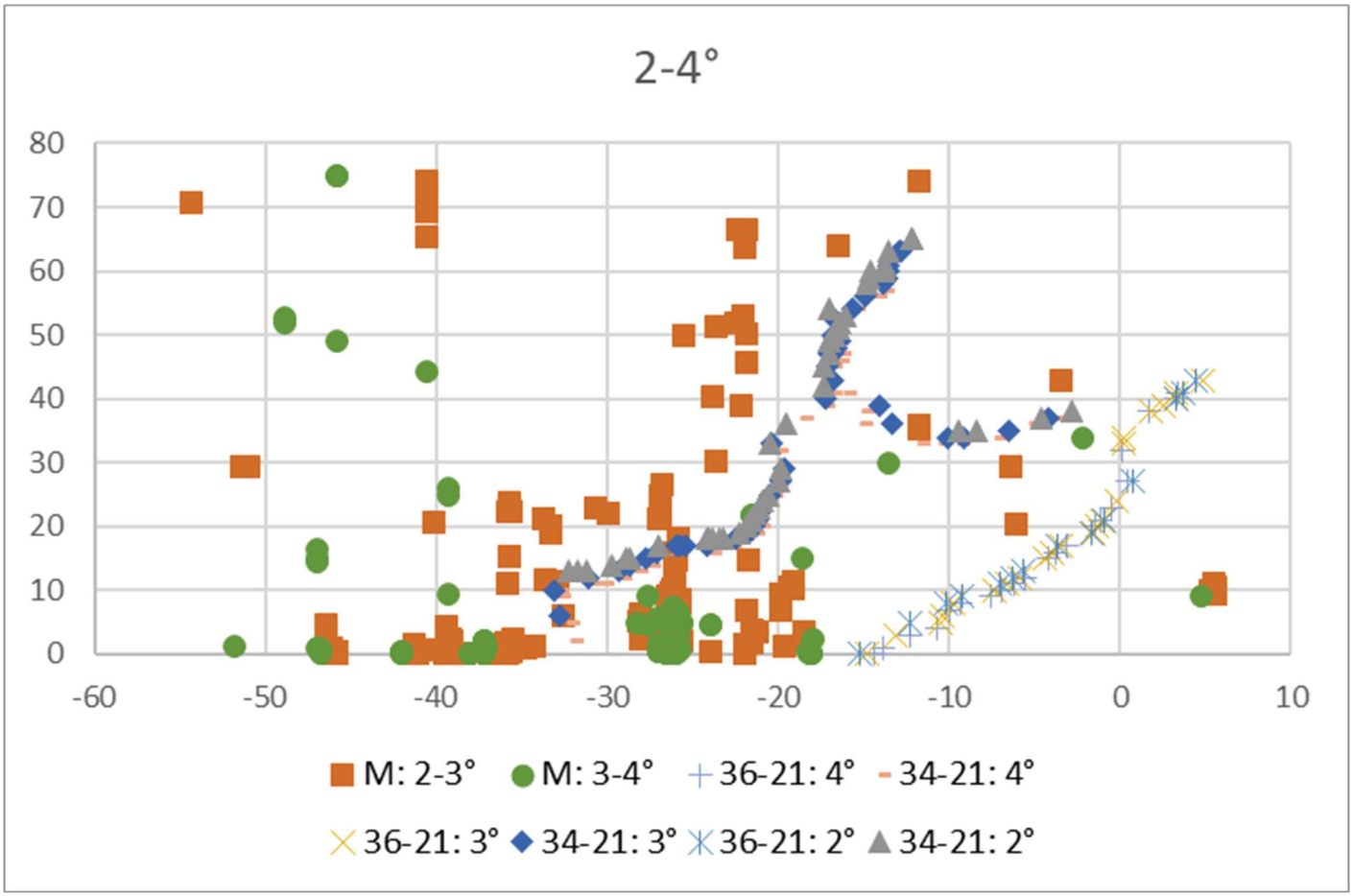

Figure 18. a: Isotopically dated *mafic* rocks from the Andes (top). b-g: Charts: Projected isotopic dates of mafic rocks in adjacent increments of 1° arc-distance from the trench along with projected intersections of modeled hotspot traces on segment boundaries, b: 0-2°, c: 1-3°, d: 2-4°, e: 3-5°, f: 4-6°. Traces are from modified GGW22 model (older Hawaiian-Emperor bend, 50 Ma, and older maximum age, 85 Ma) combined with WK08 incremental stages for traces older than 85 Ma, of Pacific-Hotspot reconstructions propagated to the Nazca plate and further reconstructed relative to South American plate. (Note, in contrast with previous projection figures, two adjacent 1° segments are shown in each chart along with three sets of trace intersections.) The traces can be thought of as partial envelopes around time-transgressive magmatic episodes. That is, in the middle of the graph, as it propagates north-south, the Juan Fernandez trace (36) bounds older from younger mafic data points. The Easter-Nazca trace (34) provides similar bounds on the northern part of the graph, although data points are sparser.

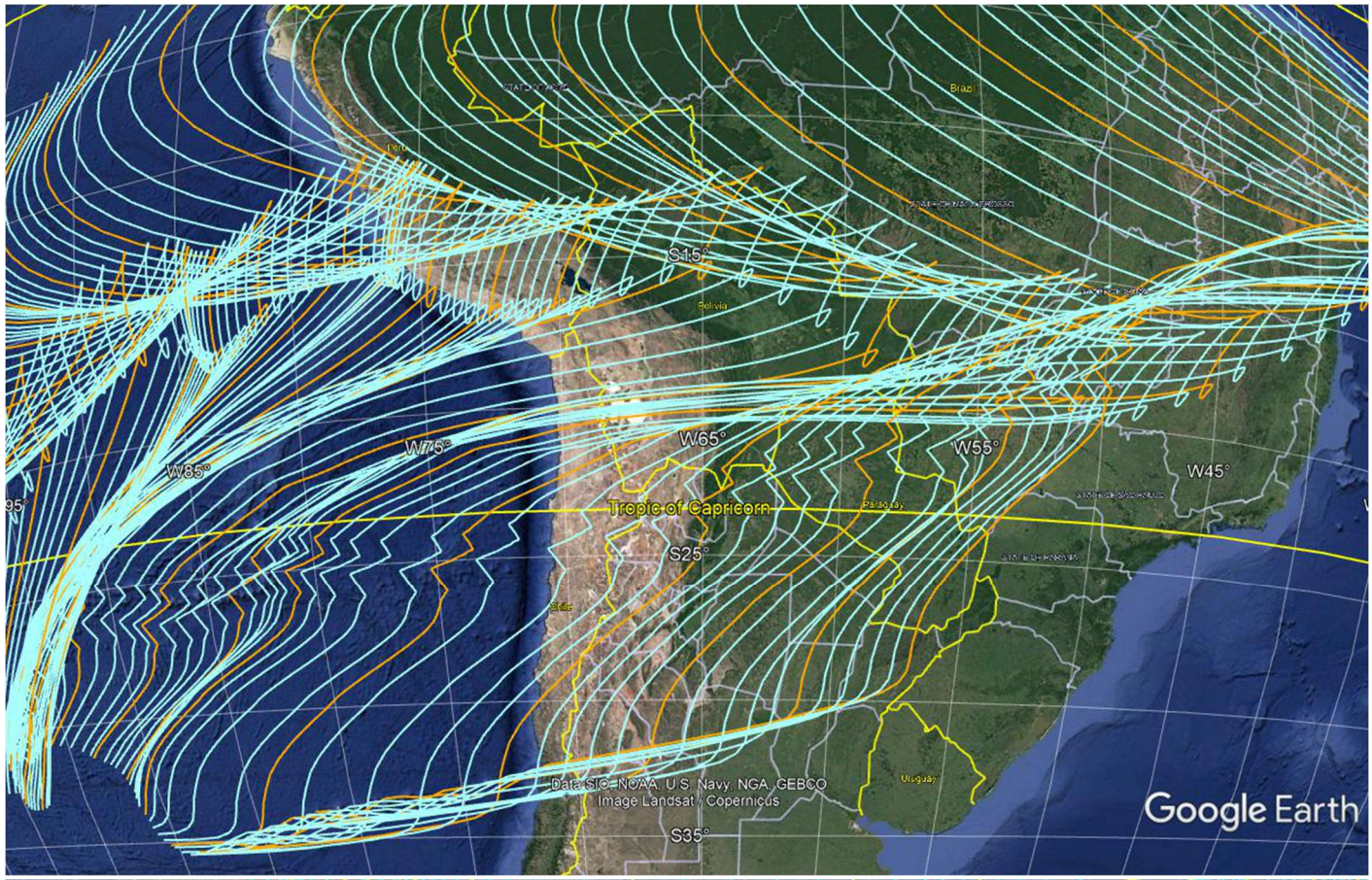
S15°
W65°
W55°
W45°
W75°
W85°
Tropic of Capricorn
S25°
S35°
Data SIO, NOAA, U.S. Navy, NGA, GEBCO
Image Landsat / Copernicus
Google Earth

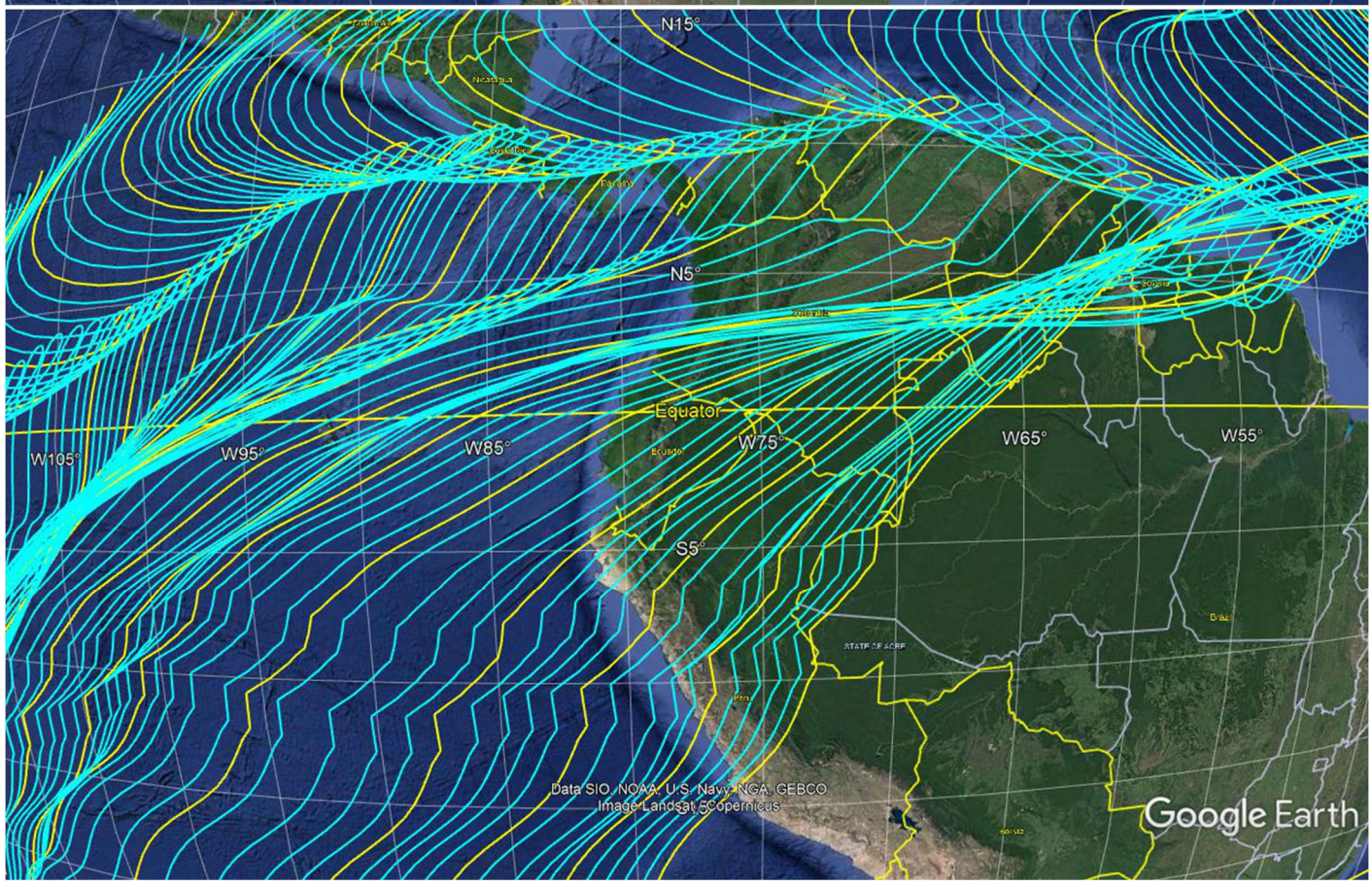
N15°
N5°
Equator
S5°
W105°
W95°
W85°
W75°
W65°
W55°
Data SIO, NOAA, U.S. Navy, NGA, GEBCO
Image Landsat / Copernicus
Google Earth

Figure 19. Juan Fernandez (upper) and Easter-Nazca (lower) hotspot traces at 1 m.y. increment, assuming GGW22 model with 50 Ma Hawaiian-Emperor Bend, and 85 Ma end, extended to the Nazca plate, reconstructed to fixed South America(as described in text). 5 m.y. intervals in orange and yellow. Google Earth format (*.kml) files are accessible in Supplementary Data files.